Analytical and Numerical Studies of 2D XY Models with Ring Exchange

by

Jason Iaconis

A thesis
presented to the University of Waterloo
in fulfillment of the
thesis requirement for the degree of
Master of Science
in
Physics

Waterloo, Ontario, Canada, 2012

I hereby declare that I am the sole author of this thesis. This is a true copy of the thesis, including any required final revisions, as accepted by my examiners.

I understand that my thesis may be made electronically available to the public.

Abstract

In this thesis we take several different analytic and numerical approaches to studying the classical J-K model. This model describes an interacting many-body system of spins with continuous symmetry which interact via 2-site nearest-neighbour exchange terms and 4-site ring-exchange terms. We begin by looking at the traditional solution of the XY model, in order to gain insight into the behaviour and general properties of the system. Classical Monte Carlo simulations will then be used to study the properties of the J-K model in different regimes of phase space. We will see that we can use properties from the theoretical solution of the XY model to study the Kosterlitz-Thouless phase transition numerically. We then extend our simulation to study the aspect ratio scaling of the superfluid density in the XY model. It will also be shown that there exists a finite temperature phase transition in the pure-K ring-exchange model. After this we will develop a mapping from the 1D quantum Bose-Hubbard model to the 2D J-K model and use this mapping to search for topological phases in classical Hamiltonians. However, we find that our mapping fails to reproduce the topological phase present in the quantum model. Finally we will look at the XY model using tools from information theory. A method for measuring mutual information in classical Monte Carlo simulations is developed. We then show that this measurement of mutual information can be used as a completely new way to identify the Kosterlitz-Thouless phase transition in Monte Carlo simulations.

Table of Contents

List of Figures

Chapter 1

Introduction

1.1 Overview

This thesis presents an analysis of the behaviour of the classical two dimensional J-K model using both numerical Monte Carlo techniques and various analytical techniques. The 2D XY model is one of the most interesting cases of a statistical mechanics problem whose properties can be used to demonstrate a wide variety of important ideas which are pervasive throughout other areas of many-body physics. Important physics behind superfluidity, continuous phase transitions, renormalization group techniques and finite-size scaling are all addressed within the basic solution of this model [1, 2]. The J-K model is an extension of the XY model to include a 4-site ring-exchange interaction term. This generalization can allow us to extend our model to study a wider range of topics.

We look at this model from several different perspectives. The first is from a purely classical standpoint, treating it as statistical mechanics problem which can be related to several interesting physical systems. From this perspective, the classical XY model can be used to study the properties of superfluid films of Helium-4 and the pure ring-exchange model can be related to the melting of two dimensional vortex solids [3, 4]. By performing Monte Carlo simulations we can infer important properties about which type of phase transitions occur in our model. Analytical analysis can be used to point out universal properties which can be measured in Monte Carlo simulations and used to infer properties of other systems which are related by universality.

We can also look at how one can learn about quantum systems when studying classical statistical mechanics models by applying the path integral formulation of quantum mechanics. Within this formulation, quantum systems in d-dimensions can always be mapped onto

classical systems in $(d+1)$-dimensions. While looking at the aspect ratio scaling of the XY model, we will see that there is a connection to 1D fermionic systems which are described by Luttinger liquid theory. We will spend more time looking at 1D bosonic systems, where we develop a mapping from the one dimensional Bose-Hubbard model to the two dimensional J-K model. As we will see, the 1D Bose-Hubbard model contains a phase which is topologically ordered. This mapping offers the tantalizing prospect of studying topological phases, which arise entirely due to nonlocal properties, by studying a classical system. We are interested in discovering whether we can realize this topological phase within a classical model and seeing how this type of order manifests itself. However, we find that our quantum to classical mapping was not able to reproduce the topologically ordered phase of the Bose-Hubbard model.

Finally, we study the XY model within the context of information theory. Recently, the use of information theory has been seen as a new tool within many-body physics which can be used to measure properties which cannot be detected using traditional measures [5, 6, 7]. We look at how information theory can be used to study properties of classical many-body systems. We then develop a method for measuring the "information entropy" of the classical system, based on techniques which are known for quantum systems. We then apply this technique to study the phase transition in the 2D XY model. We find that we can measure a quantity known as mutual information in our Monte Carlo simulations and this measurement gives a completely new way to identify the Kosterlitz-Thouless phase transition.

This thesis will be organized as follows. In the remainder of Chapter 1, I will introduce the J-K model and discuss the solution to the XY model. We will discuss the important properties of systems with continuous symmetries which will be used throughout the rest of this thesis. We rigorously show that a finite-temperature phase transition occurs in this model, the famous Kosterlitz-Thouless transition. We also discuss the main idea behind Monte Carlo simulations and an extension of this algorithm which allows us to more efficiently study the XY model.

In Chapter 2 we continue the discussion of the classical J-K model by simulating the system using the Monte Carlo algorithm. We start by discussing the scaling properties of the XY model, then study the phase transition which occurs within the pure-K ring-exchange model. Finally we extend this analysis to include the properties of the entire J-K phase space. Chapter 3 will be used to develop the connection between classical and quantum many-body systems. We discuss the quantum Bose-Hubbard model and develop a mapping to the (1+1)-d J-K model. Specifically, we will be looking for a representation of the topological Haldane phase for the quantum system in terms of a classical Hamiltonian. Finally, in Chapter 4 we discuss the XY model within the context of classical information

theory and develop a new way to detect the Kosterlitz-Thouless phase transition using numerical simulations.

1.2   The Classical J-K Model

The model describes classical continuous degrees of freedom, represented as spins with O(2) symmetry, which interact with each other via a two-site nearest-neighbour interaction and a 4-site ring-exchange interaction. Quantum versions of this model have been studied in references [8] and [9]. In practice the classical spins are simply represented as a single angle θ which takes a value between 0 and 2π. The ring-exchange term sums over the elementary plaquettes of the lattice, that is smallest 4-site clusters of spins which appear on the lattice (Fig. 1.1).
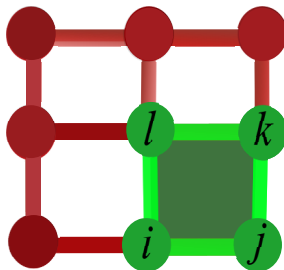
Figure 1.1: The smallest plaquette $\langle ijkl \rangle$ on a square lattice

The ring-exchange term acts in a way such that the total sum of the spins on each plaquette wants to be either 0 or π, depending on the sign of the exchange term. The Hamiltonian is given by:

$$\mathcal{H} = -J \sum_{\langle ij \rangle} \cos(\theta_i - \theta_j) - K \sum_{\langle ijkl \rangle} \cos(\theta_i - \theta_j + \theta_k - \theta_l). \tag{1.1}$$

For positive J and K terms, it is clear that the most energetically favoured state would be one where all the spins align in the same direction. However, the Mermin-Wagner theorem states that in dimensions $d \leq 2$ and at finite temperatures, it is impossible to have a state with long range order which breaks continuous symmetries of the system [10]. In the XY model in two dimensions it is well known that there does exist a finite temperature phase transition into an ordered low temperature phase, which does not break any continuous

3

symmetries of the system but is instead mediated by the unbinding of magnetic vortex-antivortex pairs. Such a transition is classified as an infinite order phase transition since there are no discontinuities in any derivatives of the free energy, and is known as the Kosterlitz-Thouless phase transition. Through a series of Monte Carlo simulations we show in Section 2.3 that such a transition also occurs in the pure K model, when $J = 0$. The rest of this chapter will be devoted to reviewing the properties of the XY model and discussing the general properties of the J-K model, which will be needed when using this model to study more complicated systems in future chapters.

1.3   The XY Model

There exists a finite-temperature phase transition in the 2D XY model despite the apparent problem posed in the previous section due to the Mermin-Wagner theorem. The key is that this ordering occurs in a way which does not break the rotational symmetry of the spins. This ordered phase of the XY model is characterized by a finite value of a quantity known as the helicity modulus, also called the spin stiffness. There is no magnetic order in the low temperature phase (Define $\theta \in [r - \pi, r + \pi]$. Then no magnetic order implies that $\langle \theta_i \rangle = r$ for every choice of r). Instead the spin stiffness measures the relative phase between neighbouring spins which doesn't depend on any broken symmetry property of the system. This measurement is defined as the response of the system to a uniform rotation of the spins in the direction of one of the lattice vectors [11],

$$\gamma_\mu/J = \frac{1}{Z}\frac{\partial^2 F}{\partial \theta^2} = \frac{1}{N}\left\langle \sum_{\langle ij \rangle} \cos(\theta_i - \theta_j)(\hat{\mathbf{e}}_{ij} \cdot \hat{\mu})^2 \right\rangle - \frac{J}{TN}\left\langle \left[\sum_{\langle ij \rangle} \sin(\theta_i - \theta_j)\hat{\mathbf{e}}_{ij} \cdot \hat{\mu} \right]^2 \right\rangle. \tag{1.2}$$

The advantage of this measurement is that it is defined in terms of the local spin degrees of freedom of the system and can be easily implemented in a Monte Carlo simulation. An equivalent way of defining the superfluid density measures the response to a twisting of the boundary conditions of the system. If we define γ as the energy cost of uniformly twisting the spins across the lattice, then the change in free energy associated with such a rotation would be given by $\Delta F \approx \gamma(\nabla\theta)^2 V(\Omega)$ where $V(\Omega)$ is the volume of the system.

There exists a close relationship between the XY model and a bosonic superfluid which is actually quite intuitive. In bosonic superfluid systems, the wavefunctions of individual bosons condense into a single macroscopic wavefunction for the entire system at low temperatures. The wavefunction of a boson naturally has a gauge invariance

$\psi(\vec{r}) = e^{i\theta}\psi(\vec{r})$. More formally if $\psi_0(\vec{r})$ is a single-particle wave function, then the wavefunction $\psi(\vec{r}) = e^{i\vec{q}\cdot\vec{r}}\psi_0(\vec{r}) = e^{i\theta(\vec{r})}\psi_0(\vec{r})$. Then $\nabla\theta(\vec{r}) = \vec{q}$, and $\psi(\vec{r})$ describes a wave packet moving with velocity $v_s = \langle\nabla\theta\rangle$. In a superfluid, the increment in the free energy due to a nonzero gradient $\nabla\theta$ is given by the expression $\Delta\mathcal{F} = \frac{1}{2}\rho_s(T)v_s^2 V(\Omega)$ [12]. That is, the change in energy is solely related to the increase in the velocity of the superfluid flow. In a bosonic system, the superfluid density can be related to the helicity modulus directly as $\rho_s(T) = \gamma$. By taking a phenomenological definition of the superfluid density and looking at the energy cost of a change in the superfluid flow we can identify the phase of the spin variables in our XY model with the phase of the wavefunction in a bosonic system. Hence we can identify our earlier definition of helicity modulus with the superfluid density of the bosonic system. In a superfluid, the phases of the wavefunctions of neighbouring bosons will attempt to align in order for the system to lower its energy by achieving macroscopic phase coherence. This alignment of the phases θ also occurs in the XY model at low temperature. For this reason, throughout this thesis I will often use the phrases 'helicity modulus', 'spin stiffness' and 'superfluid density' interchangeably when describing the classical XY model.

In the XY model, the phase transition from an ordered phase to a disordered phase is mediated by the binding and unbinding of vortex-antivortex pairs. I will now give a brief overview of the physics behind this transition (this can be found in many places in the literature see for example reference [13]). We start by taking the continuum limit of the XY Hamiltonian:

$$H = -J\sum_{\langle ij\rangle}\cos(\theta_i - \theta_j) \approx -\frac{J}{2}\int d\vec{x}(\nabla\theta(\vec{x}))^2. \tag{1.3}$$

A vortex is a configuration of the spins of the system where the phase of the spins changes by a multiple of 2π as one circles the core of the vortex. That is:

$$\oint d\vec{x}\cdot\nabla\theta(\vec{x}) = 2\pi n \quad n\varepsilon\mathbb{Z}. \tag{1.4}$$

The variable n is the winding number of the vortex. Using these two equations, one can solve for the energy and entropy contributions made by the presence of a vortex core:

$$(1.4) \Rightarrow \quad \theta(\vec{x}) = n\alpha \Rightarrow \nabla\theta(\vec{x}) = (n/|\vec{x}|)\hat{\alpha} \tag{1.5}$$

$$\text{Then } (1.3) \Rightarrow \quad H_v = -\frac{J}{2}\int d\vec{x}(\nabla\theta)^2 = \pi Jn^2\int_{r_0}^{L}\frac{rdr}{r^2} = \pi n^2 J\ln\left(\frac{L}{r_0}\right) \tag{1.6}$$

where α is the polar angle representation of θ, with the coordinate system centred on the vortex core. You can place a vortex core at any of the L^2 lattice sites, so that the entropy of a vortex core is given by $S_v = \ln((L/r_0)^2) = 2\ln(L/r_0)$.

Putting this together, we find that the change in free energy associated with the creation of a vortex is given by:

$$\Delta F_v = H_V - T\Delta S_v = \pi n^2 J \ln\left(\frac{L}{r_0}\right) - 2T \ln\left(\frac{L}{r_0}\right)$$

$$= (\pi n^2 J - 2T) \ln\left(\frac{L}{r_0}\right). \tag{1.7}$$

Thus as $L \to \infty$ we find that $\Delta F_v = 0$ when $T_{KT} = \frac{2}{\pi}J$.

This shows that there exists a finite temperature, T_{KT}, above which it becomes favourable to have free vortices appear in the system. This very simple argument shows that it is the appearance of vortices which can lead to a finite-temperature phase transition in this 2D model with continuous symmetries. One property which makes this possible is that in two dimensions the energy cost of vortices is logarithmic in the linear size of the system.

1.4   A Renormalization Group Treatment

Traditionally, a much more rigorous treatment of the XY model is given by deriving a set of renormalization group (RG) flow equations to describe the system. There are several important results which can only be understood within the context of this RG treatment [2, 13] . I will give a general overview of the most important steps of this procedure as the ideas listed here will be present throughout the rest of this thesis. The idea is that you formulate the problem in a way which systematically removes the short-ranged or high-momentum degrees of freedom, so that as you can isolate which properties of the system become important as you approach a phase transition and the correlation length of your field diverges. We start with the partition function for the XY model,

$$Z_{xy} = \int_0^{2\pi} \prod_i \frac{d\phi_i}{2\pi} e^{\frac{J}{T} \sum_{i,\hat{\mu}} \cos(\phi_i - \phi_{i+\mu})}. \tag{1.8}$$

There exists a series of transformations that we can apply to Z_{xy} which allows us to write the partition function of an exact dual to this model [14]. The Villain approximation [15] allows us to write the cosine as a sum over variables which are quadratic in ϕ and

6

the Hubbard-Stratonovich transformation then makes it possible to integrate over these variables. The result is called the discrete Gaussian model and can be expressed as a sum over discrete variables n_i:

$$Z_G = \sum_{n=-\infty}^{\infty} \exp\left[-\frac{T}{2J} \sum_{i\mu} (\Delta_\mu n_i)^2 \right].$$ (1.9)

We can bring back continuous variables at the cost of introducing a new set of discrete variables m_i, by applying the Poisson summation formula,

$$\sum_{m=-\infty}^{\infty} e^{-i2\pi m x} = \sum_{n=-\infty}^{\infty} \delta(x - n),$$ (1.10)

so that we find

$$Z_G = \int_0^{2\pi} \prod_i d\phi_i \sum_m \exp\left[-\frac{T}{2J} \sum_{i,\mu} (\Delta_\mu \phi_i)^2 - 2\pi i \sum_i \phi_i m_i \right].$$ (1.11)

It turns out the new variables m_i now have a useful physical meaning. Integrating over the fields ϕ by inverting the interaction matrix above, $G_{ij}^{-1} = \frac{T}{J}[4\delta_{ij} - \sum_\mu (\delta_{j,i+\mu} + \delta_{j,i-\mu})]$, gives $G_{ij} = -\frac{J}{2\pi T} \ln(|x_i - x_j|/a)$. Then using the Hubbard Stratonovich transformation again gives a long-wavelength form of the discrete Gaussian model as:

$$Z_G = \sum_{\{m\}} \exp\left[\frac{\pi J}{T} \sum_{ij} m_i m_j \ln\left(\frac{|x_i - x_j|}{a} \right) \right].$$ (1.12)

This is exactly the form of the partition function of a vortex-antivortex plasma. Our variables m_i represent the charge, or winding number, of these vortices. From our argument in the previous section we expect the appearance of unbound vortices to be solely responsible for any phase transition in the XY model. So, keeping with the physical picture of m_i being equal to the vortex charge, we then know that in the continuum limit there will be some energy cost associated with the core of a vortex. In the XY model on a discrete lattice vortex cores do not really exist, as a vortex is just centred in the middle of one plaquette on the lattice. However, as we perform our RG procedure there will be a course graining of the lattice so that the energy associated with the vortex core will become important. For a free vortex of charge m the contribution to the action of the vortex core will be $\frac{E_c}{T} m_i^2$, where E_c is the energy associated with the core of a vortex [2].

7

For this reason, we define the vortex fugacity $y = e^{-\frac{E_c}{T}}$. It represents the chemical potential of vortices. We then add the term $e^{-\frac{E_c}{T}\sum_i m_i^2} = \prod_i y^{m_i^2}$ to our partition function in Eq.(1.11). Then we expand our partition function in terms the fugacity y,

$$\sum_{m_i=-\infty}^{\infty} y^{m^2} e^{-2\pi i \phi_i m_i} = 1 + 2y\cos(2\pi\phi_i) + 2y^4\cos(4\pi\phi_i) + \cdots \approx e^{2y\cos(2\pi\phi+i)}. \qquad (1.13)$$

All this allows us to finally express the partition function in a form which is suitable for us to perform the RG analysis. Our resulting partition function, which we will write in the continuum limit, is called the sine-Gordan model and is dual to the XY model up to the very minor approximations we performed,

$$Z_{sG} = \int_0^{2\pi} d\phi(\vec{x}) \exp\left[\int d^2x \left[\frac{T}{2}\left(\vec{\nabla}\phi(\vec{x})\right)^2 - 2y\cos\left(2\pi\phi(\vec{x})\right)\right]\right]. \qquad (1.14)$$

As mentioned, the renormalization group procedure depends on course graining the lattice by assuming fluctuations which occur on the shortest length scales become unimportant as the correlation length of the system becomes large. In the momentum space picture, it is the spin fluctuations with the highest momentum that become unimportant. There exists a scale invariance, so as you integrate out the highest momentum states or average over the shortest length scales it becomes possible to write the partition function in a way which is in exactly the same form as when you started [16, 17, 18].

To achieve this, first note that there naturally exists a high momentum cutoff Λ to the system which occurs at the scale of the lattice constant a. We must divide the field $\phi(x)$ into slow and fast momentum modes $\phi(k) = \phi_<(k) + \phi_>(k)$. This allows us to write any integrals over momentum as $\int_0^{\Lambda} \phi(k)dk = \int_0^{\Lambda/b} \phi_<(k)\,dk + \int_{\Lambda/b}^{\Lambda} \phi_>(k)\,dk$ where b is a constant slightly greater than unity.

Formally, the RG procedure is this:

1. Separate the field into fast and slow modes.

2. Integrate out the fast modes.

3. Rescale the momentum and slow modes to their original form.

As you repeat this procedure one must continually rescale certain coupling parameters after each step. As $b \to \infty$, these coupling parameters will either scale to zero or a finite

value. If it goes to zero, then you know that this parameter is unimportant and you could have neglected it from the start. We call such a parameter irrelevant. However, if it flows to a finite value, or infinity, then this parameter is relevant at the largest length scale and its evolution as it scales with b needs to be followed.

It is the discrete nature of vortices in our XY model which leads to the existence of the cosine term in Eq.(1.14), and does not allow us to transform the partition function to momentum space. The RG routine then proceeds by integrating over the momentum modes while expressing the partition function in real space. Doing this leads to terms such as:

$$\langle \cos(2\pi\phi_>(x)) \rangle_{0>} = e^{-2\pi^2 \langle \phi_>^2(x) \rangle_{0>}} = e^{-\frac{1}{2}G_>(0)}, \tag{1.15}$$

where $G_>(0) = \frac{2\pi}{T} \int_{\Lambda/b}^{\Lambda} dq/q = \frac{2\pi}{T} \ln(b)$ and $\langle \cdots \rangle_{0>}$ is just an averaging taken only over the fast modes of the system. This leads to a final form of the action that looks like:

$$
\begin{aligned}
S[\phi_<] \ = \ & \frac{T}{2} \int d^2x (\nabla \phi_<)^2 - 2y e^{-\frac{1}{2}G_>(0)} \int d^2x \cos(2\pi\phi_<(x)) \\
& - y^2 e^{-G_>(0)} \int d^2x d^2x' \Big\{ \cos[2\pi\phi_<(x) + 2\pi\phi_x(x')] \cdot [e^{-G_>(x-x')} - 1] \\
& + \cos[2\pi\phi_<(x) - 2\pi\phi_x(x')] \cdot [e^{G_>(x-x')} - 1] \Big\}.
\end{aligned}
\tag{1.16}
$$

The exact meaning of all the terms in this action is not critical for our understanding. All that matters is that if you let

$$\frac{\Lambda}{b} \to \Lambda, \tag{1.17}$$

$$y' = yb^2 e^{-\frac{1}{2}G_>(0)}, \tag{1.18}$$

$$\text{and} \quad T' = T + 2\pi^2 y^2 e^{-G_>(0)} \int d^2x x^2 [e^{-G_>(x)} - 1], \tag{1.19}$$

then it is possible to make Eq.(1.16) look exactly the same as Eq.(1.14), now using the new 'primed' variables. The last step is to write $b = e^{\Delta \ell} \approx 1 + \Delta \ell$. Then substituting $G_>(0)$ into (1.18) and (1.19) and taking the limit $b \to \infty$ gives the equations:

$$\frac{dy}{d\ell} = \left(2 - \frac{\pi}{T}\right)y, \tag{1.20}$$

$$\frac{dT}{d\ell} = \frac{y^2}{2T}. \tag{1.21}$$

This is our main result which describes the evolution of the parameters y and T as we continuously integrate out the fast momentum modes of our Hamiltonian. We plot the family of parametric curves which result from these equations in Fig. 1.2.
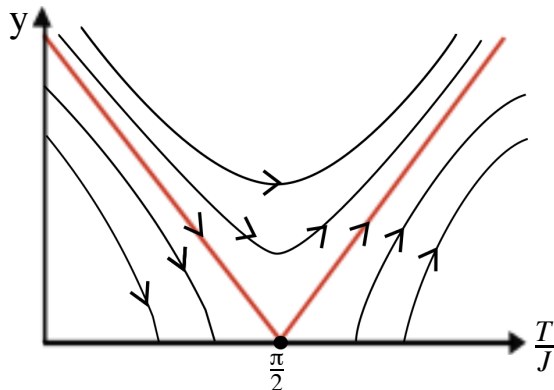
Figure 1.2: The RG flow curves for the XY model. The red lines correspond to special values of initial conditions which separate the family of curves into those which flow to ordered fixed points $T < \frac{\pi}{2}$ and those which flow to $y = \infty$, where free vortices kill any superfluid order in the system.

We will focus on three main properties of the XY model which we can identify from the RG flow curves. The first is there exists a set of curves which flow to a line of fixed points with $y^* = 0$ and $T^* < T_{KT} = \frac{\pi}{2}$. For all $T < T_{KT}$, y is an irrelevant variable since it always flows to $y = 0$. On the other hand, for all $T > T_{KT}$ y is relevant. So for T greater than some temperature, the vortex fugacity suddenly becomes a relevant quantity which is allowed to obtain a nonzero value. Recall, we defined $y = e^{-E_c/T}$, so that $y = 0$ implies that there is an infinite energy associated with the existence of vortex cores and a vanishing probability that free vortices will appear. Since y is the chemical potential for free vortices, this shows rigorously that below a transition temperature, T_{KT}, vortices can only occur in bound vortex-antivortex pairs while above T_{KT} free vortices can and do exist. We have thus shown that there is a phase transition in the XY model which is mediated by the binding and unbinding of free vortices. It can be shown [13] that in the ordered phase where there are no free vortices we can use the Gaussian approximation to calculation the correlation function to be:

$$\langle e^{i\phi(x)} e^{-i\phi(0)} \rangle \sim |x|^{-T_{KT}/2\pi}. \tag{1.22}$$

When correlations decay as a power law such as this we say the phase is quasi-long range

ordered. In the high temperature phase, free vortices kill this algebraic ordering and the correlation functions decay exponentially.

The second property comes from looking at the RG curves slightly away from the fixed point $y^* = 0$, $T^* = \frac{\pi}{2}$. If one makes a change of variables $z = y^2$, $x = 2 - \frac{\pi}{T}$, then the RG equations (1.21) become:

$$\frac{dz}{d\ell} = 2xz, \qquad \text{and} \qquad \frac{dx}{d\ell} = \left(\frac{2}{\pi}\right)^2 z, \tag{1.23}$$

$$\Rightarrow \quad z = \left(\frac{\pi}{2}\right)^2 x^2 + \sigma. \tag{1.24}$$

That is, we can solve the differential RG equations to find a family of curves which make up the RG flow diagram, Fig. 1.2, and where the constant σ depends on the initial conditions. Assume that at $b = 1$ and $x = 0$ we have $z = \sigma$, then determine the value of the rescaling parameter b at which $z(b) = 1$. We want to find the behaviour slightly above the critical point $T \gtrsim T_{KT}$ so that we associate $\sigma \sim (T - T_{KT})/T_{KT}$. We want to integrate along an RG curve away from T_{KT} to see how the parametric scaling parameter changes with temperature. Then integrating Eq.(1.23), gives:

$$\int_0^\ell d\ell' = \frac{\pi}{2} \int_\sigma^1 \frac{dz'}{z'\sqrt{z' - \sigma}} = \frac{\pi^2}{4\sqrt{\sigma}} \quad \Rightarrow \quad \ell = \frac{\pi^2}{4} \sqrt{\frac{T_{KT}}{T - T_{KT}}} \ . \tag{1.25}$$

Away from a critical point, the correlation length is given by the amount of course graining that is necessary to characterize the long-wavelength properties of the system. For this reason, we associate the term $b \sim \xi$, and note that we can write $b = e^\ell$. Putting this together we finally find that

$$\xi \sim e^{c\sqrt{\frac{T_{KT}}{T - T_{KT}}}} \ , \tag{1.26}$$

where c is some nonuniversal constant. Thus, we are able to derive the scaling of the divergence of the correlation length as one approaches the Kosterlitz-Thouless critical temperature from above. This exponential divergence is an essential singularity, where ξ diverges much faster than any power law.

The final important property we will look at is the behaviour of the superfluid density ρ_s. Usually, the exact value of the fixed point couplings y^* and T^* are nonuniversal and do not carry physical significance. However, let's look at the quantity $K = \frac{J}{T}$. In particular, we want to look at the flow of K as we iteratively perform the RG and take b from 1 to

∞. Look at $K(b,T) = J(b)/T$ as a function of RG parameter b and temperature T. Just by looking at the RG flow diagram we can see that:

$$\lim_{\Delta T \to 0} \lim_{b \to \infty} [K(b, T_{KT} - \Delta T) - K(b, T_{KT} + \Delta T)] = \frac{2}{\pi}. \tag{1.27}$$

We can write the action of the XY model in the continuum limit as:

$$S[\phi(\vec{x})] = \frac{J}{T} \int d^2x (\nabla\phi(\vec{x}))^2 = \frac{\rho_s}{T} \int d^2x (\nabla\phi(\vec{x}))^2. \tag{1.28}$$

This is a definition of the superfluid density ρ_s. It is the coefficient of the effective action in the long wavelength limit. Therefore, $K(b,T) = \rho_s/T$ in Eq.(1.27). In a mean field type analysis, ρ_s just equals J for all temperatures below the transition. The flow of the coupling K can then be understood as the renormalization of ρ_s as we take b from 1 to ∞ and the presence of vortex-antivortex pairs in the ordered phase at finite temperature lowers the value of ρ_s from $\rho = J$. Then, from (1.27) and (1.28), we find that at the transition temperature:

$$\rho_s = \frac{2}{\pi} T_{KT}. \tag{1.29}$$

This is the famous Nelson-Kosterlitz universal jump [19]. In the thermodynamic limit, at temperatures below T_{KT} the superfluid density will have a finite value. At temperatures above T_{KT} the RG analysis shows us that the superfluid density is zero since y flows to infinity. The Nelson-Kosterlitz condition tells us that at exactly T_{KT}, the superfluid density is exactly eqaul to $\frac{2}{\pi} T_{KT}$. There is a discontinuous jump in the superfluid density as you move from T_{KT}^+ to T_{KT}^-. This discontinuous jump has actually been measured in experiments on thin films of superfluid Helium-4, where the value of the superfluid density is calculated by looking at a loss of the moment-of-inertia of the sample as it undergoes a superfluid transition [3].

Fig. 1.3 is an example of the superfluid density curve as a function of temperature on a finite-size system as measured in the 2D XY model via a Monte Carlo simulation. This quantity is measured using the definition of spin-stiffness given in Eq.(1.2). As described in Section 1.3 , I will frequently refer to the helicity modulus γ as the superfluid density ρ throughout this thesis, even though strictly speaking the superfluid density only exists in quantum models, since ρ maps onto the helicity modulus γ if you associate the phase of bosons a quantum system with the parameter ϕ in the XY model. The green line is the function $f(T) = \frac{2}{\pi} T$. The intersection of this line with the ρ_s curve gives the value of

the temperature T_{KT} where $\rho_s = \frac{2}{\pi}T$. Note that the jump of ρ_s is not discontinuous as we simulated a finite size $L \times L$ system with $L = 120$. It is only in the limit that L$\to \infty$ that we can compare to the results from the RG analysis where we let our effective length scale $b \to \infty$. In this case when $L \to \infty$, then ρ_s will jump discontinuously to zero at the point where it meets with the Nelson-Kosterlitz line $f(T)$ based on the result of Eq.(1.27).
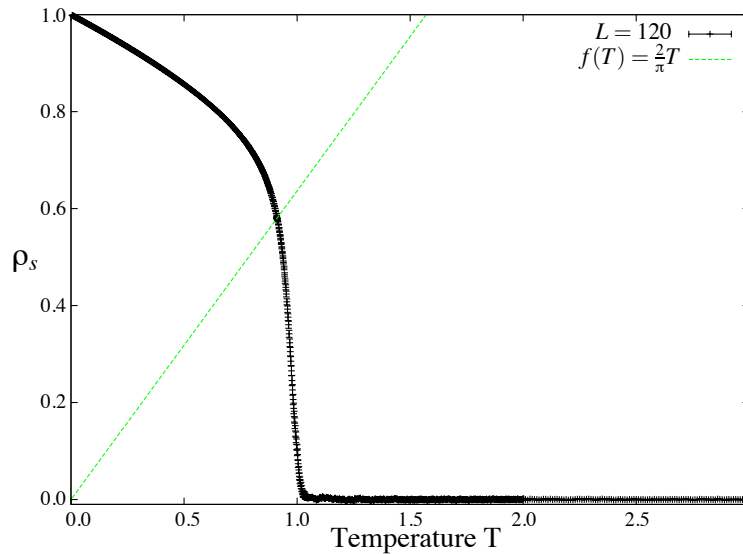
Figure 1.3: Monte Carlo measurement of the helicity modulus as a function of temperature for a 120x120 size system. The intersection with the green line shows the Nelson-Kosterlitz universal jump condition $\rho_s = \frac{2}{\pi}T_{KT}$.

1.5   The Monte Carlo Algorithm for XY Models

A Monte Carlo algorithm is a name given to a broad class of techniques which use importance sampling as a way to numerically solve problems which have practical complications making exact solutions difficult or impossible. For example, to study a general interacting classical many-body system, we can simply calculate the value of the partition function Z as a function of the relevant thermodynamic variables such as temperature and particle number. Equilibrium statistical mechanics is based on the idea that from the partition function, one can calculate all thermodynamic properties of the system. For the simplest case of the Ising model which describes a system of N variables which can only take on the value 0 or 1 and which interact only with their nearest neighbours, the partition function would be written as:

$$Z \;=\; \sum_{\text{all states}} e^{-\beta \mathcal{H}} \tag{1.30}$$

$$=\; \sum_{\sigma_1 \epsilon \{0,1\}} \sum_{\sigma_2} \cdots \sum_{\sigma_N} \exp\left[-\beta \sum_{\langle ij \rangle} \sigma_i \cdot \sigma_j \right] \tag{1.31}$$

Extending this to the XY model, where our variables, ϕ can now take on any real value between 0 and 2π gives:

$$Z = \int_0^{2\pi} d\phi_1 \int_0^{2\pi} d\phi_2 \cdots \int_0^{2\pi} d\phi_N \ \exp\left[-\beta \sum_{\langle ij \rangle} \cos(\phi_i - \phi_j) \right] \tag{1.32}$$

A method for solving this problem is known in principle, however in practice numerically performing such an integration over N variables becomes impossible as N becomes even moderately large. The solution provided by Monte Carlo algorithms is to not solve this system exactly, but to use randomness and probability theory to approximate the solution in a way that is statistically significant [20]. A naive approach to this problem using Monte Carlo integration would be to randomly choose points in an [N+1] dimensional configuration space in some bounded region V. Counting the ratio of points which fall below the function $f(\phi_1, \ldots, \phi_N) = e^{-\beta H}$ to the total number of points in the region would give an estimate of the area beneath the curve $f(\{\phi_i\})$. However, even for the Ising model on N variables, there exist 2^N possible configurations from which one can sample and it becomes more complicated when you try to account for continuous variables. One cannot hope to sample a large enough region of such a configuration space to gain an accurate estimate of the integral in any reasonable amount of time.

The solution to this problem is to use importance sampling via Markov chains [21] in order to only sample the most important regions of the configuration space. The idea is that new configurations are generated from only the previous configuration using transition probabilities which depend on the energy difference between the initial and final states. Consider an ensemble consisting of a large number of configurations which appear with a probability corresponding to the strength of their contribution to the partition function. If X_n and X_m are two different configurations which occur with probability P_n and P_m, then we want to move along our Markov chain in a way in which the transition rate from state n to m mimics these probabilities so that:

$$P_n W_{n \to m} = P_m W_{m \to n}, \tag{1.33}$$

where $W_{n \to m}$ is the rate at which we transition between the two states according to some predetermined probabilistic scheme. Instead of sampling all configurations equally, we determine which configurations occur with the highest probability using some Markov searching process combined with a proper importance sampling condition. In ignoring the vast majority of the configurations we lose the ability to directly access the partition function. However, we can use this method to estimate in a statistically relevant way any observable quantity about the system we wish.

Consider an observable property of the system, A, such as energy or magnetization.

$$\langle A \rangle = \frac{\sum_i A_i e^{-\beta E_i}}{\sum_i e^{-\beta E_i}} = \sum_i P_i A_i . \tag{1.34}$$

In a Monte Carlo simulation we use importance sampling, whereby according to Eq.(1.33), the probability the system appears in a given state i is the same as the probability P_i that such a configuration would occur in the physical system. By using this method, if we just measure our observable property A_i for every configuration our system samples, we will naturally measure the average $\langle A \rangle$ according to its definition given in Eq.(1.34).

There are really only two conditions which must be satisfied for an implementation of any Monte Carlo algorithm to follow the above properties for obtaining accurate estimates of observables [20]. The first is that the probability to transition between any two configurations must match the weights that such a configuration contributes to the partition function. This condition is known as detailed balance and has already been formulated in Eq.(1.33). The second condition is that in any given Markov chain it must be possible to transition to any configuration which appears in the partition function of the problem. This condition, known as ergodicity, ensures that you do not bias your answer by omitting important regions of configuration space.

By far the most common implementation of this method is the Metropolis Condition Monte Carlo (MCMC) algorithm [22], where transitions between different configurations are made by randomly changing a single spin in the system. Consider the following description of this algorithm implemented for the Ising model [20]:

Metropolis Condition Monte Carlo Algorithm

1. Chose an initial state

2. Randomly choose a site i

3. Calculate the energy change ΔE which results from flipping the spin at site i

4. If $\Delta E < 0$, flip the spin at site i and go to step (7)

5. Otherwise, generate a random number r such that $0 < r < 1$

6. If $r < e^{-\Delta E/T}$, flip the spin at site i

7. Randomly choose a new site i and go to step (3)

Ergodicity is satisfied since we are always flipping only one spin at a time. For a lattice with N sites, in N moves one can transition between any two possible configurations by flipping only those spins which differ between the two configurations. Detailed balance is also trivially satisfied by construction; we accept a move to a new state, with probability $e^{-\Delta E/T}$, if the change in energy ΔE is greater than 0 and we always accept the move, with probability 1, if ΔE is less than 0. Thus, our ratio of transition rates follows the ratio of the Boltzmann probabilities:

$$\frac{W_{i \to i+1}}{W_{i+1 \to i}} = \frac{e^{-\Delta E/T}}{1} = \frac{e^{-E_i/T}}{e^{-E_{i+1}/T}} = \frac{P_i}{P_{i+1}} \ . \tag{1.35}$$

Then to measure a given property we just need to keep track of that property A_i for every configuration i and average the values at the end of our simulation.

The move to studying systems with continuous symmetries, such as the XY model is very simple. Simply add a step between (2) and (3) whereby you randomly choose an angle $\Delta\phi$ between 0 and 2π. Then instead of flipping the spin at site i, rotate the angle of the spin by $\Delta\phi$.

16

One of the main difficulties in Monte Carlo simulations occurs in ensuring your algorithm consistently samples independent configurations. This problem arises when using a Markov process to generate new configurations since two configurations which are separated by a small number of Monte Carlo steps will always be very similar to each other. In order to get a true estimate of the expectation value of an observable one needs to sample configurations independently. One solution to this is to just wait long enough so that the new configuration is sufficiently independent from the old one as the simulation takes a random walk in configuration space. In the XY model, one can adjust the random update angle $\Delta\phi$ depending on the temperature of the simulation. At low temperatures one wants $\Delta\phi$ to be small so that more proposed updates are accepted, improving the speed with which correlations between separate configurations goes to zero.

This problem of correlated sampling of configurations becomes much more important as one approaches a phase transition. In this case, the correlation length of the spins within the system diverges, so in order to have sampled two independent configurations, the system must flip a far greater number of spins. The amount of time it takes for a system to move between independent configurations is called the correlation time τ. One can imagine that when the correlation length is large, large clusters of spins will point in the same direction. It becomes much more likely in this case that you will flip a spin and then flip it back to its original state than it is that you will flip enough nearby spins to effectively change the cluster shape and reach a new configuration, so τ will be quite large. Although τ is always finite for a finite system, it can be very large near a critical point. In this case, as the system size is increased, τ increases as L^z, where z is the dynamical critical exponent and L is the linear size of the system [23]. This problem is known as critical slowing down. A much more powerful method of dealing with this problem involves implementing cluster moves into the Monte Carlo algorithm. Instead of proposing changes to a single spin, the program grows a cluster of spins according to a special prescription and then flips (or rotates) the entire cluster of spins at once.

In this thesis, along with using the Metropolis algorithm, we have used a famous implementation of cluster moves which works for spins with continuous symmetry. This is known as either the Swendsen-Wang or Wolff algorithm [23, 24].

The Wolff Algorithm for Monte Carlo Simulations of Models with Continuous Symmetry

1. Randomly choose an initial site i and a random vector $\vec{r}$

2. Create a cluster C and a queue Q

3. | Add the site i to C. Let σ_i represent the spin vector with $\mathcal{O}(n)$ rotation symmetry |

4. | Refect spin i about the vector $\vec{r}$ so that $R(\vec{r})\vec{\sigma}_i = \vec{\sigma}_i - 2(\vec{\sigma}_i \cdot \vec{r})\vec{r}$ |

5. | Add all neighbours of site i which are not already in C to Q. |

6. | Choose the next site in Q as site i. If Q is empty, proceed to step (1). |

7. | For all bonds connecting i to sites $j \epsilon C$ only, calculate $\Delta E_{\langle ij \rangle} = \sigma_i \cdot [1 - R(\vec{r})]\sigma_j$ |

8. | If $\Delta E > 0$, do not flip the spin and proceed to step (6) |

9. | If $\Delta E < 0$, with probability $P = 1 - e^{-\beta \Delta E}$ add site i to C and go to step (4) |

10. | If i is not added to C, go to step (6) |

In this way, one grows a cluster C based off of an initial random seed. Spins are updated by reflecting the spin about a random axis, where in the XY model this axis could just be represented as an angle ϕ. One calculates the energy cost of reflecting the spin, but only considers the cost with respect to spins which are already in the cluster C. Growing the cluster is analogous to a percolation problem. The idea is that near a phase transition, the size of the cluster will approximately be equal to the size of a group of correlated spins. You can then flip large sections of spins at once and consequently the problem of critical slowing down is greatly improved.

It is interesting to see how ergodicity and detailed balance are satisfied within the Wolff algorithm. Ergodicity is satisfied since in each iteration of the above steps there is a finite probability that the cluster will be of size one, and reflecting about a random vector $\vec{r}$ can produce any new spin vector σ_i as long a $\vec{r}$ is a continuous vector.

Detailed balance is more interesting. If a spin i within the cluster C is completely surrounded by other spins which are also in C, then when all the spins in C are flipped, i will have no energy cost associated with it since the relative angle between i and its neighbours will not be changed. Then, the only energy change to the system occurs along

18

the boundary of the cluster ∂C. Therefore

$$\frac{W(\{\sigma_x\} \to \{\sigma_{x'}\})}{W(\{\sigma_x'\} \to \{\sigma_x\})} = \prod_{\langle xy \rangle \epsilon \partial C} \frac{e^{-\beta[R(r)\sigma_x \cdot \sigma_y]}}{e^{-\beta[R(r)\sigma_x' \cdot \sigma_y']}} = \exp\left\{ \beta \sum_{\langle xy \rangle \epsilon \partial C} \sigma_x \cdot [R(r) - 1]\sigma_y \right\}$$

$$= \exp\left\{ \beta \sum_{\langle xy \rangle} \sigma_x' \cdot \sigma_y' - \sigma_x \cdot \sigma_y \right\}. \quad (1.36)$$

The transition rates here are given by the probability that all sites y, such that bond $\langle xy \rangle$ goes across the boundary of C, are not added to the cluster. The probability of not activating bond $\langle xy \rangle$ is $1 - P = e^{-\beta R \sigma_x \cdot \sigma_y}$. The first equality also uses the fact that the same reflection operation $R(r)$ applied twice will always give the original state back, so that the forward and backward transition rates are related by the same reflection operations. The last equality uses the fact that sites that are not on the boundary ∂C cost zero energy to reflect. The algorithm proceeds in a way in which adding individual sites to the cluster does not satisfy detailed balance, but once you build the whole cluster detailed balanced is satisfied globally by rejecting spins along the boundary of the cluster with the proper probability [24].

In this thesis I perform MCMC simulations on various 2D XY models with ring-exchange terms. I have found that for the 2D XY model, implementing the Wolff algorithm gives a large increase in computational efficiency near the critical temperature. Far away from the critical temperature there is no speedup over the Metropolis algorithm. Using the Wolff algorithm has allowed me to measure the superfluid density near T_c for $L \times L$ lattices as large as 2000×2000. Studying such massive systems would likely not be feasible using only the Metropolis algorithm. When the Hamiltonian contains ring-exchange terms it is no longer possible to use the Wolff algorithm. In this case I used the Metropolis condition algorithm. When studying the pure ring-exchange model it was found that decreasing the maximum update angle $\Delta\phi$, as described above, results in a loss of ergodicity as the system can become stuck in a metastable state at low temperatures. Keeping $\Delta\phi \epsilon [0, 2\pi]$ allows us to properly sample the configuration space and obtain the correct behaviour of the ring-exchange model.

Chapter 2

Numerical Simulations of the Classical J-K Model

In this section, we will look at the results of Monte Carlo simulations of the J-K model. We start with the pure J model (also called the XY model) and show how we can extract the temperature of the Kosterlitz-Thouless transition in the thermodynamic limit by measuring the spin-stiffness and using the Nelson-Kosterlitz universal jump condition. We will also study the dependence of the spin-stiffness on the aspect ratio of the lattice. Then we will look at the pure-K ring-exchange model. A physical motivation for studying this model on a triangular lattice will be given. We will show, through numerical simulations, that there exists an ordered finite-temperature phase in this model. Finally, we will look at the general model with both J and K interactions, and map out the phase diagram for this model as the relative strength of J and K are varied.

2.1   Identifying T_{KT} in XY Model Simulations

The Kosterlitz-Thouless transition in the XY model can be identified by measuring the helicity modulus and looking at the finite size signatures of the discontinuous Nelson-Kosterlitz jump, given by Eq.(1.29). We define the finite size KT phase transition as the point where $\rho_s = \frac{2}{\pi} T_{KT}(L)$, which is clearly exact as $L \to \infty$. We expect that for large system sizes the scaling form of the transition temperature with system size is given by :

$$T_{KT}(L) = T_{KT}(\infty) \left[1 + \frac{c^2}{[\log(L/L_0)]^2} \right], \tag{2.1}$$

where L_0 is some microscopic length scale and c is the same constant which appears in the correlation length ξ [25]. We already saw an example of the ρ curve in Fig. 1.3 for a 120×120 size system. In the thermodynamic limit, $\rho(T)$ will have the same qualitative shape as the curve in Fig. 2.1, curving to intersect the line $f(T) = \frac{2}{\pi}T$, and then jumping discontinuously to $\rho = 0$ for any $T > T_{KT}$. The value quoted in the literature for T_{KT} at $L = \infty$ is $T_{KT} = 0.89294(8)$, which was found in [26] through universality arguments by comparing the RG flows of two different models, and verified by measuring the helicity modulus in reference [27].
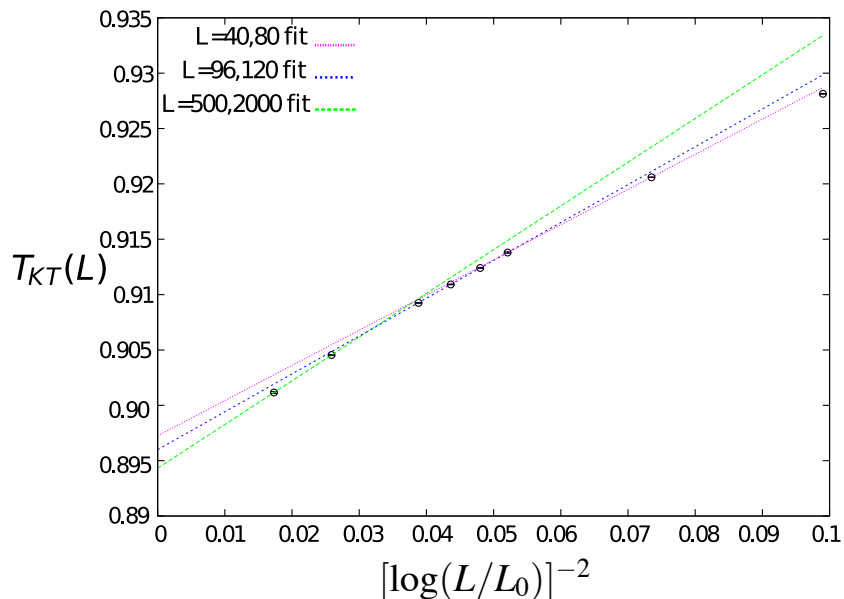
Figure 2.1: The scaling of the finite transition temperature for the XY model for system sizes from L=24 to L=2000. The three lines show the tangent of the curve at different points in L along the curve with pink being the smallest L and green the largest.

We have plotted, in Fig. 2.1, the intersection of ρ_s and $f(T)$ for various finite size $L \times L$ systems up to $L = 2000$. We plot the finite temperature transition against $[\log(L/L_0)]^{-2}$ to fit our data to the expected scaling form in Eq.(2.1). The x-intercept of our plot will then be the transition temperature at $L = \infty$. The plot appears to be approximately linear, however if we allow our error bars to become small enough we can see that there is definite curvature which is noticeable. This curvature is more noticeable when fitting to smaller system sizes, supporting the claim [25] that the scaling form follows Eq. 2.1

plus subleading corrections. The three lines in Fig. 2.1 show the extracted $T_{KT}(\infty)$, when we fit a straight line using only two neighbouring data points at different sections of the curve. These lines estimate the tangent of the curve for different linear system sizes, L. As we move to larger system sizes, the data becomes more linear and the extracted transition temperature systematically approaches the true T_{KT} from above.

In Fig. 2.2 we plot the intercepts (a) and slopes (b) of 'tangent curves', again as a function of $[\log(L/L_0)]^{-2}$. The x-intercept of these curves will tell us what the x-intercept and slope of our original scaling data is trending to as $L \to \infty$. We calculate $T_{KT}(\infty) = 0.8928(2)$, which is in very good agreement with the value quoted in the literature. We also calculate the slope of our curve to be trending to $m = 0.42(1)$. From this we can extract the value of c in Eq.(2.1) to be $c \approx 0.69$.

a)   b)
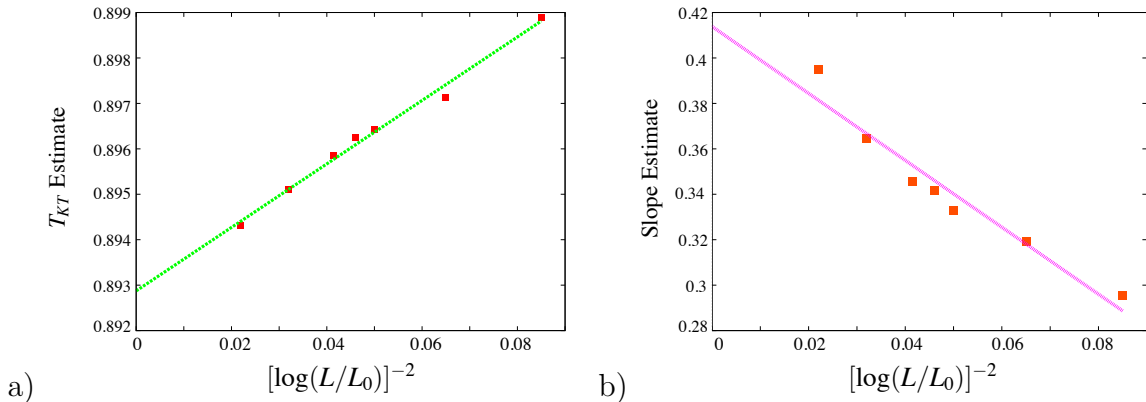
Figure 2.2: The scaling of the x-intercept and slope of the tangent curves for the finite-size T_{KT} scaling data. We can use this to extract the x-intercept and slope of a linear curve which would fit our finite-size data exactly as $L \to \infty$.

2.2 Aspect Ratio Dependence of the Superfluid Density

We will now look at the dependence of the helicity modulus on the aspect ratio of our lattice. The aspect ratio, R, is defined as $R = \frac{L_x}{L_y}$. The helicity modulus defined in Eq.(1.2) measures the spin stiffness along a particular lattice direction. For different aspect ratios

$R \neq 1$, even in the limit $L_x, L_y \to \infty$, $\rho_x(T)$ and $\rho_y(T)$ will in general not be equal to each other or to the spin-stiffness at $R = 1$.

There is a subtle point regarding two closely related but not equivalent ways of defining the superfluid density which was first discussed by Prokof'ev and Svistunov in [28]. The first way, which we have taken as our definition up to now, describes the response of the free energy to some uniform rotation of the spins in our system:

$$\delta F = \frac{\rho_x}{2} v_s^2, \tag{2.2}$$

where the subscript x refers to the direction we apply the uniform rotation. This definition is very useful since it naturally leads to a measurement which can be made within a Monte Carlo simulation. One may also define the superfluid density as a coefficient in an effective long-wavelength action which governs phase fluctuations.

$$F_{eff} = \frac{\rho_s}{2} \int dV (\nabla \Phi)^2. \tag{2.3}$$

This is the form of the superfluid density which was we used in the renormalization group calculation to give us the universal jump condition at the Kosterlitz-Thouless phase transition $\rho_s = \frac{2}{\pi} T_{KT}$. It turns out that practically, for aspect ratios $R = 1$, these two quantities are extremely close to each other and so in general these definitions have been used interchangeably in the literature. However, as shown in [25], there is in fact a strong dependence on the aspect ratio of the lattice when measuring ρ based on our first spin-stiffness definition. As discussed in [28], a calculation of the effect of topological excitations based on vortex-antivortex pairs which appear on a torus of aspect ratio $R = Lx/Ly$ leads to a renormalization of the free energy quantity δF and can be used to find a formula relating our two definitions of the superfluid density:

$$\rho_x^W = \rho_s(T_{KT}) \left(1 - \frac{4\pi^2 \rho_s(T)}{T} \frac{L_y}{L_x} \langle \ell^2 \rangle_x \right) \quad , \tag{2.4}$$

$$\text{where} \qquad \langle \ell^2 \rangle_x = \frac{\sum_\ell \ell^2 e^{-\left(\frac{2\pi^2 \rho_s L_y}{L_x T} \right) \ell^2}}{\sum_\ell e^{-\left(\frac{2\pi^2 \rho_s L_y}{L_x T} \right) \ell^2}} \ . \tag{2.5}$$

When measuring the spin stiffness along, say, the x-direction, the measurement will go to zero even in the ordered phase if the size of your lattice in the x-direction L_x is far greater than L_y. It is only when L_y is far greater than L_x and when both these values approach infinity that measurements of the spin stiffness we gave in Eq.(1.2) approaches

23

the true long-wavelength value of the superfluid density. For a square lattice geometry where $R = 1$, it can be shown from Eq.(2.4) that $\rho_x^W \approx 0.9998247 \rho_s$.

This aspect ratio dependence of the superfluid density actually gives us an opportunity to study another type of system. There is a very close connection between the XY model in two dimensions and the one dimensional Luttinger liquid model. This connection follows from a well known path integral formulation of quantum mechanics [29], which we will look at in more detail in the next chapter, which states that quantum systems in d-dimensions can always be mapped to classical systems in $(d+1)$ dimensions. Within this mapping, we associate the inverse temperature β with the extra dimension in the classical system. By studying the aspect ratio dependence of the classical system we can study our quantum system at finite system sizes and finite temperatures.

Luttinger liquid theory is the 1D analog of Fermi liquid theory [29]. In two or more dimensions, all properties of free fermions are derived from the Pauli exclusion principle. Fermi liquid theory states that when interactions are turned on their only effect is to renormalize the effective mass of the electrons [30, 31] . According to Fermi liquid theory, the exact form of the interaction between electrons is unimportant because the low energy effective theory of the model can always be described in terms of a non-interacting model where the relevant excitations are not the bare electron but an electron with a mass which is renormalized by the collective excitations of the whole system. In one dimension the situation is very similar, but Fermi liquid theory is replaced by Luttinger liquid theory [32]. Interactions play a special role in one dimensional fermionic systems due to the Pauli exclusion principle and the fact that particles cannot move around each other. In one dimension, any low energy excitation must be due to collective motion of the entire system. In higher dimensions interactions between fermions plays a negligible role while in one dimension the situation is reversed and interactions play a dominant role regardless of the precise form of the interaction.

The low energy / long wavelength theory of any general interacting system in one dimension can be found by using the Luttinger liquid Hamiltonian [33]. The collective motion of the system leads to excitations which are bosonic in nature. Bosonization [34] is a general phenomenon which is unique to one dimension. This occurs due to the linear dispersion of the high energy theory and leads to density-density correlations functions which decay algebraically with distance. Interestingly, in one dimension the distinction between fermions and hard-core bosons is not well defined since both types of particles cannot 'move around' each other and so the exact form of their exchange statistics plays a diminished role. For this reason it is also possible to describe hard-core bosonic system by an effective low-energy Luttinger liquid Hamiltonian. This mapping underlies the superfluid-insulator transition in the 1D Bose-Hubbard model which we will look at later in this thesis.

The low energy effective theory of any 1D fermionic system is described by the Luttinger liquid Hamiltonian [29]:

$$H_{LL} = \frac{1}{2\pi} \int_0^L \left[uK(\partial_x \phi)^2 + \frac{u}{K}(\partial_x \theta)^2 \right], \tag{2.6}$$

which leads to the action

$$S = \frac{1}{2\pi K} \int dx d\tau \left[\frac{1}{u}(\partial_\tau \phi)^2 + u(\partial_x \phi(x))^2 \right]. \tag{2.7}$$

What is important is that this form of the action is exactly the same as the continuum limit of the 2D XY model, Eq.(1.28), assuming we associate the temporal direction τ with the y-direction of our classical system. The superfluid density of a Luttinger liquid is zero in the thermodynamic limit and at T=0. However, at finite temperature and finite system size, some superfluidity actually survives. In [35] the superfluid fraction of a Luttinger liquid is calculated exactly within Luttinger liquid theory by calculating the probability that topological excitations, in the form of a winding of the phase field ϕ, appear as a function of system size and temperature:

$$\frac{\rho_s}{\rho} = 1 - \frac{\pi u K}{LT} \left| \frac{\theta_3''(0, e^{-2\pi v_J/LT})}{\theta_3(0, e^{-2\pi u K/LT})} \right|, \tag{2.8}$$

where I used the definition of the θ_3 function $\theta_3(z, q) = \sum_{n=-\infty}^{\infty} q^{n^2} e^{2\pi i n z}$.

Thus, $\theta_3''(z, q) = \partial_z^2 \theta_3(z, q) = \sum_{n=-\infty}^{\infty} -4\pi^2 n^2 q^{n^2} e^{2\pi i n z}$.

One can simply map our variables for temperature and coupling strength in the quantum model to the variables in the XY model Hamiltonian, (1.3) by letting $T \to u/L_y$ and $K \to J$. Then substituting these change of variables into 2.8 gives:

$$\frac{\rho_s}{\rho} = 1 - \frac{\pi u K}{TL_x} \frac{\sum_n e^{-\left(\frac{2\pi^2 u K}{L_x T}\right) n^2}}{\sum_n e^{-\left(\frac{2\pi u K}{L_x T}\right) n^2}} = 1 - \frac{\pi J L_y}{Lx} \frac{\sum_n e^{-\left(\frac{2\pi^2 J L_y}{L_x}\right) n^2}}{\sum_n e^{-\left(\frac{2\pi J L_y}{L_x}\right) n^2}}. \tag{2.9}$$

This is exactly the same form of the aspect ratio scaling in the XY model, Eq.(2.4), assuming we associate the superfluid density in the LL model with the spin-stiffness is the classical system and the boson density in the LL model with the long-wavelength superfluid density of the XY model.

Using these two equations for the scaling of the superfluid density we can show that the Luttinger liquid Hamiltonian maps directly onto the 2D XY model at $T = T_{KT}$. In
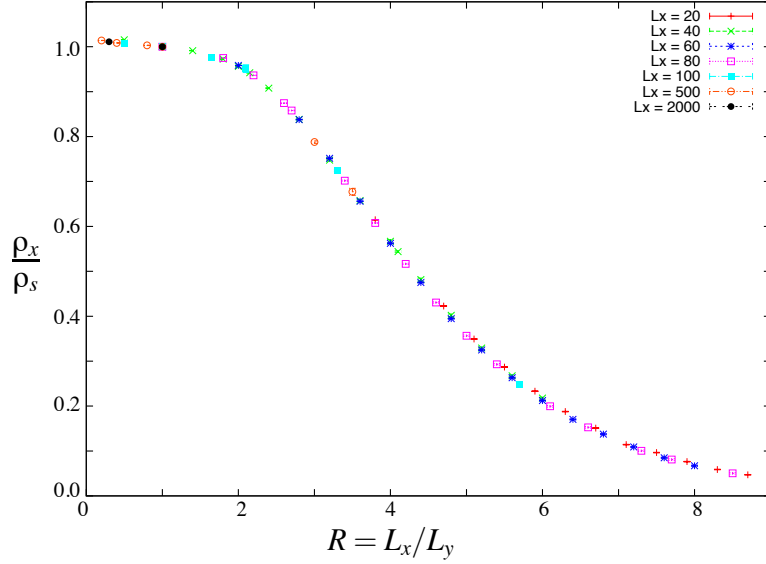
Figure 2.3: The data collapse of ρ_x over the long-wavelength superfluid density ρ_s as a function of aspect ratio R, measured at exactly $T = T_{KT} = 0.893$. We measure ρ_x by measuring the helicity modulus in Monte Carlo simulation for system sizes up to $L = 2000$, and estimate ρ_s by the helicity modulus measurement when $R = 1$.

Fig. 2.3, we verify the scaling form given in equations (2.4) and (2.8). In order for the scaling of the helicity modulus in the 2D XY model to collapse onto the proper function depending only on aspect ratio, we invoked the condition that $\frac{\rho_s}{T} = \frac{2}{\pi}$. We can use this data collapse as a formal way of finding the KT transition temperature. In Fig. 2.4 we plot the aspect ratio dependence for two system with different L_x values at a slightly higher temperature $T = 0.92 \gtrsim T_{KT}$. We see that in this case the points do not collapse onto a universal function.

We have verified, via Monte Carlo simulations, the aspect ratio dependence of the spin-stiffness based superfluid density. This data collapses onto a universal function when measured at $T = T_{KT}$ and thus can be used as a formal way of finding the KT transition temperature. The curves look very similar to the expected scaling form as found using Luttinger liquid theory. By making a connection to Luttinger liquid theory we can verify that there is a direct mapping between a 1D Luttinger liquid and the 2D XY model at exactly T_{KT}. It may be possible to use this mapping to calculate properties of the Luttinger liquid model such as the Luttinger parameters u and K used in Eqs. (2.6) and (2.7).

26
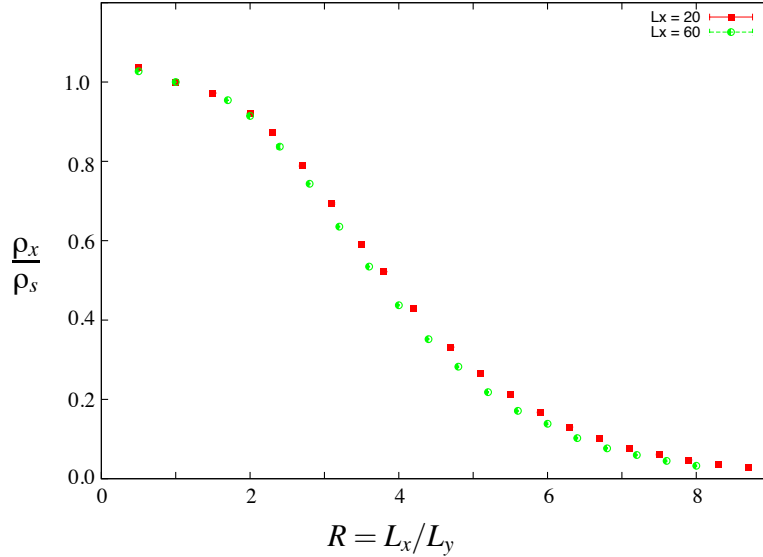
Figure 2.4: The attempted data collapse of ρ_x over ρ_s as a function of aspect ratio R at a temperature slightly higher than T_{KT}. We measure this for two system sizes at $T = 0.92 > T_{KT}$.

2.3   The Pure K Model

Next, it will be interesting to look at what happens when we set $J = 0$ in Eq.(1.1). In this section we will develop a mapping which relates two dimensional Abrikosov vortex solids [36] to the pure-K model on a triangular lattice. Recently, direct scanning tunnelling microscope imaging of the melting of a triangular vortex solid has shown that such a system undergoes a continuous phase transition [37]. It is due to the relationship between our model and this physical vortex solid that we will study the pure-K model on a triangular lattice. We will see that there exists a continuous finite temperature phase transition in our model which is described by the same theory which describes the melting of two dimensional solids. On a triangular lattice the ring-exchange interaction sums over three distinct nearest neighbour plaquette types (Fig. 2.5). For a positive 'ferromagnetic' K term, just looking at the form of the Hamiltonian Eq.(1.1), one can see that it is energetically favourable for the system to arrange its spins in a way which minimizes the term $(\theta_i - \theta_j) + (\theta_k - \theta_\ell)$.

We saw in the case of the XY model that although spontaneous symmetry breaking is forbidden by the Mermin-Wagner theorem, there is still a phase transition between a

27
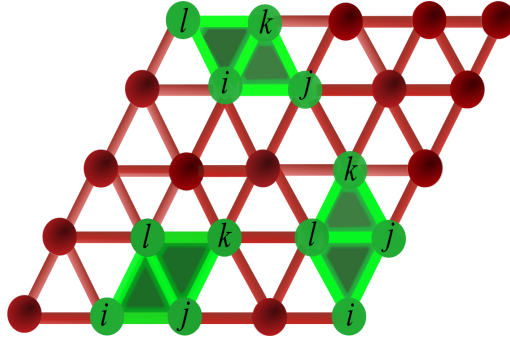
Figure 2.5: The three smallest plaquettes $\langle ijkl \rangle$ on the triangular lattice.

disordered phase and a phase with quasi-long range order. In the pure-K model, we expect thermal fluctuations to be even stronger since there is more freedom in the interaction term for neighbouring spins to vary. Indeed, one can easily see that the configuration with spins completely aligned (XY model groundstate) is just one of many degenerate groundstates that saturate the minimum possible energy which can be obtained. Any uniform rotation, ϕ, of these completely aligned spins in one of the lattice directions will cost zero energy (i.e. this would amount to the rotation $[(\theta_i - \theta_j) - (\theta_\ell - \theta_k)] \to [(\theta_i - \theta_j + \phi) - (\theta_\ell - \theta_k + \phi)]$, which would not change the total sum of any plaquette energy term). Since our previous definition of spin-stiffness, γ given in Eq.(1.2), measured the energy cost of applying a uniform twist to the system, then γ is clearly zero at all temperatures. However, by developing a measurement analogous to the helicity modulus we can show explicitly through Monte Carlo simulations of this system that there is indeed a phase transition at finite temperature which is closely analogous to the Kosterlitz-Thouless phase transition in the XY model [38] that we discussed in the previous section.

We will first show that this model gives a description of Abrikosov vortex lattices in 2D superconductors. In two dimensional crystals, there is no long-range crystal line order as this would break the continuous translational symmetry of the system and thus violate the Mermin-Wagner theorem. Crystalline solids at low temperatures are characterized by a power-law decay of the crystalline correlation functions. These correlations allow the system to possess a nonzero shear modulus and thus be characterized as true solids. The theory describing the melting of such two dimensional solids was first described by Halperin, Nelson and Young using ideas very closely related to the theory of Kosterlitz and Thouless describing 2D superfluids [4]. This theory (called KTHNY theory from now on), replaces the idea of vortices in superfluids with dislocations in a solid. A dislocation is a

topological defect which appears as an irregularity in the crystal order of the system. In the low temperature phase, dislocations are always bound into pairs which correspond to an extra row of atoms inserted along the line connecting the two dislocation cores. Above a certain temperature these dislocations unbind and any shear force applied to the system can be accommodated by the motion of the free dislocation. In this case the shear modulus of the system drops to zero and the solid has melted.

A type II superconductor placed in a perpendicular magnetic field will form what is known as an Abrikosov vortex lattice where the superconducting pieces of the system surround the non-superconducting vortex cores, which arrange themselves in a triangular lattice [36]. We start from the standard Ginzburg-Landau expression for the free energy functional of a superconductor:

$$\mathcal{H} = \int d^2\vec{r} \left[\frac{1}{2m^*} \left| \left(-i\hbar\nabla + \frac{e^*}{c}\mathbf{A} \right) \Psi(\vec{r}) \right|^2 + a|\Psi(\vec{r})|^2 + \frac{b}{2}|\Psi(\vec{r})|^4 \right], \qquad (2.10)$$

where the superconductor is placed in a perpendicular magnetic field $\mathbf{B} = \nabla \times \mathbf{A}$. When the magnetic field is near the superconductor's upper critical value, we can expand the field $\Psi(r)$ in terms of Landau-level eigenstates and note that only the lowest Landau-level (LLL) eigenstates will contribute to the action [39],

$$\Psi(r) = \sum_m c_m \phi_m(r). \qquad (2.11)$$

A little bit of algebra, defining a set of Wannier states centred on the sites of the triangular lattice, writing a set of Block states in terms of these Wannier functionals, invoking a centre-of-mass conservation of the system and taking $c_m = e^{i\theta_m}$ allows us to write down the following LLL representation of the Ginzburg Landau functional [1] :

$$\mathcal{H} = -K \sum_{\langle ijkl \rangle} \cos(\theta_i - \theta_j + \theta_k - \theta_l). \qquad (2.12)$$

Thus we have derived the pure-K model from the very general expression of a type II superconductor in a nearly critical perpendicular magnetic field. Besides providing a motivation for studying the pure-K model, the connection between our model and Abrikosov

---

[1]For a detailed explanation of this derivation see Ref [39]. The main point is that by writing the GL functional in terms of Wannier functions in the LLL basis we can use the translational symmetry of the Abrikosov vortex lattice states to derive a model with an underlying triangular lattice structure. Then, transforming to momentum space, one finds that the low lying excitations of the system obey a conservation relation $\int d^2r|\Psi(r)| \sim \delta_{m_1+m_2,m_3+m_4}$ which leads to a ring-exchange interaction in our derived model.

vortex lattices gives us a clue that our system exhibits a phase transition which is of the form described the KTHNY theory.

As stated earlier, the minimum energy states of Eq.(2.12) corresponds to all possible states with a uniform gradient of the phase θ_m along the basis directions of the triangular lattice. In the long-wavelength elastic theory of the vortex lattice, gradients of the phases $\nabla\theta$ corresponds to the displacement of the centre-of-mass position of the vortex cores $\mathbf{u} = \ell^2 \hat{z} \times \nabla\theta$. Therefore, some nonuniform twist of the phases in the pure-K model would cost energy and would correspond to some distortion of the vortex lattice (i.e. it would correspond to a shear force).

We want to derive a measurement analogous to the helicity modulus used in the XY model which will tell us whether our system is in an ordered or disordered phase. In close analogy with the XY case, we will look at the response of the system when we apply a twisting to the groundstate of our system. In this case, we will apply a non-uniform twist in one of the lattice directions. $\theta_i - 2\theta_{i+1} + \theta_{i+2} \to \theta_i - 2\theta_{i+1} + \theta_{i+2} + \phi$. We define:

$$\kappa = \frac{\partial^2 F}{\partial(\nabla^2\theta)} = \frac{T}{Z}\frac{\partial^2 Z}{\partial\varphi^2} = \frac{1}{N}\left[\left\langle\frac{\partial^2\mathcal{H}}{\partial\varphi^2}\right\rangle - \frac{1}{T}\left\langle\left(\frac{\partial\mathcal{H}}{\partial\varphi}\right)^2\right\rangle\right]_{\varphi\to 0}. \tag{2.13}$$

Here I have used the notation $\varphi = \nabla^2\theta$, and have written the free energy in terms of the partition function:

$$Z = \text{Tr}(H) = \int D\theta \, \exp\left[-\frac{K}{T}\sum_{\langle ijkl\rangle}\cos(\theta_i - \theta_j + \theta_k - \theta_\ell)\right]. \tag{2.14}$$

Now all one needs to note is that for one of the three plaquette types, we can write

$$\theta_i - \theta_j + \theta_k - \theta_\ell \;=\; \theta_{\hat{x}} - 2\theta_{\hat{x}+\hat{\lambda}_x} + \theta_{\hat{x}+2\hat{\lambda}_x}. \tag{2.15}$$

That is, it takes the form of a discrete second derivative in one of the lattice directions. In the continuum limit, $\cos(\theta_i - \theta_j + \theta_k - \theta_\ell) \to \cos(\nabla_x^2\theta) = \cos(\varphi_x)$. Substitute this into Eq.'s (2.13) and (2.14) to find an expression for the shear modulus of the pure-K model:

$$\kappa = \frac{1}{N}\left\langle K\sum_{\langle ijk\ell\rangle_2}\cos(\theta_i - \theta_j + \theta_k - \theta_\ell)\right\rangle - \frac{1}{TN}\left\langle\left[K\sum_{\langle ijk\ell\rangle_2}\sin(\theta_i - \theta_j + \theta_k - \theta_\ell)\right]^2\right\rangle. \tag{2.16}$$
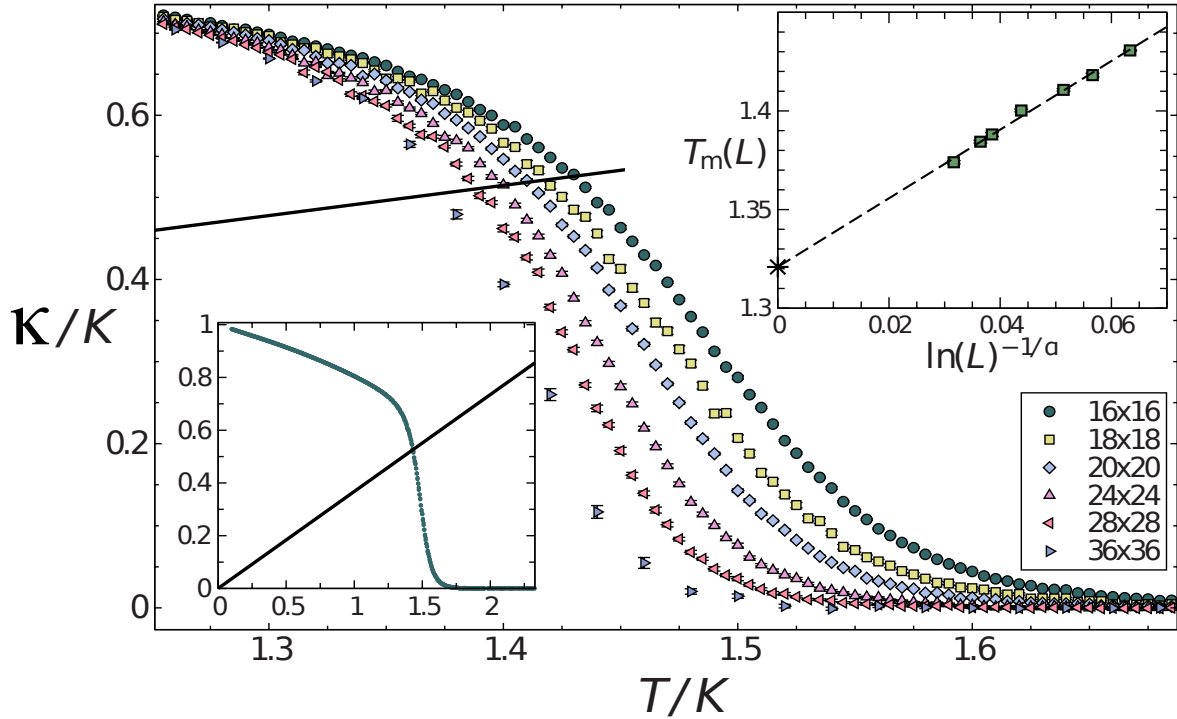
Figure 2.6: The finite-size scaling behaviour of the shear modulus of the pure-K model through the finite-temperature phase transition at critical temperature T_m. The black line is the equation $\kappa = (2/\sqrt{3}\pi)K/T$ which from Eq.(2.21) gives the finite-size estimate for $T_m(L)$. The bottom left inset shows the data for linear lattice size $L = 16$ over a larger temperature range. The upper right inset is the finite size scaling of $T_m(L)$, which gives an estimate of $T_m(\infty)$ of $T_m = 1.32K$.

We now have a measurement which we can directly implement in our Monte Carlo simulation. Fig. 2.6 shows the results of this measurement. We find that at low temperatures there exists an ordered phase with a non-zero shear modulus, and that this phase is destroyed at higher temperatures.

Due to our mapping to the KTHNY theory, it is natural to suspect that this is a continuous infinite-order phase transition. To prove that this is true we now use our previous work relating our pure-K model to that of a two dimensional vortex solid in order to derive expressions which are in close analogy to the Nelson-Kosterlitz universal jump and the divergence of the correlation length which we looked at in the XY model.

In the long-wavelength vortex lattice model, the expression for the elastic energy is $E = \mu \int d^2 r u_{ij} u_{ij} = \mu \ell^4 / 2 \int d^2 r (\nabla^2 \theta)^2$, where μ is the shear modulus of the lattice. We also choose the lattice constant $a^2 = 4\iota \ell^2 / \sqrt{3}$ in such a way that the unit cell of the lattice contains exactly one magnetic-flux quantum. We can use this to give us a relationship between the variables in our pure-K model and the KTHNY theory. Compare the elastic energy E for the Abrikosov solid with the Hamiltonian for the pure-K model in the continuum long-wavelength limit:

$$\mathcal{H} = \frac{9K}{32} \frac{a^4}{2\pi\ell^2} \int d^2 r (\nabla^2 \theta)^2 = \frac{3\pi K \ell^2}{4} \int d^2 (\nabla^2 \theta)^2, \qquad (2.17)$$

where the coefficients come from the magnetic flux condition we put on our lattice constant, $a^2 = 4\iota \ell^2 / \sqrt{3}$. Like in the XY model, the coefficient of the action in this long-wavelength limit defines the physical meaning of $K = 2\mu\ell^2 / 3\pi$ as the shear modulus of the system.

Melting of the vortex lattice is mediated by the presence of free dislocations. A single dislocation satisfies the relation:

$$\oint \nabla u_x \cdot d\ell = a, \qquad (2.18)$$

which in the pure-K model corresponds to the condition:

$$\oint \nabla^2 \theta \cdot d\ell = 2\pi n. \qquad (2.19)$$

Thus, the role of vortices in the XY model in replaced with this definition of dislocations in the K model. Integrating the elastic energy of the vortex lattice subject to the constraint (2.18) gives the energy of a dislocations as $E_d = (\mu a^2 / 2\pi) \ln(L/a)$. Comparing this to the entropy of a single dislocation gives the form of the free energy contribution of a dislocation as:

$$F = [\mu a^2 / 2\pi - 2T] \ln(L/a). \qquad (2.20)$$

32

Apparently, there is a dislocation-unbinding transition at $T = \mu a^2/4\pi$. Substituting in our expressions $a^2 = 4\pi\ell^2/\sqrt{3}$ and $\mu = 3K\pi/2\ell^2$, and recalling that our long-wavelength definition of the shear-modulus is given by $\kappa \sim K$ gives the analogy of the Nelson-Kosterlitz universal jump in the KTHNY theory as:

$$\kappa = \frac{2}{\sqrt{3}\pi} T_m. \tag{2.21}$$

The scaling of the crossing $\kappa(T)$ with the line $\kappa = (2/\sqrt{3}\pi)T$ should follow the equation

$$T_m(L) - T_m(\infty) \propto T_m(\infty)\ln(L)^{-1/\alpha} \qquad \text{with } \alpha = 0.36963. \tag{2.22}$$

The value of α in this scaling equation follows from the expression for the divergence of the correlation length in KTHNY theory $\xi \sim \exp[C/(T - T_m)^\alpha]$ (Note in the XY model under KT Theory $\alpha = \frac{1}{2}$). The upper right inset in Fig. 2.6 shows that the temperature crossings do indeed follow this scaling form. Therefore, our simulation is in exact agreement with KTHNY theory. From this scaling we can extract the transition temperature in the thermodynamic limit at $T_m/K \approx 1.32$.

We have now seen in detail the behaviour of the XY model and the pure-K model. These models are both interesting as models which obey a very special class of phase transitions (the KT and KTHNY transitions respectively) with universal properties and which relate to physical systems such as thin films of superfluid He^4 and two dimensional Abrikosov vortex lattices. Using KTHNY theory and the mapping from a vortex lattice model we were able to show that the pure-K model contains a stable low-temperature phase and that the system undergoes an infinite order phase transition. By doing this we have also proven then that the pure-K model does indeed provide an effective low-energy description of the thermal melting of the two dimensional solid.

2.4 Behaviour of the General J-K Phase Space

We will now show the results of simulations of the general J-K model at different points in phase space. In anticipation of future applications, we will omit the temperature term in our Hamiltonian. That is, we absorb one of our free parameters into the coupling constants J and K. In the previous sections we have also done this implicitly by setting the terms J and K equal to constants and varying T. Now we simply do the opposite, set T to a constant and vary either J or K. Recall the Hamiltonian for the J-K model given in Eq.(1.1) just includes a nearest-neighbour term as in the XY model and a 4-site ring-exchange term as in the pure-K model (Fig. 1.1).

$$\mathcal{H} = -J \sum_{\langle ij \rangle} \cos(\theta_i - \theta_j) \ - \ K \sum_{\langle ijkl \rangle} \cos(\theta_i - \theta_j + \theta_k - \theta_l). \qquad (2.23)$$

We will study the model on a square lattice so that the nearest-neighbour plaquette $\langle ijkl \rangle$ is just the elementary square plaquette of the lattice.

We know that when K=0, as we decrease our variable J there is a transition from a superfluid phase to a disordered phase. We will see what happens when we turn on the K-term while the system is in the superfluid phase. We will be interested in these results for both positive and negative K.
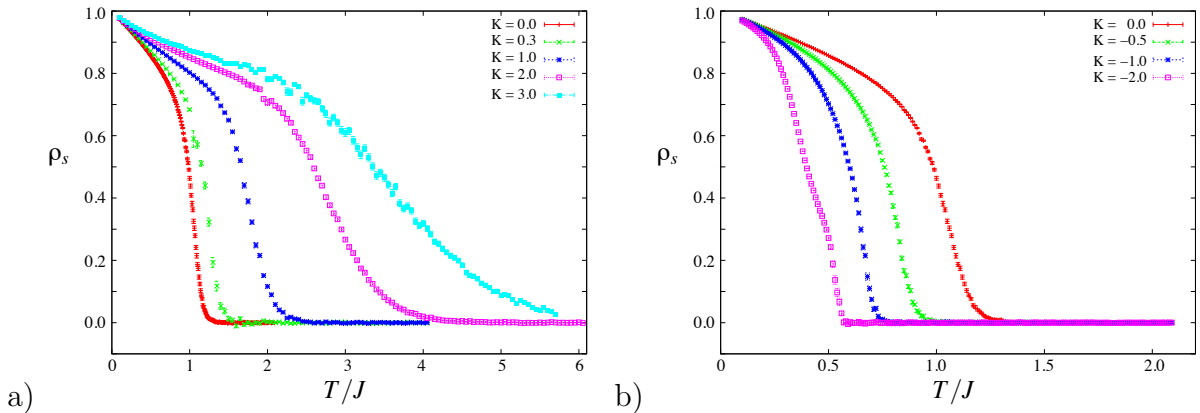

Figure 2.7: The superfluid density as a function of $1/J$ for different values of both positive (a) and negative (b) values of K. The term $1/J$ plays the role of temperature since as the J coupling goes to 0 ($1/J \to \infty$), the XY coupling becomes weaker and superfluid density is destroyed. The red curve in both figures corresponds to the pure XY case when $K = 0$.

In the pure-K model the minimum energy states are degenerate in the sense that every configuration with a uniform twisting of the spins in any of the lattice directions will have the same energy. In the XY model, only the configuration with all spins aligned in one direction will produce the minimum energy. It is interesting to note that in the quantum J-K model, the presence of a ring-exchange term kills the superfluidity[40, 41]. However, as we can see from Fig. 2.7, in our classical J-K model adding the K-term pushes back the superfluid transition and increases the superfluid density. Recall that we absorbed T into the parameter J, so then the term T/J acts like temperature in our model. For $K = 0$, as we increase T/J we see a KT transition at $J/T \sim 1$ as we expect. Then when we add a positive K interaction the spin stiffness increases and the point in T/J where the stiffness drops to zero also increases. Clearly what is happening is that the presence of the J-term breaks the degeneracy present in the pure-K model. In the low temperature phase there are two terms which want neighbouring spins to be aligned, and this increases the value of the spin-stiffness measurement and allows a non-zero spin-stiffness to persist to higher temperatures.

The situation is different, however, when a negative K-interaction is included. In this case, the minimum energy for the K-term is obtained when the sum of the spins around a plaquette $\theta_i - \theta_j + \theta_k - \theta_\ell$ equals π. This term now competes with the J interaction term. The simulations in Fig. 2.7 show that when a small negative K interaction is present, the helicity modulus goes to zero very quickly.

For a positive K term there are only two phases present, a superfluid phase and a paramagnetic phase. The degeneracy of the low temperature phase of the pure-K model is lifted by the J-term and the groundstate is always a superfluid. When a negative-K term is present, the superfluid phase is destroyed by the presence of a ring-exchange interaction. We expect, then, that for a large negative K there will be a stable phase which is similar to the stable phase in the pure-K model (except the sum of the spins on a plaquette equals π instead of 0), just as there exists a paramagnet to large-K phase transition for either sign of K when $J = 0$. If we look at the specific heat as a function of K, as in Fig. 2.8, we observe a peak which corresponds to this transition for large negative K. The last feature that we notice is that there is an energy crossing as K is made more negative and that this energy crossing occurs at some point within the paramagnetic phase of the model.

We can now determine the general features of the phase diagram for the entire phase space of the J-K model. We plot this diagram in Fig. 2.9. For J and K both positive there is only one transition which can occur, the superfluid to paramagnet (SF-PM) transition. This occurs because the superfluid groundstate is one of the degenerate groundstates of the pure-K model, so at finite J, this degeneracy is broken and the ordered phase is always the
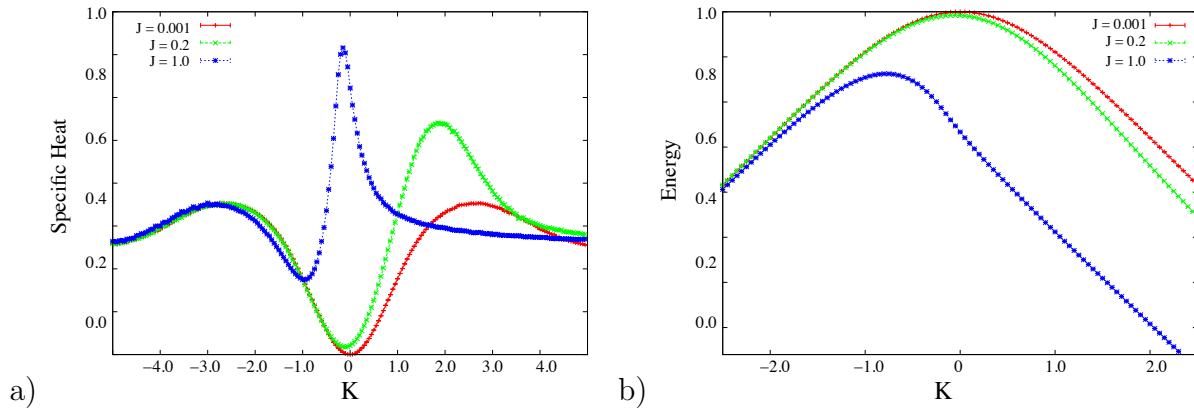
Figure 2.8: The specific heat a), and energy b), as a function of K for fixed values of J. These curves correspond to vertical cuts on the phase diagram in Fig. 2.9. The two peaks in specific heat correspond to superfluid-paramagnet and paramagnet-large K phase transitions. There also exists an energy crossing which occurs in the middle of the paramagnetic phase due to the competing interactions of the J and K terms in the Hamiltonian when K is negative and J is positive.

same as the ordered phase of the pure XY model. The specific heat curves show vertical cuts in the phase diagram where we fix $1/J$ and vary K from a large positive value to a large negative value. The red curve in Fig. 2.8 a) shows the specific heat in the limit that $1/J \to \infty$. This model essentially acts like the pure-K model since $J \approx 0$. We see that there is a transition to the ordered phase when K is larger than $K \sim 3$. When you add any finite J for $K \gtrsim 3$, regardless of how small J is the system will be a superfluid. This explains the asymptotic behaviour of the SF-PM transition at large K.

The location of the peaks in the specific heat curves correspond to the values in K where a phase transition occurs. These specific heat curves show that as K is made more negative there is another transition from the paramagnetic state to some large negative K phase. This is a state where the spins align to satisfy the antiferromagnetic ring-exchange interaction at the cost of not satisfying the XY ferromagnetic interaction. Again, we know the behaviour of this phase by comparing the shape of the specific heat curves for a general J-K interaction to the case when $J = 0$. Finally, we see from Fig. 2.8 b) that there is an energy crossing within the paramagnetic phase when K is negative due to the competing interactions of the J and K terms.
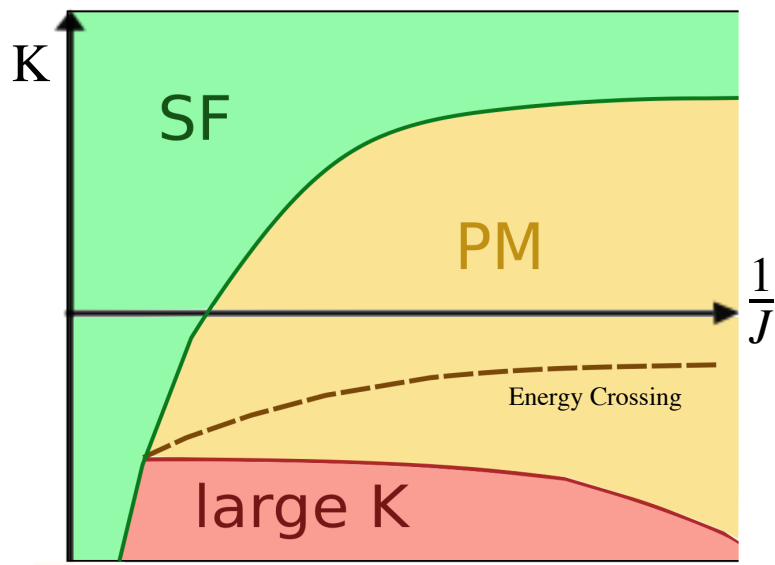
Figure 2.9: The phase diagram for the J-K model. There exist 3 distinct phases, plus an energy crossing which occurs within the paramagnetic phase.

Chapter 3

Searching for Topological Phases in the J-K Model

So far we have looked at the different phases of the classical J-K model. We have seen that the XY and pure-K models relate to physical systems of superfluids and the thermal melting of 2D solids through the universal properties of their respective phase transitions. A general rule is that universal properties only depend on essential qualitative features of the system such as symmetry of the order parameter, the dimensionality of the space and constraints placed by conservation laws. In this chapter we will take a slightly different approach to studying physical systems. We will look directly at a quantum model describing the behaviour of bosons in a one dimensional system. Such a system can be realized experimentally using, for example, ultra-cold atoms in optical lattices [42]. We will show that this model can be mapped onto an effective two dimensional classical model. This follows from a general technique known as the Trotter decomposition whereby a quantum system in d dimensions can be mapped to a classical system in $(d+1)$ dimensions [43, 44]. I will derive a mapping which sends the 1D Bose-Hubbard model at integer filling to a classical model in (1+1) dimensions with J-K type interactions.

One of the most interesting features of the Bose-Hubbard model is that it provides one of the simplest models in which a topological phase can be observed. It is simple since it is in one dimension, occurs at integer filling and contains simple two-site interaction terms. In our model, a traditional insulator is a phase of the system where strong onsite repulsion interactions restrict the system to have exactly one boson per site and all correlation functions decay exponentially. Our topological phase is also an insulator which has just one boson per site and all local correlation functions decay exponentially fast, however there is a subtle type of nonlocal order present. In this case the new order is revealed

by the presence of a special type of nonlocal string order parameter. A similar type of phase occurs in the Haldane gapped phase of quantum spin-1 chains [45], and so the new phase is known as a Haldane Bose insulator [46]. We can make this connection between the boson model and a spin-1 chain more explicit by restricting the number of particles allowed on each site to 0, 1 or 2. Then we can use the exact mapping $S_i^z = n_i - \bar{n}$, where $\bar{n}$ is the average filling. An insulating phase, for example, would then have $S_i^z = 0$ for all sites i. The Haldane insulator also has $S_i^z = 0$ on all sites, but there exists a non-local restriction on the individual particles which is very closely related to the exactly solvable Affleck-Kennedy-Lieb-Tasaki (AKLT) model [47] and leads to the existence of long-range order as measured by the string order parameter.

3.1   Phases of the 1D Bose-Hubbard Model

We begin by looking at the Bose-Hubbard model at integer filling with on-site and nearest neighbour repulsion, which has been studied in refereces [48, 49, 50, 46, 13, 29]. The system can be described by the Hamiltonian:

$$H = -t \sum_i \left(b_i^\dagger b_{i+1} + h.c. \right) + U \sum_i (\hat{n}_i)^2 - \mu \sum_i \hat{n}_i + V \sum_i \hat{n}_i \hat{n}_{i+1}. \qquad (3.1)$$

Here, $\hat{n}_i$ is the average filling of the lattice site i. The variable μ is the chemical potential and is used to set the filling factor of the lattice. We will fix the chemical potential and write the Hamiltonian in a more compact form by writing $\hat{n}_i \to \hat{n}_i - \bar{n}$ so that our variables n_i now represent the deviation of the site i from its mean filling. The variable t controls the strength of the boson hopping operators, while the variables U and V control the strength of the onsite and nearest-neighbour repulsive interactions respectively.

Consider first the system when $t = 0$ and $V = 0$. In this case there is no hopping term and only onsite repulsion, so you can solve this system exactly [29]. The number operator n_i commutes with the Hamiltonian $[\hat{H}, \hat{n}_i] = 0$ and the ground state is just given by $|\psi\rangle = \prod_i |n_i\rangle$ where $n_i = \bar{n}$ $\forall i$ and $\bar{n}$ is the smallest integer larger than $U/2\mu$. The lowest excited state of our system occurs when a boson is removed from one lattice site and placed on another. Since our variables n_i are eigenvalues of the system, the energy cost of such a move is just the difference between the two diagonal states $\Delta E = U \times [(n+1)^2 - 2n^2]$. Therefore, there exists an energy gap between the groundstate and the first excited state [29]. If the bosons carried an electric charge the system would be an insulator since the bosons do not move between lattice sites. The energy gap between the groundstate and

first excited state tells us that this insulating phase will be stable when a small hopping term is turned on. In fermionic systems, trivial insulators as described by band theory and exist when an energy band is completely filled and the fermions cannot move around the lattice due to the Pauli exclusion principle. When a fermionic system which is predicted by band theory to be a conductor actually behaves as an insulator due to strong interactions within the system, we get what is known as a Mott insulator. Of course in our bosonic system there is no Pauli exclusion principle, so any insulating phase must be due entirely to interactions. In one dimension, interactions play an especially important role since particles cannot move around one another. In the limit that $U \to \infty$ we have what are known as hard-core bosons, and in this case there is no real difference between a fermionic and bosonic system since exchange statistics have no effect. Thus, for large U the Bose-Hubbard model is in a Mott insulating phase.

Now, when we turn off all interactions, the difference between bosons and fermions becomes extremely important. At T=0, free bosons will all condense into the lowest energy state. However, when you include even an infinitesimal interaction such a state will become unstable since the energy cost of such an interaction term will grow like N^2. Adding a hopping term will create a superfluid with $\langle b_i \rangle \neq 0$. When the repulsion term U is turned on there is a critical value t_c where if $t > t_c$ the superfluid order survives, while if $t < t_c$ the Mott insulating phase is favoured [49].

When the system is in the Mott phase, the number of particles per site is the smallest integer greater than $2\mu/U$. Since the number of particles per site doesn't change with small changes in the chemical potential, we say that the system is incompressible. In the superfluid phase, on the other hand, the system is gapless and compressible. This is because the parameter $\langle b_i \rangle \neq 0$, and the operators b_i and n_i do not commute, so in the superfluid phase it is impossible to know a precise value for the total particle number of the system. Since the total particle number is allowed to fluctuate freely, the system must be compressible.

When we include nearest-neighbour repulsion ($V > 0$), we see that for large V/t, this repulsion term dominates the Hamiltonian and we get a charge density wave where there are alternating particles and holes occupying neighbouring sites along the chain(this minimizes the $\hat{n}_i \hat{n}_{i+1}$ term) [50]. Note that this density wave phase breaks the translational invariance of the lattice.

The most interesting phase of this model occurs at intermediate values of U/t and V/t, where there exists a subtle type of order which is characterized by a breaking of a hidden $Z_2 \times Z_2$ symmetry of the system signifying that the ordering of the system in this region is topological. In the Mott insulator phase, there is a gap to the lowest excitations of

the system and all correlation functions of the system decay exponentially. The lowest excitations of the system are tightly bound particle-hole pairs. In the charge density dave (CDW) phase there is a breaking of the translational symmetry of the lattice and the correlation function $(-1)^{|i-j|}\langle\delta n_i\delta n_j\rangle$ approaches a constant at long distances. This intermediate topological phase is gapped as in the Mott insulator and does not break translational symmetry, so the density wave correlation function decays exponentially. The ground state of this phase favours one particle on each lattice site, so that it behaves locally like a Mott insulator. However, the excitations of this phase are special. They consists of particle and hole fluctuations which appear in alternating order along the chain and are separated by strings of sites with $\delta n_i = 0$ of arbitrary length.

This intermediate phase is the Haldane phase. It is characterized by a breaking of hidden $Z_2 \times Z_2$ symmetry which is related to the string order parameter [46]. The Mott-insulator phase will have $n_i = \bar{n}$ on every site with tightly bound particle-hole excitations. The CDW phase will have $n_i = (-1)^i$, so particles and holes appear on alternating sites along the chain. The Haldane phase, on the other hand, consists mainly of sites at average filling $n_i = \bar{n}$, but the excitations will appear as strings with particle and hole fluctuations appearing in an alternating order along the chain separated by strings of zeros of arbitrary length. This ordering can be seen in the string correlation function, which measures the decay of these strings and approaches some constant non-zero value at long distances. This correlation function measures a highly nonlocal property of the system. The density fluctuations can be separated along the string by any distance, all that matters is the constraint that if you are moving along the string in one direction every particle fluctuation ($\delta n_i = +1$) must be followed by a hole fluctuation ($\delta n_i = -1$). Formally, this is characterized by the string correlation function

$$R_{\text{string}} = \langle\delta n_i e^{i\pi\sum_{k=i}^{j}\delta n_k}\delta n_j\rangle \rightarrow \text{constant} \ \text{as} \ r_{ij}\rightarrow\infty. \tag{3.2}$$

This type of order is very closely related to a phase which appears in quantum spin-1 chains. Haldane's conjecture states that Heisenberg antiferromagnetic spin-1 chains have a gap to the excitation spectrum, while the spin-1/2 case has no gap and algebraically decaying correlations [45]. It has been shown that the appeerence of this so called Haldane gap in the $S = 1$ Heisenberg chain corresponds to the breaking of a hidden $Z_2 \times Z_2$ symmetry and that such a phase contains string correlations, like in our model. This is the reason we call this phase a Haldane insulator [45].

3.2 The Haldane Phase and Spin-1 Chains

To understand the topological order present in the Bose-Hubbard model, it is instructive to look at the mapping to a spin-1 chain [46]. In order to map our boson system to an effective spin model we need to restrict the number of bosons which can occupy each site to $\{0, 1, 2\}$. Then we use the mapping $S_i^z = n_i - \bar{n}$, and $S_i^+ = b_i^\dagger$, $S_i^- = b_i$. Since we are at integer filling, our effective spin model has integer spin. Then $S_i^z = 1$ implies there are two bosons occupying site i, and $S_i^z = 0$ and $S_i^z = -1$ imply one and zero bosons respectively. If we apply these transformations to our Hamiltonian in (3.1), we find an effective spin-1 Heisenberg antiferromagnet Hamiltonian with an S^z anisotropy term:

$$\mathcal{H} = \sum_i S_i^z S_{i+1}^z + (S_i^+ S_{i+1}^- + S_i^- S_{i+1}^+) + D(S_i^z)^2. \tag{3.3}$$

Haldane's conjecture implies that this system is gapped. There is also a theorem by Lieb, Schultz and Mattis which states that translationally invariant spin-$\frac{1}{2}$ antiferromagnetic Hamiltonians are either gapless or possess a groundstate degeneracy [51]. Taken together, these two theorems can be used to construct a model with integer spin and a groundstate degeneracy. Such a model was created by Affleck, Kennedy, Lieb and Tasaki [47] by creating a spin-$\frac{1}{2}$ chain in which the Hamiltonian forces neighbouring spins to always form singlet states. Then after contracting two of the spin-$\frac{1}{2}$'s into the singlet state, the next two spins are free to form a triplet or a singlet state. By creating a Hamiltonian that projects out this singlet state, so that the neighbouring spins of different singlets form a triplet, every pair of neighbouring spins forms an effective spin-1 site. Then, Haldane's conjecture on the spin-1 system implies that this system is gapped, while Lieb-Schultz-Mattis theorem on the spin-1/2 system then states that since the groundstate is gapped there must exist a groundstate degeneracy.

Figure 3.1: A cartoon diagram of the spin-1 Haldane phase. The red bonds represent spin-1/2 singlet states. The green circles are effective spin-1 states formed by the neighbouring halves of two singlet bonds. Fig. a) shows that on a chain with open boundary conditions one needs to include free spin-1/2's on the edges. Fig. b) shows a possible state where each site has S_z either 1, 0 or -1.

Consider the properties of such a chain [47, 52]. Since unbound neighbouring spin-$\frac{1}{2}$'s must form a triplet state, then it is impossible for two neighbouring spin-1's to have $S^z = 2$.

That is, if one of the spin-1's has $S^z = +1$, then both spin-$\frac{1}{2}$'s must have $S^z = +\frac{1}{2}$. Then, since the spin bound to this spin-$\frac{1}{2}$ must form a singlet, this spin must have $S^z = -\frac{1}{2}$. This implies that the neighbouring spin-1 must have S^z equal to either 0 or -1. This property forms the basis of the string-order excitations in the system. Once one pair of spin-$\frac{1}{2}$'s form a triplet state with S^z equal to either +1 or -1, then as you move in one direction the bound singlet spin-$\frac{1}{2}$ nature of the groundstate forces the next excitation to be of the opposite sign, S^z equals -1 or +1.

The other important feature of this AKLT state is related to the nature of the edges when the boundaries of the system are open [52]. When periodic boundary conditions are in place, all the spin-$\frac{1}{2}$'s of the system are bound to one neighbouring spin in a singlet state and form an effective spin-1 site with another neighbouring spin. When the boundary conditions are opened, then we are forced to break apart one of these singlet states (so that all sites in our chain still form effective spin-1 states) resulting in our chain containing two free spin-$\frac{1}{2}$ sites on its ends which are not forced to be bound into a singlet state. This freedom accounts for the $Z_2 \times Z_2$ symmetry of the groundstate since each of the spin-$\frac{1}{2}$'s on the edges can have S^z equal to either $+\frac{1}{2}$ or - $\frac{1}{2}$. This implies that the spin-1 states on the edges are free to fluctuate plus or minus one eigenvalue each and the groundstate with open boundary conditions is hence 4-fold degenerate. This illustrates two important properties: that the degeneracy of the groundstate depends on the boundary conditions (i.e. it depends on the one dimensional topology), and that when the system has open boundary conditions the sites on the boundary can fluctuate freely even though the sites within the bulk of the chain are highly constrained.

Although we have looked at a model which has been finely tuned to rigorously demonstrate this topological order, it has been shown [52] that a phase with this type of string order does exist in spin-1 chains which interact under the Hamiltonian given by (3.3). It has been shown that for large D, the ground state of $\mathcal{H}$ is unique, has exponentially decaying correlation functions and a finite excitation gap, i.e. it describes the Mott phase of our original boson Hamiltonian. However, for small D the groundstate is gapped and has exponentially decaying correlations but contains a hidden antiferromagnetic order which breaks a hidden $Z_2 \times Z_2$ symmetry and leads to a nonzero value of the string correlation function. That is, this phase has the same properties as the AKLT state described above.

Now, in order to map our boson system to a spin-1 system we had to truncate our Hilbert space to include states with only 0,1 or 2 bosons per lattice site. Technically, this approximation is only valid for large U where the system will favour one boson per site. However numerical simulations of the boson system [46] show that this order survives in the limit of smaller U. Then, the Haldane phase in the boson picture has the same properties as the spin-1 system. That is, the excitation are alternating particle and hole excitations

separated by strings of zeros (no excitations) of arbitrary length. Also, when the boundary conditions are open, the lattice site on the edges of the chain a free to fluctuate. That is, even though in the bulk of the system there is an energy gap to the excited states, at the edges a particle or hole excitation can be added with zero energy cost. Therefore, the bulk of the system is incompressible but the edges are compressible. This is an important property which we will exploit in our attempt to identify topological order in the classical J-K model. In fact, the presence of edge states is a general property of any manifestation of topological order and is not unique to the Haldane phase.

We now know the properties of the Bose-Hubbard model in different regimes of phase space. At intermediate values of U/t and V/t this Haldane phase exists, which has a subtle topological ordering. It would be interesting to see whether this type of non-local order can be seen in a classical Hamiltonian. If it is possible then we could use classical Monte Carlo simulations to study a wide range of interesting systems which may be topologically ordered. We address this question now.

3.3 Mapping Quantum Systems to $(d+1)$-dimensional Classical Systems

In the path-integral formulation of quantum mechanics the main difference between quantum and classical systems is that classical particles follow a path in phase space which minimizes a classical action, while quantum particles traverses all possible paths in phase space with some probability [53]. This formulation allows us to draw a connection between quantum systems in d dimensions and classical systems in $(d+1)$-dimensions. A classical system will exist in a state which minimizes the free energy, $F = -T \ln Z$ with $Z = \text{Tr}[e^{-\beta H}]$. In the quantum case, however, you must also deal with fluctuations caused by the fact the all operators do not commute with each other. The off-diagonal operators in the Hamiltonian make it difficult or impossible to explicitly evaluate the trace in the partition function. However, by expanding the partition function in an extra dimension you can decompose the partition function so that at every point in time all the operators commute with each other and in this way the quantum fluctuations are just classical fluctuations of the system in the imaginary time direction [20].

We start with the 1D quantum Bose-Hubbard Hamiltonian which contains a 2-site boson hopping term, t, as well as onsite and nearest-neighbour repulsion terms, U and V respectively.

$$H = -t \sum_i (b_i^\dagger b_{i+1} + h.c) \ + U \sum_i n_i^2 \ + V \sum_i n_i n_{i+1}. \tag{3.4}$$

We will first show the general procedure of expanding the Hamiltonian in the imaginary time direction. To do this, we will write the boson hopping operators in terms of the phase operator θ:

$$b_i = e^{i\theta_i} \ \text{so that} \ b_i^\dagger b_{i+1} = e^{i(\theta_i - \theta_{i+1})}, \tag{3.5}$$

$$\text{and with} \ [\hat{\theta}_i, \hat{n}_j] = i\delta_{i,j} \ . \tag{3.6}$$

Then our quantum Hamiltonian becomes:

$$H = -t \sum_i cos(\theta_i - \theta_{i+1}) + U \sum_i n_i^2 + V \sum_i n_i n_{i+1}. \tag{3.7}$$

Next, write down the partition function

$$Z = \text{Tr}[e^{-\beta H}] = \int_0^{2\pi} \prod_i D\theta \ \langle\theta|e^{-\beta H}|\theta\rangle \qquad \text{where} \ |\theta\rangle = \prod_i |\theta_i\rangle \ \text{and} \ D\theta = \prod_i d\theta_i \ . \tag{3.8}$$

All we have done is choose a basis where the θ operators are diagonal and hence the n_i variables are off-diagonal operators. Then write the partition function in a form where we divide the exponential into a product over M pieces where each piece commutes with each other in the limit of large M.

$$\text{Now let} \qquad \varepsilon = \frac{\beta}{M} \ \text{for} M \gg 1, \tag{3.9}$$

$$\text{so that} \qquad Z = \text{Tr}(e^{-\beta H}) = \text{Tr}(e^{-\varepsilon H} e^{-\varepsilon H} \dots e^{-\varepsilon H}). \tag{3.10}$$

Insert an identity operator $1 = \int D\theta(\tau_p) \left|\theta(\tau_p)\right\rangle\langle\theta(\tau_p)|$ between every copy of $e^{-\varepsilon H}$. We index each independent copy of the resolution of the identity operators with the variable τ_p, so that we get:

$$Z = \int D\theta(\tau_m) \cdots D\theta(\tau_1) \prod_{p=0}^{M-1} \langle\theta(\tau_{p+1})|e^{-\varepsilon H}|\theta(\tau_p)\rangle. \tag{3.11}$$

For each copy of $e^{-\varepsilon H}$ we can again break up the exponential into the different components present in the Hamiltonian H:

$$
\begin{aligned}
e^{-\varepsilon H} &= \exp\left\{ -\varepsilon\left[-K\sum_i \cos(\theta_i - \theta_{i+1}) + U\sum_i n_i^2 + V\sum_i n_i n_{i+1} \right] \right\} \\
&= \exp\left\{ -\varepsilon\left[-K\sum_i \cos(\theta_i - \theta_{i+1}) \right] \right\} \times \exp\left\{ -\varepsilon U\sum_i n_i^2 \right\} \times \exp\left\{ -\varepsilon V\sum_i n_i n_{i+1} \right\} \\
&= e^{-\varepsilon H_1} e^{-\varepsilon H_2} e^{-\varepsilon H_3},
\end{aligned}
\tag{3.12}
$$

where $e^{\mathbf{A}+\mathbf{B}} = e^{\mathbf{A}}e^{\mathbf{B}}$ only if $[\mathbf{A}, \mathbf{B}] = 0$. In our case, $[\varepsilon H_1, \varepsilon H_2] = 0$ in the limit $\varepsilon \to 0$

Now

$$
\begin{aligned}
\int D\theta(\tau_p) e^{\varepsilon t \sum_i \cos(\theta_i - \theta_{i+1})} |\theta(\tau_p)\rangle &= \int D\theta(\tau_p) \left(\int D\theta(\tau_p) e^{\varepsilon t \sum_i \cos(\theta_i - \theta_{i+1})} |\theta\rangle\langle\theta| \right) |\theta(\tau_p)\rangle \\
&= \int D\theta(\tau_p) |\theta(\tau_p)\rangle \ e^{\varepsilon t \sum_i \cos(\theta_i - \theta_{i+1})}.
\end{aligned}
\tag{3.13}
$$

We expand the trace in the $|\theta\rangle$ basis, so the t term of the Hamiltonian (i.e. H_1) is diagonal in this basis and we can take this term outside of the trace and replace the operators $\hat{\theta}_i$ with the classical variables θ_i

Now, we need to deal with the off-diagonal terms (n_i terms) in the Hamiltonian:

$$
\langle\theta(\tau_{p+1})|e^{-\varepsilon H_2} e^{-\varepsilon H_1}|\theta(\tau_p)\rangle = \langle\theta(\tau_{p+1})|e^{-\varepsilon U \sum_i \hat{n}_i^2 - \varepsilon V \sum_{\langle ij \rangle} \hat{n}_i \hat{n}_j}|\theta(\tau_p)\rangle.
\tag{3.14}
$$

We use the projection of the number operator, $\hat{n}$, in θ space, so that

$$
\langle\theta_i|n_i\rangle = \frac{1}{\sqrt{2\pi}} e^{-in_i\theta_i} \quad \Rightarrow \quad \langle\theta|n\rangle = \prod_i \langle\theta_i|n_i\rangle = \frac{1}{(2\pi)^N} e^{-i\sum_i n_i\theta_i},
\tag{3.15}
$$

and $\quad e^{-\varepsilon U \sum_i \hat{n}_i^2 - \varepsilon V \sum_{\langle ij \rangle} \hat{n}_i \hat{n}_j} = \sum_{n=0}^{\infty} |n\rangle\langle n| \ e^{-\varepsilon U \sum_i n_i^2} \quad \text{with} \quad |n\rangle = \prod_i |n_i\rangle, \quad (3.16)$

46

to get:

$$
\begin{aligned}
(3.11) \quad &= \sum_{n=0}^{\infty} \langle \theta(\tau_{p+1}) | n(\tau_p) \rangle \langle n(\tau_p) | \theta(\tau_p) \rangle \ e^{-\varepsilon U \sum_i n_i^2 \ -\varepsilon V \sum_i n_i n_{i+1} \ + \ \varepsilon \ t \sum_i \cos(\theta_i - \theta_{i+1})} \\
&= \sum_{n=0}^{\infty} e^{i \sum_i n_i(\tau_p)\theta_i(\tau_{p+1})} e^{-i \sum_i n_i(\tau_p)\theta_i(\tau_p)} e^{-\varepsilon U \sum_i n_i^2 \ -\varepsilon V \sum_i n_i n_{i+1} \ + \ \varepsilon t \sum_i \cos(\theta_i - \theta_{i+1})} \\
&= \sum_{n=0}^{\infty} e^{i \sum_i n_i[\theta_i(\tau_{p+1}) - \theta_i(\tau_p)] \ - \ \varepsilon U \sum_i n_i(\tau_p)^2 \ -\varepsilon V \sum_i n_i(\tau_p)n_{i+1}(\tau_p)} \,\big] e^{\varepsilon t \sum_i \cos(\theta_i - \theta_{i+1})}.
\end{aligned}
$$

$$(3.17)$$

$$
\therefore Z = \int \prod_{p=0}^{M-1} D\theta(\tau_p) \sum_{n=-\infty}^{\infty} \exp\left\{ \varepsilon t \sum_i \cos(\theta_i - \theta_{i+1}) \right\} \times \cdots \qquad (3.18)
$$

$$
\cdots \exp\left\{ i \sum_i n_i[\theta_i(\tau_{p+1}) - \theta_i(\tau_p)] \ - \ \varepsilon U \sum_i n_i(\tau_p)^2 \ - \ \varepsilon V \sum_i n_i(\tau_p)n_{i+1}(\tau_p) \right\}.
$$

What we have done is write our quantum Hamiltonian entirely in terms of classical variables in (1+1)-dimensions.

3.4 Mapping the Bose-Hubbard Model to the Classical J-K Model

We now use the partition function given by (3.18) to connect the Bose-Hubbard model with the classical 2D J-K model. The diagonal part of (3.18) just transfers directly to the classical partition function as an interaction in the spatial direction, so we will omit that component from the following derivation. Then,

$$
Z_{\text{off diag}} = \int D\theta \sum_{n_{i,p}=-\infty}^{\infty} \exp\left\{ -\varepsilon U \sum_{i,p} n_{i,p}^2 \ - \varepsilon V \sum_{i,p} n_{i,p} n_{(i+1),p} \ - \ i \sum_{i,p} n_i[\theta_{i,(p+1)} - \theta_{i,p}] \right\}.
$$

$$(3.19)$$

47

What follows is a series of tricks and transformations which we will apply to the off-diagonal part of the partition function in order to write it solely in terms of our diagonal variables in $(d+1)$-dimensions. This transforms our quantum problem into a statistical mechanics problem with simple interactions that can be solved with, for example, classical Monte Carlo simulations.

The first step is to apply the *Poisson Summation Formula*

$$\sum_{n=-\infty}^{\infty} \delta(x-n) \;=\; \sum_{m=-\infty}^{\infty} e^{-2\pi i m x}, \tag{3.20}$$

$$\Rightarrow \quad \int dx \sum_{n=-\infty}^{\infty} \delta(x-n) \;=\; \int dx \sum_{m=-\infty}^{\infty} e^{-2\pi i m x}. \tag{3.21}$$

Doing this gives us:

$$Z = \int D\theta \sum_{m_{i,p}=-\infty}^{\infty} \left(\prod_i \int dx_i \; \exp\left\{ -\varepsilon U \sum_{i,p} x_{i,p}^2 - \varepsilon V \sum_{i,p} x_{i,p} x_{(i+1),p} \cdots \right. \right.$$
$$\left. \left. \cdots - i \sum_{i,p} x_i [\theta_{i,(p+1)} - \theta_{i,p} + 2\pi\, m_{i,p}] \right\} \right). \tag{3.22}$$

By writing (3.19), as an integral over delta-functions we can send our discrete n-variables to continuous variables. We can then perform the integral over x by using the Hubbard-Stratonovich transformation in order to write our Hamiltonian in terms of our θ variables only.

The *Hubbard-Stratonovich transformation* is:

$$\frac{1}{(2\pi)^{N/2}} \int_{-\infty}^{\infty} d\phi_1 \cdots d\phi_N \; e^{-\frac{1}{2}\phi_i A_{ij}\phi_j + \phi_i \gamma i} \;=\; \frac{1}{\sqrt{\det A}} \, e^{\frac{1}{2}\gamma_i A_{ij}^{-1}\gamma_j}. \tag{3.23}$$

In our case we let: $\phi_i = x_i$
and $\gamma_i = -i \times (\theta_{i,(p+1)} - \theta_{i,p} - 2\pi\, m_{i,p})$.

We see from (3.22), that by choosing our variables like this our partition function is in exactly the same form as the left hand side of (3.23). We find that we only need to invert the interaction matrix A_{ij}, in order to express our model entirely in terms of the classical θ_i variables.

3.4.1   U-only Model leading to the Classical XY model

In the case when there is only on-site repulsion so that V=0, inverting the interaction matrix is quite simple and the resulting mapping between the quantum and classical systems is well known [53]. In this case we have:

$$A_{ij} = \varepsilon U \,\delta_{ij}. \tag{3.24}$$

Then inverting this diagaonal matrix is simple and $A_{ij}^{-1} = \frac{1}{\varepsilon U}\delta_{ij}$. Thus:

$$
\begin{aligned}
e^{\frac{1}{2}\gamma_i A_{ij}^{-1}\gamma_j} &= e^{\frac{1}{2}\sum_{ij,p}[-i\times(\theta_{i,(p+1)}-\theta_{i,p}-2\pi\,m_{i,p})]\frac{1}{\varepsilon U}\delta_{ij}[-i\times(\theta_{j,(p+1)}-\theta_{j,p}-2\pi\,m_{j,p})]} \\
&= e^{-\frac{1}{2\varepsilon U}\sum_{i,p}(\theta_{i,(p+1)}-\theta_{i,p}-2\pi\,m_{i,p})^2} \\
&= e^{\frac{1}{\varepsilon U}\sum_{i,p}\cos(\theta_{i,(p+1)}-\theta_{i,p})},
\end{aligned}
\tag{3.25}
$$

where the last step uses the *Villain Approximation*:

$$\sum_{m=-\infty}^{\infty} e^{-\frac{1}{2}(\theta_i-\theta_j+2\pi\,m)} = e^{\cos(\theta_i-\theta_j)}. \tag{3.26}$$

When V=0, the quantum model maps onto the classical 2D model with Hamiltonian (once again including the diagonal term):

$$H = -\varepsilon t \sum_{i,p} \cos(\theta_{i,p}-\theta_{(i+1),p}) - \frac{1}{\varepsilon U}\sum_{i,p}\cos(\theta_{i,p}-\theta_{i,(p+1)}), \tag{3.27}$$

which is just the 2D-XY model with different couplings in the spatial and temporal directions.

Consider this result for a moment. The Bose-Hubbard model with just $t-U$ interactions has two phases, a superfluid phase at $U/t \sim$ small and a Mott insulator at $U/t \sim$ large. We want to study the groundstate of this model in the thermodynamic limit so that $\beta \to \infty$ and $M \sim L_y \to \infty$. But then, we have a freedom to choose the value of the parameter coupling $\varepsilon = \beta/M$. To study the critical properties of the system it is sufficient to choose the coupling so that the interaction is isotropic in the spatial and temporal (x and y) directions, $\varepsilon = 1/\sqrt{tU}$. The point being that we now have an isotropic XY model with coupling $J = \sqrt{t/U}$, and if we fix t, the parameter U acts like temperature in our model. As we increase U, there will be a Kosterlitz-Thouless transition from a disordered phase to a superfluid phase in our classical 2D model. This is exactly the same transition which occurs in the Bose-Hubbard model [49].

When the XY model is in its ordered phase, the θ variable obtains a coherent value throughout the system corresponding to a coherent phase of the boson operators in the quantum model and hence a superfluid state. Now, the value n_i is a conjugate variable to θ_i in the quantum system with the commutation relation $[n_i, \theta_i] \sim i$, or $\Delta n_i \Delta \theta_i \gtrsim 1$. When the system is in the superfluid phase, there is a high uncertainty in the particle number, $\Delta n_i \sim$ large. On the other hand, when the system is in the disordered phase there is a greater uncertainty in the phase $\Delta \theta_i$. In this case, the conjugate variable n_i has $\Delta n_i \sim$ small and so n_i can obtain a definite value on each site. This describes the Mott insulator phase in the quantum model where the particle number on each site is fixed.

3.4.2   U-V Model leading to J-+K classical model

The mapping in the previous section from the $t - U$ model to the 2D-XY model is well known in the literature [53, 13]. We will now look at a new situation and examine what happens when we include a small V interaction in our quantum model, that is:

$$\mathrm{A}_{ij} = \varepsilon U \, \delta_{ij} \ + \ \varepsilon V \, \delta_{i,j\pm 1}, \tag{3.28}$$
$$\text{with } V \ll U.$$

Now to derive the classical model we need to invert this non-trivial interaction matrix. The way to do this is by Fourier-transforming the interaction into K-space, inverting that matrix and then performing a Fourier transform back to real space.

$$\mathbf{A}(q) = \frac{1}{N} \sum_{ij} \mathbf{A}_{ij} e^{-i\vec{q}\cdot\vec{r}_{ij}}, \tag{3.29}$$

with $q = \dfrac{2\pi n}{L_x}$ and $n \,\epsilon\, \left[\dfrac{-L_x}{2}, \dfrac{-L_x}{2}+1, \cdots, \dfrac{L_x}{2}-1, \dfrac{L_x}{2}\right) \Rightarrow q \,\epsilon\, [-\pi, \pi)$.

Then $\mathbf{A}(q) = \dfrac{1}{N} \sum_{ij} \left(\varepsilon U \delta_{ij}\, e^{-i\cdot\vec{r}_{ij}} \;+\; \varepsilon V \delta_{i,j\pm1} e^{-i\vec{q}\cdot\vec{r}_{ij}} \right)$,

but $\delta_{ij}\, \vec{r}_{ij} = 0$ and $\delta_{i,j\pm1}\, \vec{r}_{ij} = \pm a$; a the lattice spacing constant,

$$\Rightarrow \mathbf{A}(q) = \frac{1}{N} \left[N \cdot \varepsilon U + 2N\varepsilon V \cos(qa) \right],$$

Then
$$\mathbf{A}(q) \;=\; \varepsilon U \;+\; \varepsilon V \cos(qa) \tag{3.30}$$
$$\Rightarrow \mathbf{A}^{-1}(q) \;=\; \frac{1}{\varepsilon U \;+\; \varepsilon V \cos(qa)} \;=\; \frac{1}{\varepsilon U \times \left(1 \;+\; \frac{V}{U}\cos(qa) \right)},$$
$$\Rightarrow \mathbf{A}^{-1}(q) \;\approx\; \frac{1}{\varepsilon U} - \frac{1}{2}\frac{V}{\varepsilon U^2}\cos(qa) \quad \text{for} V \ll U. \tag{3.31}$$

It is now easy to Fourier transform back to real space, as $\mathbf{A}^{-1}(q)$ is in the same form as $\mathbf{A}(q)$

$$\Rightarrow \mathbf{A}_{ij}^{-1} = \frac{1}{\varepsilon U}\, \delta_{ij} \;-\; \frac{1}{2}\frac{V}{\varepsilon U^2}\, \delta_{i,j\pm1}. \tag{3.32}$$

Putting this into the Hubbard-Stratonovich transformation, (3.23), gives us our partition function in terms of classical variables as:

$$e^{\frac{1}{2}\gamma_i A_{ij}^{-1}\gamma_j} \;=\; \exp\Bigg\{ -\frac{1}{2}\frac{1}{\varepsilon U} \sum_{i,p}(\theta_{i,(p+1)} - \theta_{i,p} - 2\pi\, m_{i,p})^2 \cdots$$
$$\cdots + \frac{1}{2}\frac{V}{\varepsilon U^2} \sum_{\langle ij\rangle p}[\theta_{i,(p+1)} - \theta_{i,p} - 2\pi\, m_{i,p}][\theta_{j,(p+1)} - \theta_{j,p} - 2\pi\, m_{j,p}] \Bigg\}. \tag{3.33}$$

We want to get this in a form where we can apply the Villain approximation. Use the identity:

$$x_i x_j = \frac{1}{2}\left[(x_i + x_j)^2 - (x_i - x_j)^2\right], \tag{3.34}$$

to get

$$(\theta_{i(p+1)} - \theta_{ip} - 2\pi\, m_{ip})(\theta_{(i+1)(p+1)} - \theta_{(i+1)p} - 2\pi\, m_{(i+1)p}) =$$
$$\frac{1}{2}\left[(\theta_{i(p+1)} - \theta_{ip} - 2\pi\, m_{ip} + \theta_{(i+1)(p+1)} - \theta_{(i+1)p} - 2\pi\, m_{(i+1)p})^2 \cdots \right.$$
$$\left. \cdots - (\theta_{i(p+1)} - \theta_{ip} - 2\pi\, m_{ip} - \theta_{(i+1)(p+1)} + \theta_{(i+1)p} + 2\pi\, m_{(i+1)p})^2\right]. \tag{3.35}$$

Now, we make the assumption that all the variables vary slowly on the scale of the lattice spacing. This is certainly true, at least, when $V \ll U$, and the V-term is just some small perturbation above the XY-model that we derived for the $V = 0$ case.

That is :
$$\theta_{ip} + \theta_{(i+1)p} \approx 2\theta_{ip},$$
$$\text{and} \qquad m_{ip} + m_{(i+1)p} \approx 2m_{ip}.$$

Then, the first term in (3.35) goes to $\qquad \to 2^2 \times (\theta_{i(p+1)} - \theta_{ip} - 2\pi m_{ip})^2$,

while the second term goes to $\qquad \to (\theta_{i(p+1)} - \theta_{ip} - \theta_{(i+1)(p+1)} + \theta_{(i+1)p} + 4\pi\, m_{(i+1)p})^2.$

In this way, the first term above simply acts as an XY-type interaction and will just renormalize the two-site XY term that we get from the $\sum_i \hat{n}_i^2$ term in our mapping. The second term maps onto a ring-exchange type term which is in the proper form to apply the Villain approximation to.

Our partition function can be written as:

$$Z = \int D\theta \sum_{\{m\}} \exp\left(\sum_{i,p} -\frac{-1}{2\varepsilon\, U}(\theta_{i(p+1)} - \theta_{ip} - 2\pi\, m_{ip})^2 + \frac{2V}{\varepsilon\, U^2}(\theta_{i(p+1)} - \theta_{ip} - 2\pi\, m_{ip})^2 \right.$$
$$\left. -\frac{1}{2}\frac{V}{\varepsilon\, U^2}(\theta_{i(p+1)} - \theta_{ip} - \theta_{(i+1)(p+1)} + \theta_{(i+1)p} - 4\pi\, m_{(i+1)p})^2\right) \tag{3.36}$$

As mentioned, the second two-site term can just be absorbed into the first term since $\frac{V}{U}$ is small. Then, we apply the Villain approximation

$$\sum_{\{m\}} e^{-\frac{1}{2}\frac{1}{\varepsilon U}(\theta_{i(p+1)}-\theta_{ip}-2\pi\,m_{ip})^2} = e^{\frac{1}{\varepsilon U}\cos(\theta_{i(p+1)}-\theta_{ip})}, \tag{3.37}$$

and

$$\sum_{\{m\}} e^{-\frac{1}{2}\frac{V}{\varepsilon U^2}(\theta_{i(p+1)}-\theta_{ip}-\theta_{(i+1)(p+1)}+\theta_{(i+1)p}-4\pi\,m_{ip})} = e^{\frac{1}{2}\frac{V}{\varepsilon U^2}\cos(\theta_{i(p+1)}-\theta_{ip}-\theta_{(i+1)(p+1)}+\theta_{(i+1)p})}. \tag{3.38}$$

Which leads us to the final form of our partition function

$$Z = \int D\theta\ \exp\left\{\frac{1}{\varepsilon U}\sum_{\langle ij\rangle}\cos(\theta_i-\theta_j) + \frac{V}{\varepsilon U^2}\sum_{\langle ijkl\rangle}\cos(\theta_i-\theta_j+\theta_k-\theta_l)\right\}. \tag{3.39}$$

Including the diagonal interaction term then leads to the Hamiltonian:

$$H = -\varepsilon t\sum_{ip}\cos(\theta_i p-\theta_{(i+1)p}) - \frac{1}{\varepsilon U}\sum_{ip}\cos(\theta_{ip}-\theta_{i(p+1)})$$

$$-\frac{V}{\varepsilon U^2}\sum_{ip}\cos(\theta_{ip}-\theta_{(i+1)p}+\theta_{(i+1)(p+1)}-\theta_{i(p+1)}). \tag{3.40}$$

To study the critical properties of the system we can choose the coupling constant ε so that our model is isotropic. That is choose $\varepsilon = \sqrt{\frac{1}{tU}}$. This coupling choice allows us to study a simpler model and will not affect the important physics of the system near a phase transition. In the case when $V = 0$, this choice of ε allows us to write the Hamiltonian as the usual isotropic 2D XY model.

Thus, we find that our system maps onto a (1+1)-D classical system with an isotropic XY interaction and a ring-exchange interaction:

$$H = -\sqrt{\frac{t}{U}}\sum_{\langle ij\rangle}\cos(\theta_i-\theta_j) - \frac{V}{U}\sqrt{\frac{t}{U}}\sum_{\langle ijkl\rangle}\cos(\theta_i-\theta_j+\theta_k-\theta_l). \tag{3.41}$$

3.4.3 More General U-V Model leading to the J-$\bar{\text{K}}$ Model

If we now go back to our Hubbard-Stratonovich transformation of the U-V model and instead of making the approximation $V \ll U$ we invert our interaction-matrix numerically, we can derive a more general form of the classical model.
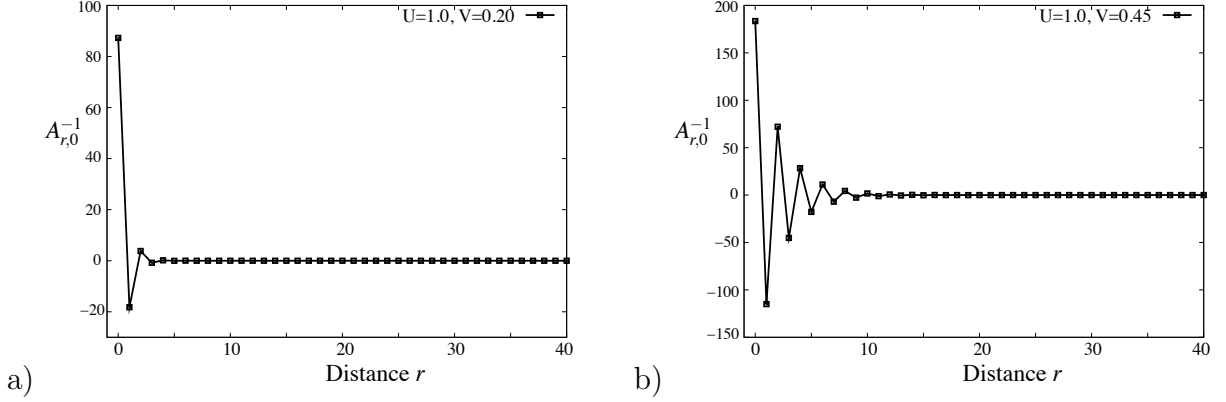

a)　　　　　　　　　　　　　　　b)

Figure 3.2: a) The coefficient of the δ_{ij} terms in the interaction matrix as a function of distance r_{ij}. In b) The next-nearest neighbour interactions become stronger as V is increased. $A_{0,0}^{-1}$ maps onto the XY interaction term. All other $A_{r,0}^{-1}$ terms map onto FM and AMF ring-exchange interactions in the (1+1)-d effective Hamiltonian.

As before we start with:

$$\text{A}_{ij} = \varepsilon U \, \delta_{ij} \, + \, \varepsilon V \, \delta_{i,j\pm 1}, \tag{3.42}$$

$$\mathbf{A}(q) = \frac{1}{N} \sum_{ij} \mathbf{A}_{ij} e^{-i\vec{q}\cdot\vec{r}_{ij}}, \tag{3.43}$$

with $\quad q = \dfrac{2\pi n}{L_x} \quad$ and $\, n \, \epsilon \left[\dfrac{-L_x}{2}, \dfrac{-L_x}{2}+1, \cdots, \dfrac{L_x}{2}-1, \dfrac{L_x}{2} \right) \Rightarrow q \, \epsilon \, [-\pi, \pi). \, (3.44)$

Then $\quad \mathbf{A}(q) \;=\; \dfrac{1}{N} \sum_{ij} \left(\varepsilon U \delta_{ij} \, e^{-i\cdot\vec{r}_{ij}} \, + \, \varepsilon V \delta_{i,j\pm 1} e^{-i\vec{q}\cdot\vec{r}_{ij}} \right),$

$$\;=\; \frac{1}{N} \left[N \cdot \varepsilon U + 2N\varepsilon V \cos(qa) \right]. \tag{3.45}$$

54

Giving
$$\mathbf{A}(q) \;=\; \varepsilon U \;+\; 2\varepsilon V\cos(qa), \tag{3.46}$$

$$\Rightarrow \mathbf{A}^{-1}(q) \;=\; \frac{1}{\varepsilon U \;+\; 2\varepsilon V\cos(qa)},$$

$$\Rightarrow \mathbf{A}_{ij}^{-1} \;=\; \sum_{q} \frac{e^{i\vec{q}\cdot\vec{r}_{ij}}}{\varepsilon U \;+\; 2\varepsilon V\cos(qa)}, \tag{3.47}$$

$$\Rightarrow \mathbf{A}_{ij}^{-1} \;=\; \sum_{q} \frac{\cos(\vec{q}\cdot\vec{r}_{ij})}{\varepsilon U \;+\; 2\varepsilon V\cos(qa)}. \tag{3.48}$$

We can evaluate this last expression numerically by simply calculating the sum over all q in (3.44). As long a $V < U/2$, this is easy since the denominator is always analytic in this case. Calculating the sum numerically gives the values of the effective (1+1)-d interaction matrix A_{ij}^{-1}. Fig. 3.2 shows A_{ij}^{-1} for different values of (i, j) as calculated at two different points (U, V) in parameter space, and it leads to interactions like in Fig. 3.2. For small V, we recover the results of the previous section, where there is a 2-site XY interaction term and a 4-site ferromagnetic ring-exchange term. However, as V gets larger we begin to notice the higher-order terms in the Taylor expansion of A. We see that there is the same type of 4-site ring-exchange interaction but with opposite sign and between next-nearest-neighbours. As we change the relative values of U/V, it changes the effective classical Hamiltonian. The three lowest order terms in the Hamiltonian are a nearest-neighbour XY interaction, a nearest-neighbour FM ring-exchange interaction and a next-nearest-neighbour AFM ring-exchange interaction. The higher order terms alternate in the same fashion, with each higher order term mapping onto a longer-range ring-exchange term. When we include the nearest-neighbour repulsion, V, our quantum to classical mapping ceases to be exact. For relatively small V/U, we can ignore the terms beyond the third order in the Taylor expansion and study a local classical system. However, for large values of V/U our mapping ceases to be well-behaved. In this case we find that the interactions do not monotonically decrease with distance and we derive a complicated long-ranged classical model. We have run Monte Carlo simulations on the short ranged model to look for signs of the Haldane phase. We will see, in the next section, that we were not able to find evidence of this topological phase in the local classical model and will conclude that the Haldane phase does not exist in the well-behaved region of the mapping.

55

3.5   Looking for the Haldane Phase in the J-K Model

So far we have gone through a rather detailed process to map our quantum 1D system onto a 2D classical model with both XY and ring-exchange interactions. For small V, to first-order, the ring exchange term is ferromagnetic. In our study of the general J-K model we saw that a ferromagnetic interaction increases the strength of the superfluid phase. However, we also saw that a very small negative ring-exchange term will quickly destroy the superfluid order. Since there is no qualitative difference between the system with positive ring-exchange and the regular XY model we claim that this term in the expansion of the interaction matrix only works to renormalize the XY interaction. That is, in our derivation of the (1+1)-d classical Hamiltonian, we Taylor expand our quantum interaction matrix in terms of small $\frac{V}{U}$, which leads to a ferromagnetic ring-exchange term. However, the lowest order term in this Taylor expansion does not capture the proper physics of our quantum model, so we look to the next term in the Taylor expansion which gives an antiferromagnetic ring-exchange interaction term.

The system we are now studying contains an isotropic XY interaction in both the spatial and temporal direction as well as an antiferromagnetic next-nearest-neighbour ring-exchange term. We can easily simulate this system and see that the basic properties are the same as the J-K model when K is negative. As V becomes more negative, the superfluid density dies off more rapidly as a function of U. This recreates the shape of the superfluid to Mott insulator transition in the quantum model. Since the nearest-neighbour repulsion term V favours an insulating phase over a superfluid phase, when this term is added to the quantum model a smaller value of the onsite repulsion U is required for the KT transition from a superfluid to a Mott insulator to occur. Recall that the disordered paramagnetic phase of our classical statistical model maps onto an insulating phase in the quantum model since large fluctuations in the θ_i variable allow the conjugate particle number variable n_i to be well defined on each site.

We can recreate the small V/U section of the phase diagram for the Bose-Hubbard model, which describes the superfluid-to-insulator transition. Our goal was to see if it is possible to study topological phases using $(d+1)$-dimensional statistical mechanics models. Specifically, we would like to study the Haldane insulator phase using our classical J-K type model. The main difficulty arises in finding good signatures of the topological order which can be measured in our simulation. By definition, any local measurement of the system cannot distinguish between the insulating phase with exponential decay of all correlation functions and the topological phase. In the Haldane phase all local order parameters decay exponentially. The Bose-Hubbard model was studied numerically by Torre et al.[46] using the Density Matrix Renormalization Group (DMRG) algorithm, which is a powerful

variational method used to study one dimensional quantum systems [54]. In the 1D DMRG simulations the Haldane insulating phase was identified by measuring the nonlocal string order parameter which approaches a constant value at long distances. However it is not clear exactly how one would measure this type of correlation function in our classical model. Instead, we will focus on trying to see signatures of the gapless excitations which occur at the edges when the system has open boundary conditions. The system should be compressible at the edges and incompressible in the bulk, which is a reflection of the nonlocal nature of the low lying excitations. Recall that a compressible system is one in which there is no energy cost associated with adding a particle to the system. In the quantum model, the set of conjugate variables $\hat{n}_i$, $\hat{\theta}_i$ obey the uncertainty principle $\Delta\theta\Delta n \gtrsim 1$. When the system is in the superfluid phase with $\Delta\theta \sim$ small, this uncertainty principle implies that Δn is large. Thus, a finite spin-stiffness γ implies that there are large fluctuations in particle number n, and the phase must be compressible. When we are in an insulating phase, where the spin-stiffness is zero, bosons are localized in space and Δn_i is small. In this case there would be an energy cost associated with adding a particle to the system and so the system is incompressible. For this reason, the uncertainty relationship for conjugate variables n and θ implies that the spin-stiffness measurement is also a measurement of the compressibility of the system.

Our first attempt in searching for these edge states involved naively measuring the helicity modulus along 1D lines in the temporal direction. The set of sites (i, j) on our lattice such that $(i, j) = (x, \tau)$ for fixed x and all τ is taken as our definition of the local spatial position x. The edges of the system are then the two lines with $x = 0$ and $x = L$ (See Fig. 3.3). We thus want to measure the superfluid density locally as a function of spatial position x. However, there is a subtlety in that the way we defined the helicity modulus measurement for the XY model necessarily sums over all bonds of the lattice. Recall Eq.(1.2):

$$\gamma_\mu/J = \frac{1}{N}\left\langle \sum_{\langle ij \rangle} \cos(\theta_i - \theta_j)(\hat{\mathbf{e}}_{ij} \cdot \hat{\mu})^2 \right\rangle - \frac{J}{TN}\left\langle \left[\sum_{\langle ij \rangle} \sin(\theta_i - \theta_j)\hat{\mathbf{e}}_{ij} \cdot \hat{\mu}\right]^2 \right\rangle. \qquad (3.49)$$

The second term sums over the entire lattice within the square brackets, so when we try to sum over only one temporal line of the lattice we will find that there is some offset from the true value of the spin stiffness. A physical picture of this may be trying the measure the spin stiffness of a 1D system which is coupled to a heat bath. We find that even in regimes where we know the value of the stiffness to be zero, when we measure it locally we
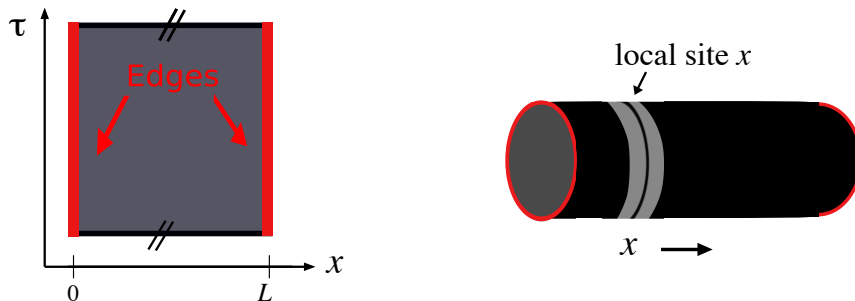
Figure 3.3: The topology of the lattice with open boundary conditions in the spatial direction x and periodic boundary conditions in the temporal direction τ. The local position x is defined as the line of sites, each at the xth spatial coordinate, which wrap around the periodic direction of the cylinder.

find $\gamma(x)$ has a nonzero value. This causes major problems when trying to use this as a definitive measurement for determining whether edge states are present. These states are either compressible or they are not. If the spin-stiffness is allowed to take on a non-zero value even when the system is in an incompressible phase then we can not use the absolute value of this measure to say anything definitive about the compressibility. However, it is still instructive to look at what we find for this quantity.

Fig 3.4 shows the local helicity modulus as a function of the spatial position along the lattice for two regions in phase space. The first figure is in the superfluid phase. We see that at the edges of the system the helicity modulus is slightly lower in value, which simply reflects the fact that the sites on the edge have fewer neighbours and hence are more free to fluctuate. A similar behaviour is observed in a region which is known to be a Mott insulating phase (i.e. at large U, $V = 0$). When we look at a region we suspect contains the Haldane phase, if it is present at all (at intermediate values of $\frac{V}{U}$ when the total superfluid density is zero and beyond the energy crossing in negative V), we see interesting behaviour. The value of the local helicity modulus at the edges of the system is clearly greater than within the bulk of the system. These peaks in superfluid density die off as one moves towards the centre of the system where the curve becomes a flat line presumably indicating the bulk insulating behaviour of the system.

This appears to be promising evidence for the existence of edge states in our classical model, however it is not at all definitive and could just be some energetic feature of the system. We want a way to study whether the sites on the edge have a qualitatively different behaviour then those in the bulk. This does, however, naturally lead to what we claim to
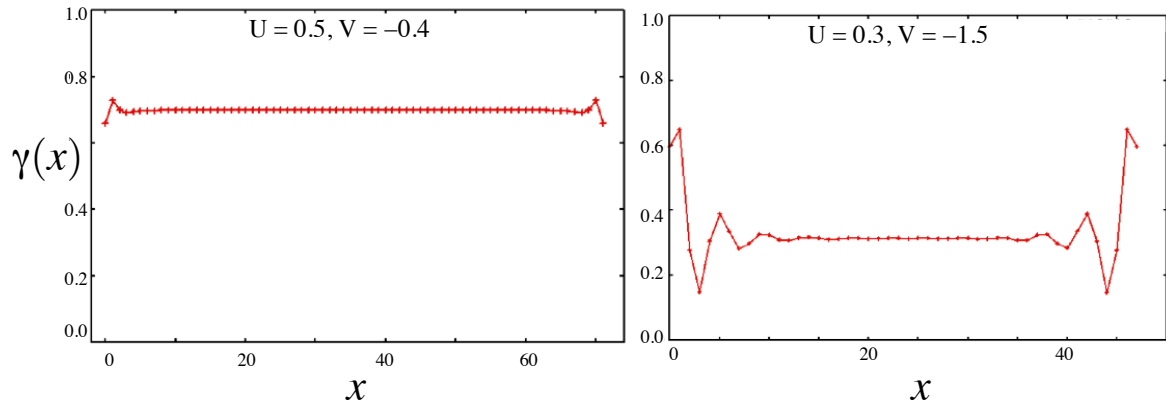
Figure 3.4: The local helicity modulus as a function of spatial position for two points in phase space. The first figure occurs in the superfluid phase and the second is in the disordered phase with large negative V.

be a definitive test for compressible edge states in our system. This is a measurement of the scaling of the correlation functions at the edges of the system as a function of distance in the temporal direction.

We measure the expectation value

$$C = \langle S_x S_{x+\tau} \rangle = \langle \cos(\theta_x - \theta_{x+\tau}) \rangle, \tag{3.50}$$

where the index x gives the spatial position on the cylinder where we measure this correlation. The index τ gives the distance in the temporal direction (which has periodic boundary condition) between the two spins for which we measure our two-point correlation function. A compressible state with a finite superfluid density will have the correlation function decay algebraically at large distances demonstrating the quasi-long range order which is present in the system. The paramagnetic or insulating phase, on the other hand will show an exponential decay of all correlation functions at large distances. In order to measure this scaling of the correlation function without finite size-effects from the periodic boundaries of the lattice ruining the measurement we use the method of measuring the correlation between two points separated by a distance $r_{ij} = L/6$. We make this measurement on an $L \times L$ lattice and scale L to larger values to extract an unbiased scaling form for $C = \langle S_i S_j \rangle$.

We first perform measurements for two test cases, in the regime where we know the
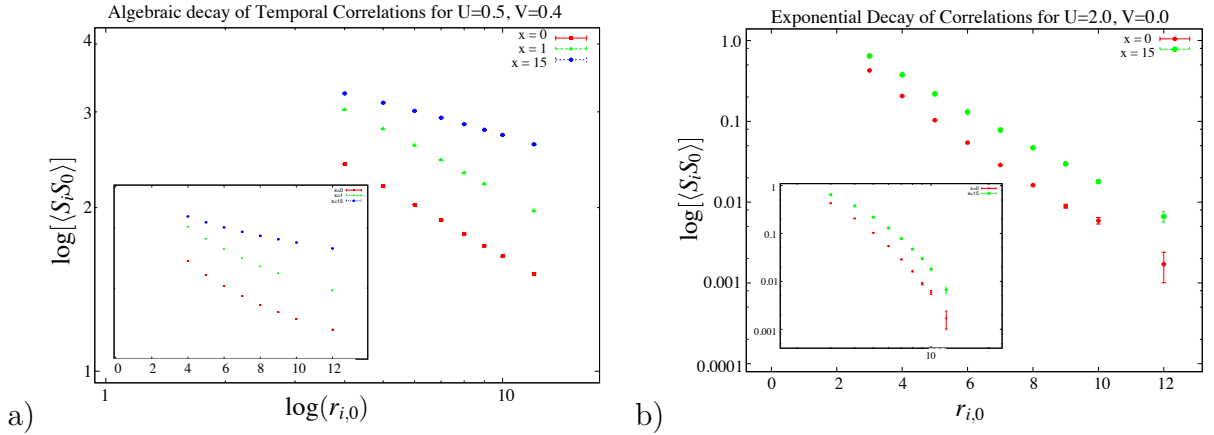
Figure 3.5: The correlations for the regimes in phase space that are known to be super-fluid(a) or Mott insulator (b) phases, showing algebraic and exponential decays respectively.

system to be either a superfluid, Fig 3.5a), and an insulator, Fig 3.5 b), to show that we can indeed extract this form of the scaling. For a system in which the correlations C decay algebraically we have $C \sim r^{-\eta} \rightarrow \log[C] \sim -\eta \log(r)$, so that if we plot C(r) on a log-log graph it should form a straight line. Similarly, if C decays exponentially we find $C \sim e^{-r/\xi} \rightarrow \log[C] \sim -\frac{r}{\xi}$, which forms a straight line on a log-linear plot. We have plotted both of these cases in Fig 3.5, and see that the correlations form the expected linear plots in both cases. If we try to plot the superfluid case on a log-linear plot or the insulator on a log-log plot we can clearly see there is curvature in the lines (see the insets on both plots). Thus this measurement is able to distinguish between the compressible and incompressible phases of the system in two well behaved regions of phase space.

So we now perform this same measurement on a region which is a candidate for the Haldane phase. If there exist compressible edge states we would expect to see an algebraic decay of the correlations when measured on the edges and exponential decay when measured in the bulk. Instead, the data in Fig. 3.6 clearly shows an exponential fit on the edges of the system (as well as in the bulk). So, although there did exist indications that the Haldane phase may exist in this J-K model, these results show that this is in fact not the case.

We can go back to our quantum-to-classical mapping to see why our classical model does not pick up this topological phase. The assumption we made in our mapping was that the term $\frac{V}{U}$ was small. We expect the Haldane phase to exist at intermediate values
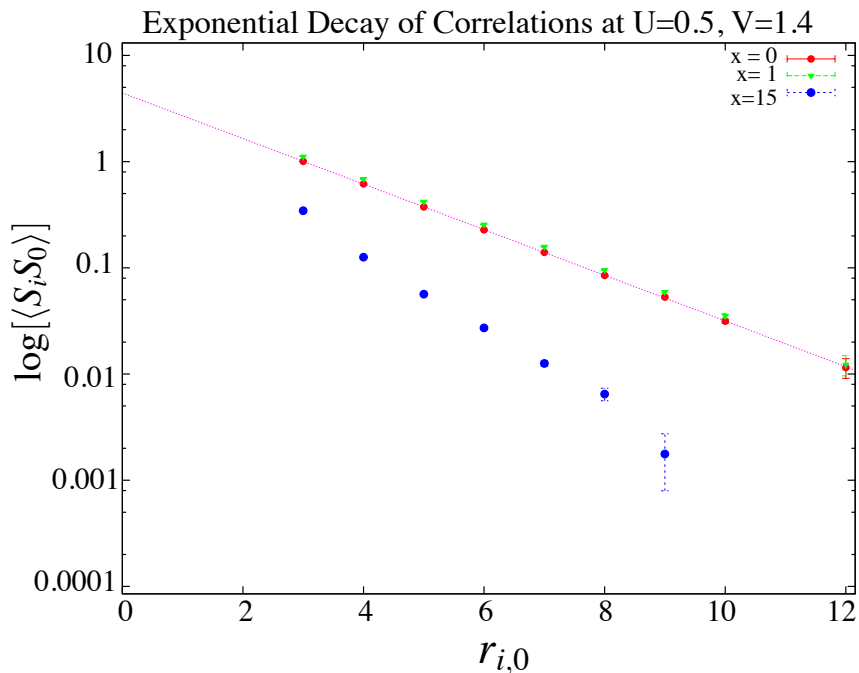
Figure 3.6: The correlations for the regime in phase space that is suspected to be topologically ordered, which would lead to algebraically decaying edges and exponentially decaying bulk spin correlations. We see here that the edge states in this region are in fact exponentially decaying.

of $\frac{V}{U}$ (while large values of $\frac{V}{U}$ correspond to a charge density wave). In our mapping we inverted the interaction matrix A_{ij} in equation (3.42). We transform this to write A_{ij}^{-1} in the form of Eq.(3.48). However, at the point $V = \frac{U}{2}$, the sum over q in (3.48) contains a pole which must be integrated around using a complex contour integral. When we do this we find that the A_{ij}^{-1} becomes some complicated long-ranged function which would lead to a complicated nonlocal classical model.

We conclude that our mapping from the 1D Bose-Hubbard model to the 2D classical J-K model is only successful in replicating the physics for small values of V/U where we can pick up the KT transition between the superfluid and insulating phases of the quantum model. This small V/U approach does not allow us see any signs of topological order which would be present in the Haldane phase of this model in the large V regime. The mapping between the quantum and classical models is not exact. Despite this, we were able to

probe the small V/U region in phase space, but we could not find the Haldane phase in our classical (1+1)-d model. There is a special point in the model at $V = U$ where we can derive a different classical model which amounts to a simple XY model in different variables (see Appendix A). This mapping, however, also does not produce a local classical model with topological order.

Chapter 4

An Information Theory Approach to the XY Model

In this chapter we will look at the concepts of information entropy and mutual information. It will be seen how these concepts can be applied to solve problems in condensed matter physics. We will define the concept of mutual information and see why it is useful for studying interacting many-body systems. We then show how mutual information can be measured in classical Monte Carlo simulations based on the so called "replica trick". Surprisingly, this technique has so far only been applied to quantum systems and is not even well-defined for classical systems. We develop an extension of this technique for classical systems and show that it works by testing the technique on the classical Ising model. This method will then be applied to study the 2D XY model where we show that it gives a completely new and more general way of identifying the Kosterlitz-Thouless phase transition.

4.1 von Neumann Entropy and Condensed Matter Systems

4.1.1 Definition of Information Entropy

The study of two-point connected correlation functions has traditionally been a fundamental component of our understanding of the behaviour of interacting many-body systems. Indeed, connected correlation functions have largely been the tool we have used to detect all important quantities within our Monte Carlo simulations. Properties such as long-range order due to symmetry breaking or the onset of a nonzero superfluid density can all be related back to some special long-distance behaviour of the correlation function. An alternative way of studying general statistical models is provided by classical information theory. This new approach involves dividing a system into two regions and studying how information is shared between the two regions. If you look at information as being the fundamental quantity which can be extracted from a system then understanding the way in which this information is shared across the two regions can allow us to measure any relevant physical property, including those which cannot be measured using more traditional methods. This approach has been used to measure the central charge in conformal one dimensional systems [5, 55] and the topological entanglement entropy in 2D spin liquid phases [6]. By studying the scaling of information with region size we may be able to identify universal quantities which we can use to identify the type of phase a system is in or to identify phase transitions.

Classical information theory was pioneered by Claude E. Shannon in his 1948 paper [56] in which he developed the notion of describing a general source with n bits of information in terms of its entropy function $H(X)$, defined as:

$$H(\{p_i\}) = \sum_{i=1}^{n} -p_i \log p_i,\tag{4.1}$$

where outputs $i \in \{1...n\}$ are output with probability p_i. When two random variables X and Y depend on each other, the maximum amount of information which can be communicated between the two variables is given by the mutual information [57]:

$$\begin{aligned}
\mathcal{I}(X;Y) &= H(Y) - H(Y|X) & (4.2)\\
&= H(X) + H(Y) - H(X,Y) & (4.3)
\end{aligned}$$

The first line gives the expression in terms of the conditional entropy, $H(Y|X)$, which measures the entropy of the variable Y given that we know the value of variable X. The

second line writes this expression in terms of the entropy of the individual variables minus the entropy of the joint system. In a many body system, we can partition our lattice into two or more regions. Say we partition the system into regions A and B as in Fig. 4.1. In this case instances of the random variables X and Y would just correspond to configurations of the spins in regions A and B respectively. For classical systems the conditional entropy $H(Y|X)$ is always positive. However, this is not necessarily true for a random variable representing quantum spins [58].
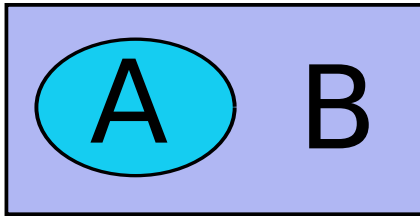

Figure 4.1: One way to partition a lattice into two regions A and B. The perimeter of the circular region is the boundary between A and B.

4.1.2 Quantum Systems, Entanglement and the Density Matrix

The analogous quantity to the Shannon entropy for quantum spins is known as the von Neumann entropy. A complete description of a quantum system is contained within its density matrix:

$$\rho = \sum_i p_i |\psi_i\rangle\langle\psi_i|. \tag{4.4}$$

If ρ can be written in terms of a single wavefunction $\rho = |\psi\rangle\langle\psi|$, then we say that ρ is a pure state. Otherwise, ρ is a mixed state and the probabilities p_i describes the relative mixture of the independent states, $|\psi_i\rangle$, which ρ is composed of. The quantity ρ is a positive semi-definite matrix whose eigenvalues lie in the interval $[0,1]$, so that we can associate these eigenvalues with the probability distribution of a quantum system. We can then define the von Neumann entropy in terms of the density matrix as:

$$H_{\text{vN}} = -\text{Tr}[\rho \log \rho]. \tag{4.5}$$

To gain some intuition about how quantum mechanics can affect the von Neumann entropy, imagine you had a system of N spins which were oriented either $|\uparrow\rangle$ or $|\downarrow\rangle$ in

the S^z basis. If the orientation of the spins was completely random then the system would be at its maximum randomness and the entropy would be $\log(2^N) = N \log 2$. If instead your spins appeared as $| \uparrow \rangle$ or $\frac{1}{\sqrt{2}}(| \uparrow \rangle + | \downarrow \rangle)$ each with probability $\frac{1}{2}$, there is a lot less randomness in your system due to the non-commuting nature of the spin Z and spin X basis states. Now, for a spin system which emerges from the description of a model Hamiltonian, at finite temperature the system will be a thermal mixed state where the probability of each configuration is given by the Boltzmann weight $p_i \sim e^{-\beta E_i}$. As temperature approaches zero the system will generally approaches a single groundstate $|\psi\rangle = \sum_i c_i |b_i\rangle$, where $\{|b_i\rangle\}$ form a complete basis for the spin system. If $|\psi\rangle$ is not entangled we can write it as a product state $|\psi\rangle = \prod_i^N \otimes |s_i\rangle$, where $|s_i\rangle$ are suitable basis states for spins at site i. We want to measure the amount of information which is shared between separate regions of the system. We can define the reduced density matrix by taking the partial trace Tr_B over spins $|s_i\rangle$ in region B only:

$$\rho_A = \text{Tr}_B[\rho] = \sum_{i\epsilon B} \langle s_i | \rho | s_i \rangle. \tag{4.6}$$

The most important properties of the density matrix for our purposes are:

- $\rho^2 = \rho$ if and only if ρ is a pure state.

- $\text{Tr}[\rho] = 1$ always.

- A pure state ρ is entangled if and only if $Tr[\rho_A^2] \neq 1$ (i.e. $\rho_A^2 \neq \rho_A$).

We can use these properties to see how the density matrix can quantify the entanglement in quantum many-body systems. Assume that as $T \to 0$, the system approach a single ground state, described by a pure state $|\psi\rangle$. If the system is not entangled then the reduced density matrix will also be a pure state and the trace of ρ_A^2 will be equal to unity implying that the von Neumann entropy will equal zero. However, if $|\psi\rangle$ is entangled then ρ_A will not be a pure state and $\text{Tr}(\rho_A^2)$ will necessarily be less than 1. In this case the von Neumann entropy will be greater than zero. At least for a pure state, then, the von Neumann entropy of the reduced density matrix at zero temperature characterizes the amount of entanglement present in the system.

$$H_{\text{vN}}(\rho_A) = S(\rho_A) = -\text{Tr}[\rho_A \log \rho_A] \tag{4.7}$$

This works because at zero temperature the only information which can be shared between two regions of the system is due to the entanglement, as any thermal fluctuations go to zero at $T = 0$. If there exists a groundstate degeneracy, then state at zero temperature

must be described by a mixed state ρ and the entropy $S(\rho_A)$ will not in general be zero even if the state is not entangled. In the case of spontaneous symmetry breaking, the density matrix would be an even mixture of a finite, non-extensive number of states which would add a constant value to $S(\rho_A)$. This is an example of a classical phenomenon which contributes to the entanglement entropy at $T = 0$. Since it only gives a constant contribution, the amount of entanglement can still be determined by measuring how the entanglement entropy scales with the area of the boundary between regions A and B. We will see that at finite temperature the scaling of the entropy $S(\rho_A)$ can be used to determine classical properties of the system.

4.1.3 The Area Law at Zero and Finite Temperatures

The actual amount of entanglement which is present in such a system can be quantified using the famous 'area law', which states that the entanglement entropy scales with the area of the boundary between the two regions [59, 60]. Note that in two dimensions, the 'area' of a boundary is the length of a one dimensional line separating the two regions. Intuitively, correlations in systems with local interactions have a characteristic length scale, ξ, so that only sites near the boundary of region A will be entangled to sites in region B. This gives an entanglement entropy which scales as the length of this boundary.

We can extend the concept of entanglement entropy to finite temperature by using our definition of mutual information introduced earlier. The advantage of this quantity is that at zero temperature it reduces to the entanglement entropy and at finite temperature the mutual information shared between two regions scales like an area law [61]. The definition of entanglement entropy at finite temperature remains the same as in the $T = 0$ case given by Eq.(4.6). Then the mutual information is given by:

$$\mathcal{I}(A; B) = S(\rho_A) + S(\rho_B) - S(\rho_{A \cup B}). \tag{4.8}$$

It is important to note that at finite temperature the density matrix of the system is a thermal mixed state. Thermal fluctuations will affect how mixed the state is. The long-distance behaviour of connected correlation functions will directly affect how much information travels across the boundary of a region. The mutual information formula given by (4.8) describes how much more random our knowledge of the individual regions A and B are than that of the combined system of $A \cup B$. The mutual information at finite temperature describes quantum and classical correlations, it is not a measure of the 'quantumness' of the system. In a purely classical system the von Neumann entropy reduces to the Shannon entropy between the random variables ρ_A and ρ_B, two variables

which depend on each other and describe the probability that regions A and B of the system will be found in a certain configuration. Under the property that the entropy is non-decreasing upon throwing away information about a part of the system, the mutual information at finite temperature must always be positive [62].

To understand the behaviour of the mutual information measurement, consider a system of classical d-component spins arising from a Hamiltonian with short-range interactions. All configurations which arise in this manner are Markov fields. This means that if x_A, x_B and x_C are three regions of the system where C separates A and B, then the conditional probabilities $\rho(x_A|x_B, x_C) = \rho(x_A, x_C)$. That is, since all communication between regions A and B must travel through region C, then the configurations x_A and x_B both mutually depend on the configuration x_C, but do not directly depend on each other.

Now, separate our system into regions A and B. Use the definition $I(A; B) = H(A) - H(A|B)$ and write A and B as $A = A_1 \cup \partial A$ and $B = B_1 \cup \partial B$, where ∂A and ∂B are the sites on the boundary between A and B. Then:

$$
\begin{aligned}
I(A; B) = I(A; B_1 \cup \partial B) &= H(A) - H(A|B_1, \partial B) \\
&= H(A) - H(A|\partial B) \\
&= I(A; \partial B).
\end{aligned}
\tag{4.9}
$$

Similarly, we can write the information shared across the boundary ∂A as:

$$
I(\partial B; A) = I(\partial B; \partial A).
\tag{4.10}
$$

Now we can use the fact that the classical conditional probability is always positive and the fact that the Shannon entropy of a single d component spin is bounded by the entropy of the maximally mixed state $S = -\sum_{i=1}^d (1/d) \log[(1/d)] = \log(d)$ to find:

$$
I(A; B) = I(\partial A; \partial B) \leq H(\partial A) \leq |\partial A| \log d.
\tag{4.11}
$$

We have just proven that the area law holds for the mutual information of classical d-component spins [62].

The mutual information picks up all quantum and classical correlations in an interacting many-body system. The coefficients of the area law and any sub-leading corrections to the area law term in the mutual information are completely determined by the interactions between the two regions of the system. We will attempt to use this to identify phase transitions in classical systems.

4.2 The Replica Trick and Measuring Mutual Information in Spin Systems

In Monte Carlo simulations, one cannot directly access the partition function of the system so one cannot easily calculate the trace of the reduced density matrix. It is thus very difficult to calculate the von Neumann entropy and the mutual information for an arbitrary many body system using Monte Carlo. To get around this problem in our simulations, we instead measure the generalized n$^{\text{th}}$ Renyi entropies defined as [61]:

$$S_n(A) = \frac{1}{1-n} \ln[\text{Tr}(\rho_A^n)]. \tag{4.12}$$

This definition reduces to the von Neumann entanglement entropy of ρ_A in the limit that $n \to 1$. The advantage of defining Renyi entropies in this way is that the calculation of the trace $\text{Tr}[\rho_A^n]$ for positive integers $n > 1$ can be written as the partition function of a system on a modified Riemann surface [63].

The idea behind measuring Renyi entropies is that we can write the reduced density matrix ρ_A as an operator of the form $e^{\beta \hat{H}'}$. Then the Renyi entropy $S_n(A)$ is the trace over ρ_A^n and can be written as the partition function of a slightly modified system which can be simulated using Monte Carlo techniques.

The density matrix of a thermal state at inverse temperature β is

$$\rho(\{\phi(x)\}|\{\phi(x')'\}) = Z(\beta)^{-1}\langle\{\phi(x)\}|e^{-\beta\hat{H}}|\{\phi(x')'\}\rangle. \tag{4.13}$$

Then the trace over the sites in region B can be evaluated by expanding the partition function of the sites in region B in imaginary time with temporal length β (since we are at finite T) and ensuring that we have periodic boundary conditions in the temporal direction.

$$
\begin{aligned}
Z(\beta) \cdot \text{Tr}_B(\rho) &= Z(\beta) \cdot \rho_A = \sum_{\{\phi\}\epsilon B} \langle\phi|e^{-\beta\hat{H}}|\phi\rangle & (4.14) \\
&= e^{-\beta\hat{H}_A} \prod_{\tau=0}^{\beta} \sum_{\{\phi_i\}\epsilon B} \langle\phi_1|e^{-\beta H}|\phi_2\rangle\langle\phi_2|e^{-\beta H}|\phi_3\rangle \cdots \langle\phi_{N-1}|e^{-\beta H}|\phi_N\rangle & (4.15) \\
&= e^{-\beta\hat{H}_A} Z_B(\beta). & (4.16)
\end{aligned}
$$

Then we can write :

$$
\begin{aligned}
\rho_A^2 &= Z_B(\beta)^2 e^{-\beta\hat{H}_A} e^{-\beta\hat{H}_A} = [Z_B(\beta)]^2 e^{-2\beta\hat{H}_A}, & (4.17) \\
\Rightarrow \text{Tr}(\rho_A^2) &= \frac{Z_A(2\beta)[Z_B(\beta)]^2}{[Z(\beta)]^2} = \frac{Z[A, 2, \beta]}{Z(\beta)^2}. & (4.18)
\end{aligned}
$$

When we take the trace over the sites in region A we ensure that the boundary conditions are periodic in imaginary time with temporal extent 2β.

One can write $\text{Tr}[\rho]$ in a path integral representation where integrating over the fields ϕ_i amounts to pasting the two temporal edges of lattice together in a cylindrical topology so that the system is periodic in imaginary time. If we also write the spins in region A in the path integral representation then there is no such periodicity condition, since we have not yet taken the trace over these spins. Then one can represent the ρ_A^n system by pasting together n copies of ρ_A where each site in region B is periodic with temporal extend β, but the only condition on sites in region A is that $\phi_j(x, \tau = \beta^-) = \phi_{j+1}(x, \tau = 0^+)$. Then finally taking the last trace $\text{Tr}[\rho_A^n]$ amounts to ensuring that the sites in region A are periodic over the entire n copies of the system. Thus, the overall system consists of n-copies of spins in region B which are periodic with length β in imaginary time, and one copy of sites in region A which are periodic with length $n\beta$ in imaginary time.

From this we can write the Renyi entropy as:

$$S_n(A) = \frac{1}{1-n} \ln[\text{Tr}(\rho_A^n)] = \frac{1}{1-n}\left(\ln Z[A, n, \beta] + n \ln Z(\beta) \right). \qquad (4.19)$$

What we have done is map the function $\text{Tr}[\rho_A^n]$ to the partition function of a general quantum system written in the path integral representation with a modified topology in the temporal direction. This is the so called "Replica Trick"; simulating powers of the reduced density matrix of a system can be done by creating n replicas of the system and pasting them together with boundary conditions which are periodic in β for region B and $n\beta$ for region A, as illustrated in Fig. 4.2.

Writing out the derivation of this replica trick has the advantage that we can try to extend this trick to study classical systems. The easiest way to see this is to take the definition in Eq.(4.18) which describes a general system where sites in region A are at temperature T/n when site in region B are at temperature T. We can implement this in the classical Monte Carlo simulations in the same way as in the quantum case, but in the classical case we collapse the imaginary time direction of the pictures in Fig. 4.2 a). To calculate $S_2(A)$ we start by taking two copies of our d-dimensional system. For sites in region B we allow the values of the spins within the two copies of our system to fluctuate independently of each other. On the other hand, for sites in region A, the values of the spins at identical sites must have the same value between the two copies. This reflects the fact that in the path integral formulation, sites in region A extends double the length in imaginary time. It is just that in the classical picture, there are no off-diagonal operators to change the value of a spin between different imaginary time slices. Or looking at this
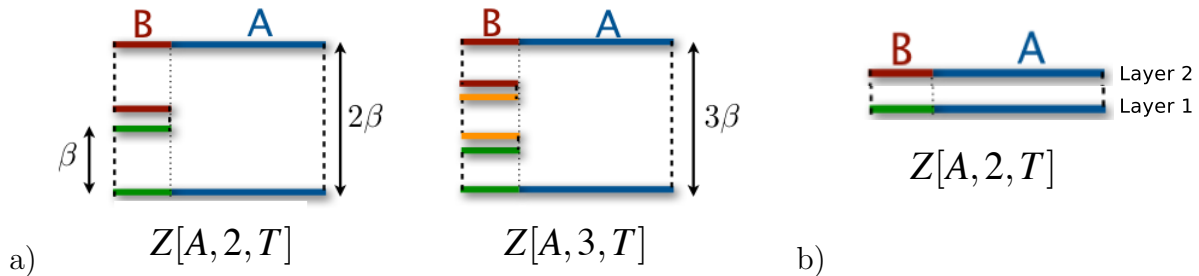
Figure 4.2: The 'Replica Trick'. Simulating the system with this modified topology allows us to measure the S_n Renyi entropies in MC Simulations. a) shows the quantum replica trick where a system has an extent of length $n\beta$ in imaginary time. b) shows the classical replica trick which is taken by collapsing the systems in a) to include n copies of a single layer with modified boundary conditions.

classically, any fluctuations of the spins in region A will cost twice as much energy because the fluctuation needs to occur on both slices of the system and so the spins in region A are effectively at half the temperature as the spin in region B.

4.3 Applying the Classical Replica Trick to Study Phase Transitions

In order to test our extension of the replica trick for classical systems we first implement our simulation with the modified topology on the simplest interacting classical model, the Ising model. The Hamiltonian for such a system is given by $H = -J\sum_{\langle ij \rangle} \sigma_i \sigma_j$ where $\sigma_i \in \{0, 1\}$. This model has been solved exactly in two dimensions by Lars Onsager using the transfer matrix method, where it has been shown that there is a phase transition at $T_c \approx 2.269185J$ [64]. One of the most useful properties of the mutual information is its ability to find the temperature transition, T_c, by directly measuring the singularity in the free energy which occurs as the system approaches a phase transition.

To measure the mutual information using the second Renyi entropies we require two separate simulations; one for $Z[A, 2, T]$ and one for $Z(T)$.
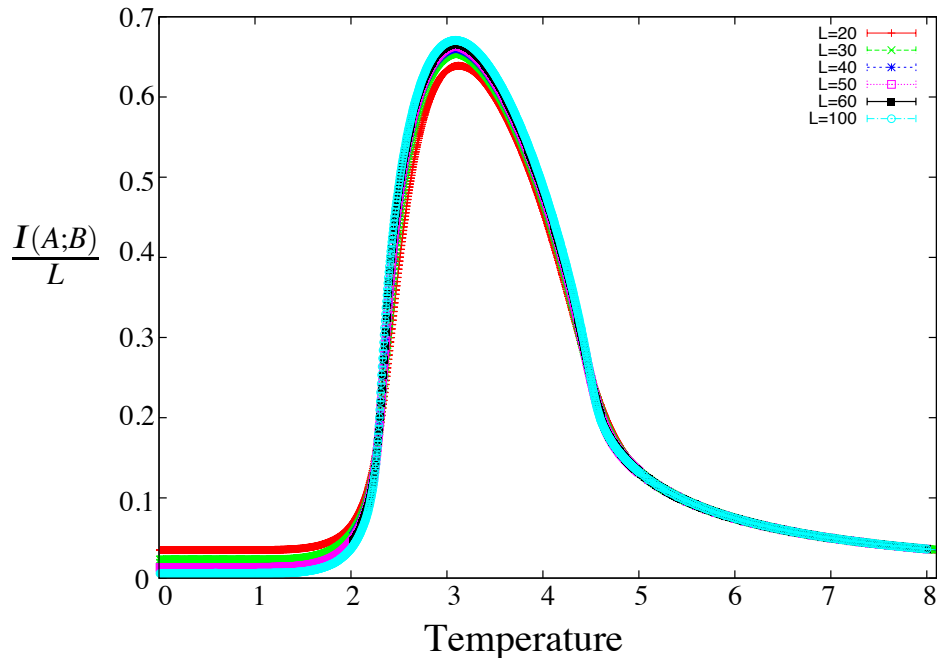
Figure 4.3: The mutual information $\mathcal{I}/L$ curves for the 2D classical Ising model for system sizes up to $L = 100$. The crossings of the different curves occur at T_c and $2T_c$.

$$
\begin{aligned}
S_2(T) &= -\ln Z[A, 2, T] + 2\ln Z(T) & (4.20) \\
&= -S_A(\beta = 0) + \int_0^\beta \langle E \rangle_{A,\beta} \, d\beta + 2S_0(\beta = 0) - 2\int_0^\beta \langle E \rangle_{0,\beta} \, d\beta , & (4.21)
\end{aligned}
$$

where $\langle E \rangle_{A,\beta}$ and $\langle E \rangle_{0,\beta}$ are the energies of the modified and unmodified systems respectively, as function of β.

Near a phase transition, the mutual information near the critical point scales like [61]:

$$
\mathcal{I}_n(A; B) = a_n(\beta) \cdot L + d_n(\beta) + \mathcal{O}(1/L). \tag{4.22}
$$

In Fig. 4.3, we plot $\mathcal{I}_2(A; B)/L$ vs. temperature for different system sizes. We can explain the shape of the curve as follows. At $T = \infty$, the spins in either region fluctuate completely independently of each other and so the mutual information approaches zero. As

the temperature is lowered, initially the MI increases as spins begin to communicate with each other and then decreases again below the phase transition as all thermal fluctuations in the system become frozen out. We see that for large L the $\mathcal{I}/L$ curves converge to a limiting function, verifying the proposed area law scaling of the mutual information $\mathcal{I}_2/L \sim a_2(\beta)$.

The most striking feature about these curves, however, is the appearance of crossing points very close to $T = T_c$ and $T = 2T_c$. We can see that this should occur from our formula for the scaling of $\mathcal{I}_n(A; b)$ given in Eq.(4.22). As $T \to T_c$ the MI is given by:

$$\frac{\mathcal{I}(A; B)}{L} = a(\beta) + \frac{d(\beta)}{L} + \mathcal{O}\left(\frac{1}{L^2}\right). \tag{4.23}$$

The term $d_n(\beta)$ is related to the symmetry breaking of the lattice. At $T < T_c$, the spontaneous breaking of the Ising symmetry means that the partition functions $Z[\beta], Z[n\beta]$, $Z[A, n, \beta]$, $Z[B, n, \beta]$ all have a multiplicative factor of 2 in addition to the area law term. This leads to a constant $\ln(2)$ being added to the MI according to Eq's (4.8) and (4.20). Similarly, when $T_c < T < 2 * T_c$, spins in region A are in a symmetry broken state but not spins in region B. Only the partition functions $Z[n\beta], Z[A, n, \beta]$ and $Z[B, n, \beta]$ carry a multiplicative factor of two leading to a constant term of $d_n = -\ln(2)/(n-1)$ being added to the MI. According to Eq.(4.23), when the symmetry breaking causes $d_n(\beta)$ to change signs $d_n(\beta)$ must be zero and the function $\mathcal{I}/L$ will be independent of system size (up to order $\mathcal{O}(1/L^2)$). This is what leads to the crossing of the MI curves for different system sizes.

Fig. 4.4 a) shows the crossings of a set of MI curves from $L = 20$ to $L = 100$. From these curves, even without accounting for the effects of the $\mathcal{O}(1/L^2)$ terms (which should be small), we can estimate the transition temperature to be $2.265 < T_c < 2.280$. We have also plotted in 4.4 b) the full $d_2(\beta)$ function. We can see the plateaus of $\ln(2)$ and $-\ln(2)/(n-1) = -\ln(2)$ in the two symmetry broken regions.

We can also compare our results to those done using Quantum Monte Carlo (QMC) and Exact Diagonalization (ED) on the quantum XXZ models which belongs to the Ising universality class and which has been studied in references [65] and [61]. We see that all the properties we have studied correspond exactly to the XXZ case, mainly the mutual information follows the same scaling form, the function $d_n(\beta)$ has all the same qualitative properties, and the crossings between the curves for different system sizes is able to identify the critical temperature at T_c and $2T_c$. With further analysis of the scaling functions it is proposed that it would be possible to extract universal terms of the scaling and in particular there should exist a $t \ln t$ singularity in the area law piece of $\mathcal{I}$ which is related to the scaling of the correlation length $\xi \sim t^{-\nu} = t^{-1}$ [61].
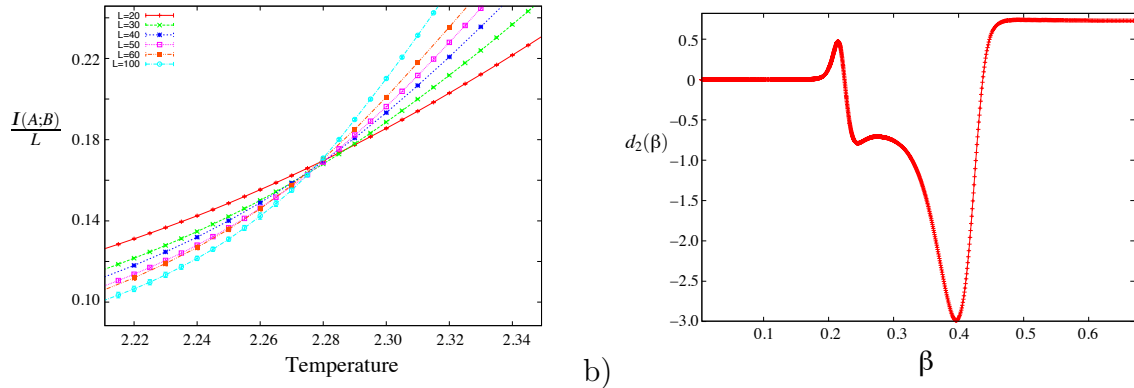
Figure 4.4: a) A close up view of the crossings of the MI curves for different system sizes shows that the curves collapse onto a point very close to the transition temperature of $T_c = 2.27$. b) The constant term d_n in the scaling of the mutual information as a function of β

4.4 Scaling of the Mutual Information near T_{KT}

Having tested our method for calculating the mutual information of classical systems on the 2D Ising model, we now turn our attention to the 2D XY model. The question then becomes whether we can identify the Kosterlitz-Thouless phase transition using this measurement. This is a nontrivial problem as the Kosterlitz-Thouless transition is a very special type of phase transition which breaks no symmetries of the system and has no singularity in any finite derivative of the free energy. In fact, the only method of identifying the phase transition is through a measurement which is related to the universal jump of the superfluid density $\rho_s = \frac{2}{\pi}T_{KT}$. If we can identify some universal scaling behaviour of the mutual information at the transition temperature it would provide a new way to identify whether a general many body system, either quantum or classical, undergoes a KT type phase transition. It is also a test of our MI measurement and whether it can in fact detect all types of phase transitions.

Figs. 4.5 and 4.6 show the mutual information curves for different system sizes for the 2D XY model. We can clearly see that there are indeed approximate crossings of the MI curves for different system sizes. Looking closely at the lower temperature crossing in Fig. 4.6 shows that for smaller system sizes the crossing of any two lines actually occurs quite far from the KT transition temperature, at around $T \sim 1.0$ compared to $T_{KT} \approx 0.893$. We can also see, however, that the crossings seem to be drifting towards T_{KT} as the system size is increased.
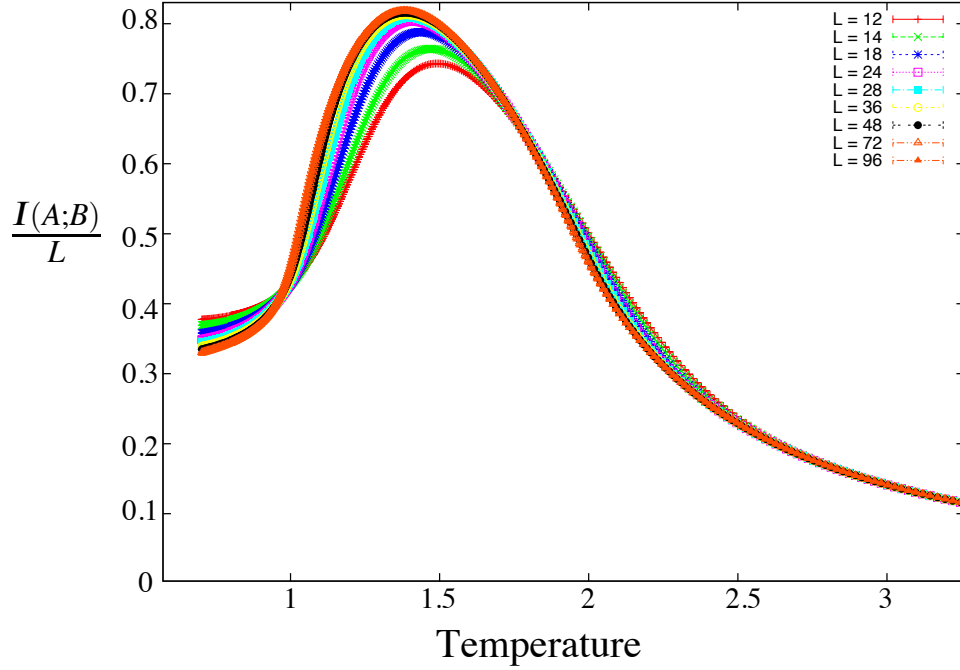
Figure 4.5: The scaling of the mutual information divided by the linear system size for the XY model in 2 dimensions. We simulate system sizes from $L = 12$ to $L = 96$. Notice that any two curves have two clear crossings, occuring slightly above $T_{KT} \approx 0.893$.

We can conjecture a scaling form of the mutual information which is the same as in the Ising case:

$$\mathcal{I}_2(A; B) = a_2(T) \cdot L + d_2(T) + \mathcal{O}(1/L). \tag{4.24}$$

The singular part of the free energy in the XY model diverges very quickly as a function of $\xi \sim e^{c\sqrt{\frac{T_{KT}}{T - T_{KT}}}}$. As you approach the critical temperature, the correlation length ξ
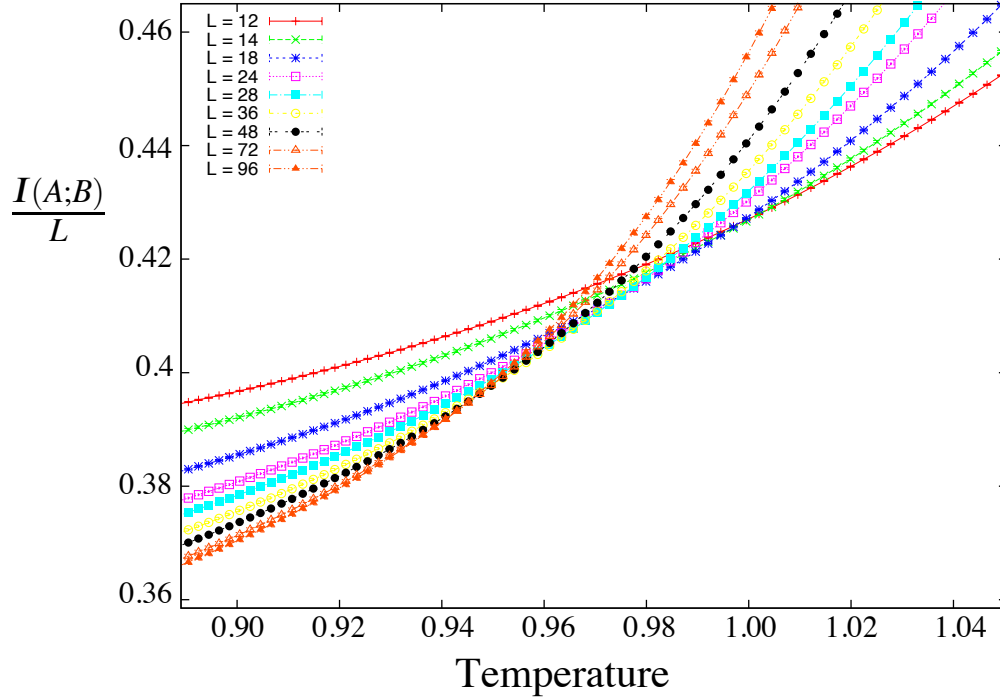
Figure 4.6: A close up of the crossings of the mutual information curves.

becomes commensurate with the size of the system.

$$\xi = \frac{L}{L_0}, \tag{4.25}$$

$$e^{c\sqrt{\frac{T_c}{T-T_c}}} = \frac{L}{L_0}, \tag{4.26}$$

$$T_{KT}(L) - T_{KT}(\infty) = \frac{c^2 \cdot T_{KT}(\infty)}{[\log \frac{L}{L_0}]^2}, \tag{4.27}$$

$$T_{KT}(L) = T_{KT}(\infty) \left[1 + \frac{c^2}{[\log \frac{L}{L_0}]^2}\right]. \tag{4.28}$$

Where in the above derivation we identify the temperature T with the finite size transition temperature $T_{KT}(L)$. We have already seen in Chapter 2 a fit to this scaling form for the superfluid crossings with the Nelson Kosterlitz universal jump condition $\rho_s = \frac{2}{\pi} T_{KT}$. We saw,

in Fig 2.1, a strong linear fit of this scaling form for larger system sizes, while for smaller system sizes it appears that higher order terms add some curvature to the line. Using this scaling form we can calculate the KT transition temperature to be $T_{KT} = 0.8928 \pm 0.0002$. Recall, we estimated the transition in the thermodynamic limit by systematically fitting pairs of data points to a straight line for successively larger linear system sizes, L.

We perform a similar analysis on the crossing points for pairs of mutual information curves. We claim that the crossings of these lines represents the transition to the ordered phase of the XY model. We look at the crossing point between two curves for linear system sizes L and $2L$. The results are plotted in Fig. 4.7, where the straight lines show linear fits of the data using successive pairs of data points at different locations in L. The intercept of these 'tangent lines' gives an estimate of T_{KT} in the thermodynamic limit.

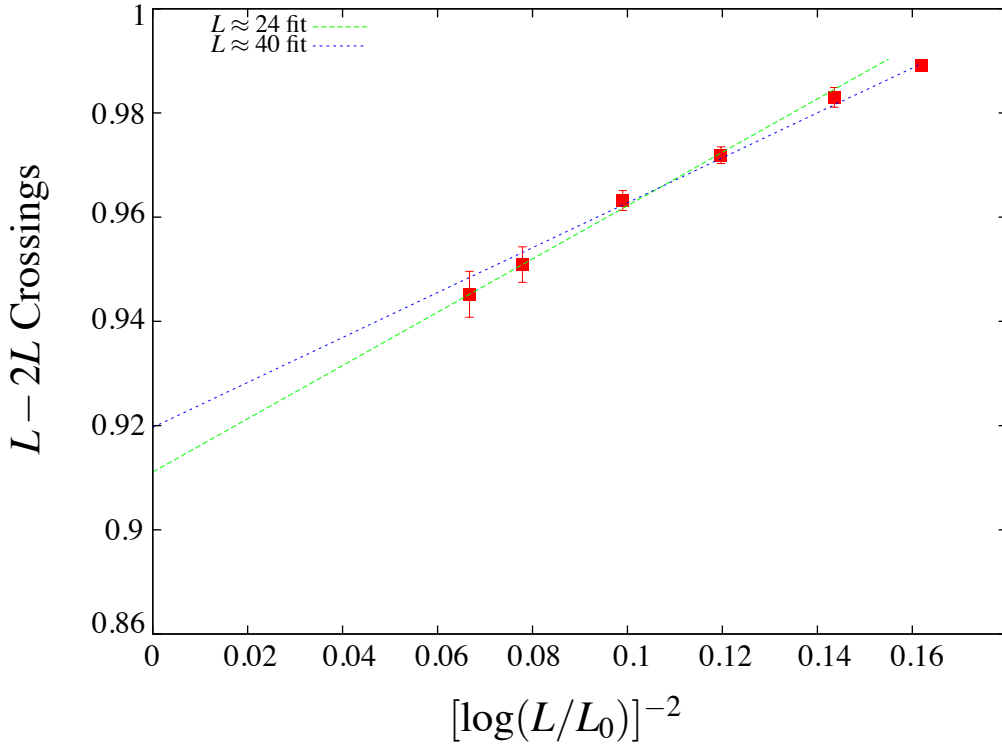Figure 4.7: The value of the MI crossing points for successive plots of L and 2*L plotted on a $\log(L)^{-2}$ scale, to fit the expected scaling of the correlation length ξ near the Kosterlitz-Thouless transition.

We see here a very similar behaviour to the case of the superfluid jump method. The crossing points clearly seem to be approaching a value which is very close to the KT transition temperature. There also seems to be some curvature in the fit, even when plotted against $[1/\log(L)]^2$. In Fig. 4.8, we plot the intercept of the tangent curves as we fit with successively larger points in L from Fig. 4.7. We see that there is some scatter in the data but there is a definite trend to an estimate of T_{KT} in the large L limit. From our data we calculate the value of the transition temperature to be $T_{KT} = 0.885 \pm 0.010$. This is within error bars of the Kosterlitz -Thouless transition temperature of $T_{KT} = 0.893$, and we take this to be strong evidence that we can extract the KT transition from measuring the crossings of our mutual information curves.
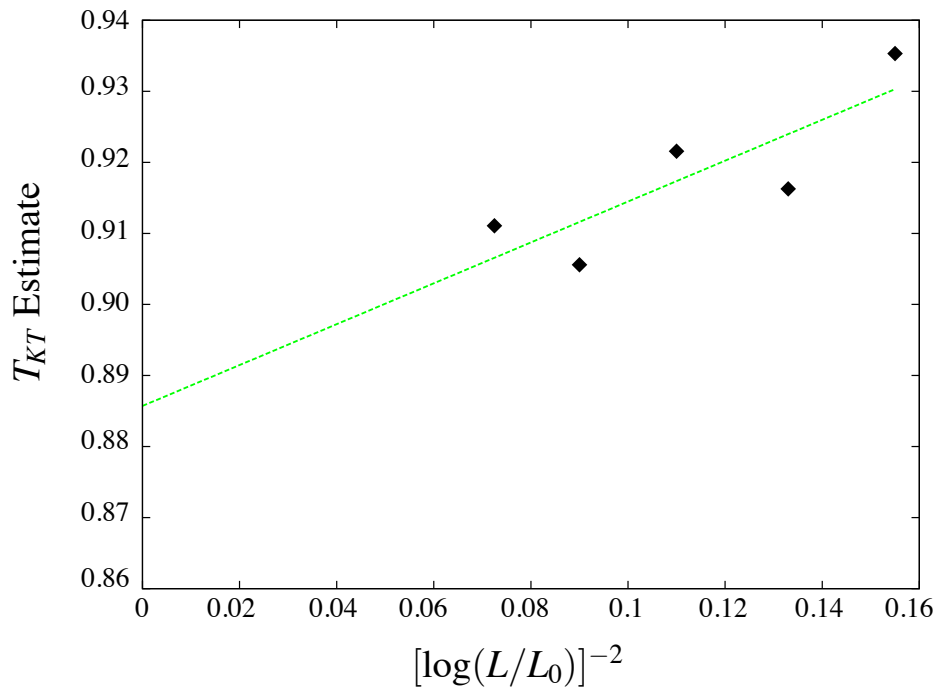
Figure 4.8: The estimates of T_{KT} using successive paris of point from Fig. 4.7. There is a clear trend in the data from which we can see that as L becomes large, we would extract $T_{KT}(\infty) \approx 0.885$ from a linear fit of our MI crossings versus $[\log(L/L_0)]^{-2}$.

Further analysis is needed to understand theoretically the full scaling form of the mutual information in our model. It is likely that there are universal parts of the scaling function which can be used to uniquely characterize a phase transition as a Kosterlitz-

Thouless type transition. We have shown that the mutual information measurement can provide a completely new way of identifying the KT transition point in the XY model, a transition which has historically been very difficult to measure and one in which there are few techniques available for identifying the transition point precisely. We have shown that the mutual information provides us with a new measurement technique which can be used in general Monte Carlo studies to detect phase transitions. This technique requires no knowledge of the order parameter of the model to find the transition, it draws only on the probabilities which appear in the definition of the Shannon entropy. For the XY model, no knowledge about the Nelson-Kosterlitz universal jump condition or any measurements of the superfluid density are needed. We can extract the transition point solely from the scaling of the mutual information.

Chapter 5

Conclusions

In this thesis we have examined the behaviour of two dimensional XY models with ring-exchange terms from several different perspectives. We began by studying the system as a classical statistical mechanics model. We made connections between the J-K model and several physical systems. First we saw that the pure-J XY model can be solved using a renormalization group procedure which looks at the behaviour of bound and unbound vortex pairs. We also looked at the connection between the ordered phase of the XY model and the superfluid phase of bosonic systems. We used this model to test our Monte Carlo algorithm and saw that we could extract, to high accuracy, the Kosterlitz-Thouless transition temperature of $T_{KT} = 0.8928(2)$. We also studied the scaling of the superfluid density in the XY model with respect to the aspect ratio of the lattice and verified claims in the literature for the form of the scaling of ρ_s with $R = L_x/L_y$. We used this aspect ratio scaling to draw a connection between the XY model at the KT transition point and a one dimensional Luttinger liquid. Next, we saw that the pure-K ring-exchange model on a triangular lattice is directly related to the thermal melting of Abrikosov vortex lattices in type-II superconductors. This connection to the physical system prompted us to study the pure-K model and find that this system contains a finite-temperature phase transition which agrees perfectly with KTHNY theory describing the melting of two dimensional solids. To conclude our study of the J-K model from a classical perspective we mapped out the phase diagram of the general J-K phase space. The main feature of this phase diagram is that the presence of a positive/negative ring-exchange term either increases/decreases the strength of the superfluidity in the system.

The second approach to studying this model involved making a connection between quantum systems in d dimensions and classical systems in $(d+1)$ dimensions using the path-integral formulation of quantum mechanics. Using this connection we derived a mapping

from the quantum 1D Bose-Hubbard model to the 2D J-K model, allowing us to study the quantum system using classical Monte Carlo simulations in $(d+1)$ dimensions. The goal of this analysis was to look for manifestations of topological order in classical Hamiltonians. We were able to reproduce, with our classical model, the regions of the Bose-Hubbard phase diagram where the nearest-neighbour repulsion term was relatively small. However, our quantum to classical mapping stopped being well-behaved as the nearest-neighbour repulsion was increased and we showed that we could not reproduce the region of the phase diagram where topological order was present. We came to this conclusion by studying the correlations at the edges of our lattice. In a general topological phase with open boundary conditions, sites are compressible on the edges and incompressible within the bulk of the system. We studied the edges of our system by measuring the decay of the spin-spin correlation function and found that there were no edge states present.

Finally, we studied the XY model from the perspective of classical information theory. We looked at techniques which have recently been employed with great success to study quantum systems with hidden correlations, and saw that we could use these techniques to study phase transitions in classical Hamiltonians. Specifically, we looked at the concept of mutual information, $\mathcal{I}(A;B)$, between two regions in a many-body system. We developed a method of measuring $\mathcal{I}(A;B)$ in classical Monte Carlo simulations using the replica trick. We saw strong evidence that there is some universal behaviour in the finite-size scaling of the mutual information which is manifest in the crossings of the curves. We then showed that these crossing can be used to produce a completely new way to identify the Kosterlitz-Thouless transition without any a priori knowledge of the order parameter or any other microscopic property of the system.

In conclusion, we have taken several analytic and numerical approaches to studying the classical J-K model and have found relationships that exist to several physical systems. We have also used this model to test new classical Monte Carlo techniques which can be applied to a broad range of interesting systems. We have used this model as a window to study a wide range of ideas and phenomena which arise in condensed matter models.

APPENDICES

Appendix A

Exact Quantum to Classical Mapping at Special Point U=V

We can actually find an exact quantum to classical mapping for the 1D Bose-Hubbard model at the special points in phase space where $U = V$, by performing a series of canonical transformations.

Let's start again from our original quantum Hamiltonian

$$H = -t \sum_i \cos(\theta_i - \theta_{i+1}) \; + \; U \sum_i \hat{n}_i^2 \; + \; V \sum_i \hat{n}_i \hat{n}_{i+1}. \tag{A.1}$$

We now apply our first canonical transformation

$$\theta_i \; \rightarrow \; (-1)^i \, \theta_i, \tag{A.2}$$

$$\hat{n}_i \; \rightarrow \; (-1)^i \, \hat{n}_i. \tag{A.3}$$

We can see that the commutation relation still holds since:

$$[(-1)^i \, \theta_i \, , \; (-1)^j \, \hat{n}_j] = (-1)^{i+j}[\theta_i, \hat{n}_j] = \delta_{ij}. \tag{A.4}$$

Then, substituting this into our Hamiltonian gives us

$$
\begin{aligned}
H \; &= \; -t \sum_i \cos(\theta_i(-1)^i - \theta_{i+1}(-1)^{i+1}) \; + \; U \sum_i \hat{n}_i^2 (-1)^{2i} \; + \; V \sum_i \hat{n}_i \hat{n}_{i+1} (-1)^i (-1)^{i+1} \\
&= \; -t \sum_i \cos(\theta_i + \theta_{i+1}) \; + \; U \sum_i \hat{n}_i^2 \; - \; V \sum_i \hat{n}_i \hat{n}_{i+1}.
\end{aligned}
\tag{A.5}
$$

Use the identity $\hat{n}_i\hat{n}_{i+1} = \frac{1}{2}\left[\hat{n}_i^2 \cdot \hat{n}_{i+1}^2 - (\hat{n}_i - \hat{n}_{i_1})^2\right]$ to give:

$$
\begin{aligned}
H &= -t\sum_i \cos(\theta_i + \theta_{i+1}) \;+\; U\sum_i \hat{n}_i^2 \;-\; V\sum_i \frac{1}{2}\left[\hat{n}_i^2\hat{n}_{i+1}^2 - (\hat{n}_i - \hat{n}_{i_1})^2\right], \\
\Rightarrow\; H &= -t\sum_i \cos(\theta_i + \theta_{i+1}) \;+\; (U - V)\sum_i \hat{n}_i^2 \;+\; \frac{V}{2}\sum_i (\hat{n}_i - \hat{n}_{i+1})^2. \qquad \text{(A.6)}
\end{aligned}
$$

In the case where $U \approx V$, our Hamiltonian can be written as

$$
H = -t\sum_i \cos(\theta_i + \theta_{i+1}) \;+\; \frac{V}{2}\sum_i (\hat{n}_i - \hat{n}_{i+1})^2. \qquad \text{(A.7)}
$$

We are now in a position to apply another canonical transformation, which will put the Hamiltonian into a form that we can deal with the same way as our previous mappings.

$$
\begin{aligned}
\text{Let} \qquad & N_i = \hat{n}_i - \hat{n}_{i-1} & \text{(A.8)} \\
\text{and} \qquad & \phi_i = \sum_{k \geq i} \theta_k. & \text{(A.9)}
\end{aligned}
$$

Then

$$
\begin{aligned}
\left[N_i, \phi_j\right] &= \left[\hat{n}_i - \hat{n}_{i-1}, \sum_{k \geq j} \theta_k\right] & \text{(A.10)} \\
&= \left[n_i, \sum_{k \geq j} \theta_k\right] - \left[n_{i-1}, \sum_{j \geq k} \theta_k\right] \\
&= \left([n_i, \theta_j] + [n_i, \theta_{j+1}] + [n_i, \theta_{j+2}] + \cdots\right) \\
&\qquad\qquad - \left([n_{i-1}, \theta_j] + [n_{i-1}, \theta_{j+1}] + \cdots\right) \qquad \text{(A.11)}
\end{aligned}
$$

If $i = j$, the first bracket in (A.11) contains $[n_i, \theta_i] = i$, and the second bracket does not contain any commutators of the form $[n_i, \theta_i]$. Therefore, $[N_i, \phi_i] = i$, (since $[n_i, \theta_i] = \delta_{ij}$)

If $i > j$, then both terms in brackets above contain exactly one commutator of the form $[n_i, \theta_i] = i$, so these cancel each other and $[N_i, \phi_j] = 0$.

If $i < j$, then both terms in bracket only contain commutators of the form $[n_i, \theta_j]$ with $i \neq j$. So all these commutators are zero and $\Rightarrow [N_i, \phi_j] = 0$.

Putting this together verifies that our canonical transformation satisfies the usual commutation relation:

$$[N_i, \phi_j] = \delta_{ij}. \tag{A.12}$$

Also, note that

$$\phi_i - \phi_{i+2} = \left(\theta_i + \theta_{i+1} + \theta_{i+2} + \cdots \right) - \left(\theta_{i+2} + \theta_{i+3} + \cdots \right) = \theta_i + \theta_{i+1}. \tag{A.13}$$

Substituting (A.8) and (A.13) into our Hamiltonian (A.7) gives:

$$H = -t \sum_i \cos(\phi_i - \phi_{i+2}) + \frac{V}{2} \sum_i N_i^2 \tag{A.14}$$

.

This Hamiltonian is in exactly the same form as the 1D Bose Hubbard model with only on-site repulsion (here nearest neighbours are sites i and i+1). We already saw that this maps onto the XY-model in two dimensions. So, in the case where $U = V$, the model maps onto two intertwined XY models where nearest-spatial neighbours are not coupled but next-nearest neighbours are coupled. This has the usual two phases in the N_i / ϕ_i variables, a Mott insulating and a superfluid phase.

The classical Hamiltonian is:

$$H = -\sqrt{\frac{t}{V}} \sum_i \cos(\phi_i - \phi_{i+2}) - \sqrt{\frac{t}{V}} \sum_i \cos(\phi_i - \phi_{i+\tau}) \tag{A.15}$$

The question now is what do the two phases correspond to in our original n_i / θ_i variables. When V/t is large, we are in the insulating phase, so our N_i variables are localized (i.e. $\Delta N_i \sim$ small). Looking at (A.14), in the large V limit the groundstate will want all variables $N_i = 0$ since any fluctuations from this would have a large energy cost.

Now, we defined $N_i = \hat{n}_i - \hat{n}_{i-1}$, where $\hat{n}_i$ is the deviation from uniform filling of our quantum model. But, recall that we also applied the first canonical transformation $\hat{n}_i \to (-1)^i \hat{n}_i$. So, in our original variables our N_i variables are expressed as : $N_i = \hat{n}_i + \hat{n}_{i-1}$.

It seems that there are two ways to satisfy $N_i = \hat{n}_i + \hat{n}_{i+1} = 0$. One is that all n_i variable equal zero. Another is that n_i, n_{i+1} are alternating particle/hole fluctuations so that $n_i = (-1)^i$ and $n_i + n_{i+1} = 0$. Clearly, one of these conditions corresponds to the Mott-insulating phase and the other corresponds to the charge density wave phase.

We have shown that we can find an exact mapping of the Bose-Hubbard model to a 2D classical model, however in performing this mapping we have had to explicitly introduce a set of long-range variables.

References

[1] J M Kosterlitz and D J Thouless. Ordering, metastability and phase transitions in two-dimensional systems. *Journal of Physics C: Solid State Physics*, 6(7):1181, 1973.

[2] J M Kosterlitz. The critical properties of the two-dimensional xy model. *Journal of Physics C: Solid State Physics*, 7(6):1046, 1974.

[3] D. J. Bishop and J. D. Reppy. Study of the superfluid transition in two-dimensional ^{4}He films. *Phys. Rev. Lett.*, 40:1727–1730, Jun 1978.

[4] B. I. Halperin and David R. Nelson. Theory of two-dimensional melting. *Phys. Rev. Lett.*, 41:519–519, Aug 1978.

[5] G. Vidal, J. I. Latorre, E. Rico, and A. Kitaev. Entanglement in quantum critical phenomena. *Phys. Rev. Lett.*, 90:227902, Jun 2003.

[6] Sergei V. Isakov, Matthew B. Hastings, and Roger G. Melko. Topological entanglement entropy of a bose-hubbard spin liquid. *Nat Phys*, 7(10):772–775, 10 2011.

[7] Matthew B. Hastings, Iván González, Ann B. Kallin, and Roger G. Melko. Measuring renyi entanglement entropy in quantum monte carlo simulations. *Phys. Rev. Lett.*, 104:157201, Apr 2010.

[8] A. W. Sandvik, S. Daul, R. R. P. Singh, and D. J. Scalapino. Striped phase in a quantum xy model with ring exchange. *Phys. Rev. Lett.*, 89:247201, Nov 2002.

[9] Roger G. Melko and Anders W. Sandvik. Stochastic series expansion algorithm for the $s = 1?2$ xy model with four-site ring exchange. *Phys. Rev. E*, 72:026702, Aug 2005.

[10] N. D. Mermin and H. Wagner. Absence of ferromagnetism or antiferromagnetism in one- or two-dimensional isotropic heisenberg models. *Phys. Rev. Lett.*, 17:1133–1136, Nov 1966.

[11] Ying-Hong Li and S. Teitel. Finite-size scaling study of the three-dimensional classical *XY* model. *Phys. Rev. B*, 40:9122–9125, Nov 1989.

[12] Michael E. Fisher, Michael N. Barber, and David Jasnow. Helicity modulus, superfluidity, and scaling in isotropic systems. *Phys. Rev. A*, 8:1111–1124, Aug 1973.

[13] Igor Herbut. *A Modern Approach to Critical Phenomena*. Cambridge University Press, Cambridge, UK, 2007.

[14] Jorge V. José, Leo P. Kadanoff, Scott Kirkpatrick, and David R. Nelson. Renormalization, vortices, and symmetry-breaking perturbations in the two-dimensional planar model. *Phys. Rev. B*, 16:1217–1241, Aug 1977.

[15] Villain, J. Theory of one- and two-dimensional magnets with an easy magnetization plane. ii. the planar, classical, two-dimensional magnet. *J. Phys. France*, 36(6):581–590, 1975.

[16] Kenneth G. Wilson and J. Kogut. The renormalization group and the expansion. *Physics Reports*, 12(2):75 – 199, 1974.

[17] Kenneth G. Wilson. Model of coupling-constant renormalization. *Phys. Rev. D*, 2:1438–1472, Oct 1970.

[18] L.P. Kadanoff. *Nature Physics*, 2:263, 1966.

[19] David R. Nelson and J. M. Kosterlitz. Universal jump in the superfluid density of two-dimensional superfluids. *Phys. Rev. Lett.*, 39:1201–1205, Nov 1977.

[20] D.P. Landau and K. Binder. *A Guide To Monte Carlo Simulations In Statistical Physics*. Cambridge University Press, 2005.

[21] J.S. Liu. *Monte Carlo Strategies in Scientific Computing*. Springer Series in Statistics. Springer, 2001.

[22] Nicholas Metropolis, Arianna W. Rosenbluth, Marshall N. Rosenbluth, Augusta H. Teller, and Edward Teller. Equation of state calculations by fast computing machines. *The Journal of Chemical Physics*, 21(6):1087–1092, 1953.

[23] Robert H. Swendsen and Jian-Sheng Wang. Nonuniversal critical dynamics in monte carlo simulations. *Phys. Rev. Lett.*, 58:86–88, Jan 1987.

[24] Ulli Wolff. Collective monte carlo updating for spin systems. *Phys. Rev. Lett.*, 62:361–364, Jan 1989.

[25] R. G. Melko, A. W. Sandvik, and D. J. Scalapino. Aspect-ratio dependence of the spin stiffness of a two-dimensional XY model. *Phys. Rev. B*, 69:014509, Jan 2004.

[26] M Hasenbusch and K Pinn. Computing the roughening transition of ising and solid-on-solid models by bcsos model matching. *Journal of Physics A: Mathematical and General*, 30(1):63, 1997.

[27] Martin Hasenbusch. The two-dimensional xy model at the transition temperature: a high-precision monte carlo study. *Journal of Physics A: Mathematical and General*, 38(26):5869, 2005.

[28] Nikolai V. Prokof'ev and Boris V. Svistunov. Two definitions of superfluid density. *Phys. Rev. B*, 61:11282–11284, May 2000.

[29] Thierry Giamarchi. *Quantum Physics in One Dimension*. Oxford University Press, Oxford, UK, 2004.

[30] L.D. Landau. *Sov. Phys. JETP*, 3:920, 1957.

[31] L.D. Landau. *Sov. Phys. JETP*, 5:101, 1957.

[32] F. D. M. Haldane. Effective harmonic-fluid approach to low-energy properties of one-dimensional quantum fluids. *Phys. Rev. Lett.*, 47:1840–1843, Dec 1981.

[33] J. M. Luttinger. An exactly soluble model of a many-fermion system. *Journal of Mathematical Physics*, 4(9):1154–1162, 1963.

[34] Daniel C. Mattis and Elliott H. Lieb. Exact solution of a many-fermion system and its associated boson field. *Journal of Mathematical Physics*, 6(2):304–312, 1965.

[35] Adrian Del Maestro and Ian Affleck. Interacting bosons in one dimension and the applicability of luttinger-liquid theory as revealed by path-integral quantum monte carlo calculations. *Phys. Rev. B*, 82:060515, Aug 2010.

[36] Zlatko Tešanović and Lei Xing. Critical fluctuations in strongly type-ii quasi-two-dimensional superconductors. *Phys. Rev. Lett.*, 67:2729–2732, Nov 1991.

[37] I. Guillamon, H. Suderow, A. Fernandez-Pacheco, J. Sese, R. Cordoba, J. M. De Teresa, M. R. Ibarra, and S. Vieira. Direct observation of melting in a two-dimensional superconducting vortex lattice. *Nat Phys*, 5(9):651–655, 09 2009.

[38] J. Iaconis, R. G. Melko, and A. A. Burkov. Continuous thermal melting of a two-dimensional abrikosov vortex solid. *Phys. Rev. B*, 82:180504, Nov 2010.

[39] A. A. Burkov. Fractional quantum hall effect and featureless mott insulators. *Phys. Rev. B*, 81:125111, Mar 2010.

[40] R.G.Melko. *Quantum Monte Carlo simulations of spin 1/2 XY models with ring exchange.* PhD thesis, University of California - Santa Barbara, 2005.

[41] Robert Schaffer, Anton A. Burkov, and Roger G. Melko. Superfluid phases of lattice bosons with ring-exchange interaction. *Phys. Rev. B*, 80:014503, Jul 2009.

[42] Markus Greiner, Olaf Mandel, Tilman Esslinger, Theodor W. Hansch, and Immanuel Bloch. Quantum phase transition from a superfluid to a mott insulator in a gas of ultracold atoms. *Nature*, 415(6867):39–44, 01 2002.

[43] H. F. Trotter. On the product of semi-groups of operators. *Proc. Amer. Math. Soc.*, 10:545–551, 1959.

[44] Masuo Suzuki. General correction theorems on decomposition formulae of exponential operators and extrapolation methods for quantum monte carlo simulations. *Physics Letters A*, 113(6):299 – 300, 1985.

[45] F.D.M. Haldane. Continuum dynamics of the 1-d heisenberg antiferromagnet: Identification with the o(3) nonlinear sigma model. *Physics Letters A*, 93(9):464 – 468, 1983.

[46] Emanuele G. Dalla Torre, Erez Berg, and Ehud Altman. Hidden order in 1d bose insulators. *Phys. Rev. Lett.*, 97:260401, Dec 2006.

[47] Ian Affleck, Tom Kennedy, Elliott H. Lieb, and Hal Tasaki. Rigorous results on valence-bond ground states in antiferromagnets. *Phys. Rev. Lett.*, 59:799–802, Aug 1987.

[48] K. Góral, L. Santos, and M. Lewenstein. Quantum phases of dipolar bosons in optical lattices. *Phys. Rev. Lett.*, 88:170406, Apr 2002.

[49] Matthew P. A. Fisher, Peter B. Weichman, G. Grinstein, and Daniel S. Fisher. Boson localization and the superfluid-insulator transition. *Phys. Rev. B*, 40:546–570, Jul 1989.

[50] D. L. Kovrizhin, G. Venketeswara Pai, and S. Sinha. Density wave and supersolid phases of correlated bosons in an optical lattice. *EPL (Europhysics Letters)*, 72(2):162, 2005.

[51] Elliott Lieb, Theodore Schultz, and Daniel Mattis. Two soluble models of an antiferromagnetic chain. *Annals of Physics*, 16(3):407 – 466, 1961.

[52] Tom Kennedy and Hal Tasaki. Hidden $z_2 x z_2$ symmetry breaking in haldane-gap antiferromagnets. *Phys. Rev. B*, 45:304–307, Jan 1992.

[53] X.G. Wen. *Quantum Field Theory Of Many-body Systems: From The Origin Of Sound To An Origin Of Light And Electrons*. Oxford Graduate Texts. Oxford University Press, 2004.

[54] Steven R. White. Density-matrix algorithms for quantum renormalization groups. *Phys. Rev. B*, 48:10345–10356, Oct 1993.

[55] Christoph Holzhey, Finn Larsen, and Frank Wilczek. Geometric and renormalized entropy in conformal field theory. *Nuclear Physics B*, 424(3):443 – 467, 1994.

[56] C.E. Shannon. A mathematical theory of communication. *The Bell Systems Tech. J.*, 27:379–423, 623–656, 1948.

[57] Peter W. Shor. Capacities of quantum channels and how to find them. *Mathematical Programming*, 97:311–335, 2003. 10.1007/s10107-003-0446-y.

[58] Mark M. Wilde. From classical to quantum shannon theory. 2011. arXiv:1106.1445v4.

[59] Mark Srednicki. Entropy and area. *Phys. Rev. Lett.*, 71:666–669, Aug 1993.

[60] J. Eisert, M. Cramer, and M. B. Plenio. *Colloquium* : Area laws for the entanglement entropy. *Rev. Mod. Phys.*, 82:277–306, Feb 2010.

[61] Rajiv R. P. Singh, Matthew B. Hastings, Ann B. Kallin, and Roger G. Melko. Finite-temperature critical behavior of mutual information. *Phys. Rev. Lett.*, 106:135701, Mar 2011.

[62] Michael M. Wolf, Frank Verstraete, Matthew B. Hastings, and J. Ignacio Cirac. Area laws in quantum systems: Mutual information and correlations. *Phys. Rev. Lett.*, 100:070502, Feb 2008.

[63] Pasquale Calabrese and John Cardy. Entanglement entropy and conformal field theory. *Journal of Physics A: Mathematical and Theoretical*, 42(50):504005, 2009.

[64] Lars Onsager. Crystal statistics. i. a two-dimensional model with an order-disorder transition. *Phys. Rev.*, 65:117–149, Feb 1944.

[65] Roger G. Melko, Ann B. Kallin, and Matthew B. Hastings. Finite-size scaling of mutual information in monte carlo simulations: Application to the spin-$\frac{1}{2}$ xxz model. *Phys. Rev. B*, 82:100409, Sep 2010.